APPLICATION OF IMAGE-BASED SENSING METHODS IN SHAKE TABLE EXPERIMENTS

by

Ferit Yardımcı

B.S., Civil Engineering, Boğaziçi University, 2015

Submitted to the Institute for Graduate Studies in
Science and Engineering in partial fulfillment of
the requirements for the degree of
Master of Science

Graduate Program in Civil Engineering

Boğaziçi University

2018

ACKNOWLEDGEMENTS

I would like to express my gratitude to my thesis advisor, Assoc. Prof. Cem Yalçın, for his guidance and patience throughout my master?s study.

I would also like to express my appreciation to Prof. Ercan Yüksel for his efforts and advices which played a crucial role during experimental work.

Special thanks extended to Assistant Prof.Ahmet Anıl Dindar for his suggestions on image-based measurements and development of source code during initial phase of my studies.

My special colleagues, PhD Students Burak Horoz and Ahmet Güllü, helped me throughout my experimental studies. Without their support, this thesis couldn?t have been completed. Their guidance and experiences in shake table were instrumental in this study.

The collaboration of the Istanbul Technical University?s Structural and Earthquake Engineering Laboratory staff made this study possible. I would like to express my sincere gratitude to them.

Finally, I would like to mention the most valuable people in my life who always stand by me and provide their unconditional support whenever I needed. My mother Fehime Yardımcı, my father Necat Yardımcı and my beloved sibling Yelda Yardımcı have always been extremely thoughtful and supportive for my entire education years.

The financial support for this study was provided by Bogazici University Research Fund (BAP) grant number 11164. Also, MIT International Science and Technology Initiatives (MISTI) collaboration was also instrumental in this study.

ABSTRACT

APPLICATION OF IMAGE-BASED SENSING METHODS IN SHAKE TABLE EXPERIMENTS

Earthquake Engineering-related experimental dynamic testing of Single Degree of Freedom (SDOF) or Multi Degree of Freedom (MDOF) structural systems involve high precision measurement devices such as strain gauges, Linear Variable Displacement Transducers (LVDTs), Linear Potentiometer (LPT), lasermeters and accelerometers. Also, high frequency data acquisition systems need to be used to collect data within a narrow time frame. Higher sensitivity and accuracy mean higher measurement costs. Thus, they are not cost effective, and this becomes a major disadvantage in dynamic shake table experiments. However, image-based sensing methods could present a feasible alternative way to perform such measurements. This study investigates the applicability of image-based methods in various forms of dynamic experiments of structural specimens. In the past, similar studies have been completed on this topic. Displacements of different structures under ambient vibrations or earthquake ground motions were investigated with different tracking methods. This study mainly focuses on two different vision-based methods to extract displacement data within short-period and high frequency dynamic motion. One method is a simple LED light source tracking, while the other one uses an existing object tracking algorithm (Kanade-Lukas-Tomasi). Quality of camera in terms of resolution and image capturing capability (frames per second) coupled with the image algorithms were compared. A computer program with an appropriate user interface was developed to analyze the video images. Displacement, velocity, acceleration and strain data provided by image-based measurements were compared with the results from conventional devices such as strain gauges, accelerometers and LVDT's.

ÖZET

GÖRÜNTÜ TEMELLİ ÖLÇÜM YÖNTEMLERİNİN SARSMA MASASI DENEYLERİNDE UYGULAMALARI

Deprem mühendisliği alanında, Tek serbestlik dereceli (TSD) ya da Çok serbestlik dereceli (ÇSD) sistemlerin deneysel dinamik testlerinde, gerinim ölçerler, Lineer Değişken Yerdeğiştirme Dönüştürücüler (LVDT), Lineer Potansiyometreler (LPT), lazermetreler ve ivmeölçerler gibi yüksek hassasiyetli ölçüm aletleri kullanılmaktadır. Bunun yanı sıra, kısa bir zaman aralığında veri toplayabilmek için, yüksek frekanslı veri alma sistemlerine ihtiyaç duyulmaktadır. Bu ölçüm cihazlarında yüksek hassasiyet ve isabetlilik beraberinde yüksek maliyetleri de getirmektedir. Bu sistemlerin maliyetleri sarsma masası deneyleri için büyük bir dezavantajdır. Görüntü temelli yöntemler ise bu ölçümleri gerçekleştirmek adına bir alternatif olarak öne çıkmaktadır. Bu çalışmada bu yöntemlerin değişik yapısal durumlar için uygulanabilirliği araştırılmıştır. Geçmişte bu konu üzerine bazı çalışmalar yapılmıştır. Bu çalışmada, kısa sürede yüksek frekanslı dinamik hareketlerde yer değiştirme ölçümlerini yapabilen iki farklı görüntü temelli metot sunulmuştur. Bu metotlardan birincisi basit bir LED ışık kaynağı takibi metodu olup diğeri ise var olan bir nesne takip algoritmasını (Kanade-Lukas-Tomasi) kullanan bir metottur. Çözünürlük ve görüntü yakalama kabiliyeti açısından kameranın kalitesi (saniye başına kare) görüntü işleme algoritmaları ile beraber kullanılarak karşılaştırılmıştır. Bu deneylerin video kayıtlarını analiz etmek için kullanıcı arayüzü de içeren bir bilgisayar programı geliştirilmiştir. Görüntü temelli ölçümlerle sağlanan yer değiştirme, hız, ivme ve gerinim verileri; gerinim ölçer, ivmeölçer ve LVDT'den elde edilen sonuçlarla karşılaştırılmıştır. Çelik kolon şeklinde bir numunenin gerinim ölçümleri hariç tüm bu karşılaştırmalardaki farklar, ihmal edilebilir seviyededir. Bu durum dinamik deneylerde görüntü temelli yöntemlerin başarısını göstermiştir.

TABLE OF CONTENTS

LIST OF FIGURES

LIST OF TABLES

LIST OF SYMBOLS

TH	Threshold value
I	Pixel grayscale intensity
c	Damping coefficient
E_a	Absorbed energy
E_d	Damping energy
E_I	Input energy
E_k	Kinetic energy
E_p	Plastic energy
E_s	Strain energy
f_s	Restoring force
k	Stiffness
m	Mass

LIST OF ACRONYMS/ABBREVIATIONS

F	Force
M	Moment

1. INTRODUCTION

1.1. General

Earthquake-induced structural damages cause intolerable sufferings such as loss of lives or permanent injuries, as well as heavy economic losses. To minimize these catastrophic damages, understanding the behavior of structures under earthquake action is crucial. In order to simulate and understand the dynamic characteristics and structural behavior of various types of scaled-down specimens under earthquake excitations researchers have often used shake table experiments.

These studies were performed through different measurement techniques, which played a key role in experiments to understand the dynamic responses of structural systems. The assessment of the behavior of specimens under seismic load during shake table experiments has always been a delicate process, which mostly plays an enormous role in the success of the experiment. Distorted response data may cause misleading conclusions and limit the potential gains of an experiment.

Measurement devices such as Linear Variable Displacement Transducer (LVDT), Linear Potentiometer (LPT), strain gauges, accelerometers and lasermeters are among the equipment utilized to measure the dynamic responses of specimens. However, these conventional measurement devices possess certain disadvantages. LVDT and LPT are the devices based on converting mechanical displacement into an electrical signal in terms of millivolts. The conversions are based on linear relationship between a known source and measured millivolts. These devices are attached to the point of interest where the required displacements on a specific point on the surface of the material are identified. However, during the movement of the specimen under excitation, additional resistance could occur due to the spring force created by these devices. This additional resistance alters the measured structural characteristics such as stiffness (and therefore the natural frequency) and damping values of the test model, and thus causes inconsistency between the designed model and its experimental results.

Strain gauges are also important measurement devices that are widely used in experimental studies. Strains occur on entire surface of the specimen during an excitation. Measuring strains on one specific surface may not yield correct characteristics of dynamic structural response. Even though these strain gauges are not so expensive (about 10 USD a piece) and quite accurate in measurements (one thousandth of a millimeter), utilizing these devices is not quite convenient. There are certain requirements and procedures to follow in the installation, such as cleaning the contact area, proper placement and wiring issues, and using the right epoxy glue. In addition, once they are removed from the surface, they cannot be used again.

Accelerometers and lasermeters are sensing devices, and their sensitivity and accuracy are directly related to their cost. Apart from cost and accuracy, all of above-mentioned devices require heavy cabling network. As length of cables increases, the sensitivity of these devices decreases. Therefore, properly insulated cables need to be used and this means further increased cost.

Even all above-mentioned devices are chosen as high-sensitive devices, one has to have a high frequency data acquisition equipment, which is highly expensive. Therefore, there is a need for accurate and yet inexpensive way, to measure the behavior of structural systems in dynamic shake table experiments. Also, the measurement technique should be applicable to entire surface rather than discrete locations of the specimens. Thus, image-based measurement technique offers a viable alternative in this case.

1.2. Image-Based Methods

While some limitations that are mentioned above exist regarding the conventional methods, remote sensing techniques provide ability to performing almost all the measurement operations similar to the contact-type classical measurement devices. Among the dynamic responses of structural models, displacement response is regarded as one of the most valuable data since all other significant quantities such as velocity, acceleration and fundamental frequencies could be analytically obtained from it. Using mathematical differentiation operations or algorithms, these quantities could readily be obtained with significantly reduced noise contamination. The image-based monitoring techniques directly identify the positions of the specified regions on test specimens in the field of measurement. Time dependent variations of these positions correspond to displacements in space. In addition, these methods of measurement require only a video recorder and few additional apparatuses such as optical target or speckle painting sprays, which are quite affordable in comparison with other widely used devices such as laser meters.

High cost in the use of high sensitive measurement equipment is a significant problem especially in dynamic experimental studies. Image-based methods could provide researchers extensive savings in their experimental studies.

When optical measurement methods are considered, there are two different types exist: the ones based on laser beams and ones based on white light. Laser-based experimental measurements could be listed as electronic speckle pattern interferometry (ESPI), Laser Doppler Vibrometry and Digital Speckle Shearography (DSS) (Baqersad *et al.*, 2017). Image-based methods utilize the white light, thus, they fall into the second category. In this study, image-based methods using video recordings were utilized to assess the responses of test specimens on shake table.

Main methods to obtain measurement of structural responses with video cameras could be divided into three categories (Baqersad *et al.*, 2017). These categories are; point based methods, digital image correlation methods and targetless methods.

1.2.1. Point Based Methods

These methods are based on extracting coordinates of specific targets on a structural specimen. Since these targets are mounted on specific locations on structures, they do not represent the entire structure but rather limited fields in the vicinity of these points. Thus, this method is more appropriate for measurement of discrete locations on a specimen rather than continuous monitoring. The points desired to be tracked are tagged with different targets, which generally create a contrast from their surrounding area. This contrast increases the recognition opportunity and makes these targets detectable whether by their color intensity or geometry. This method is less vulnerable in regards to unstable background conditions, and thus, preferable for unstable environments. In terms of the processing time, it is advantageous over the other methods. Due to the limited area in a frame as a range of interest, it demands shorter duration of process.

1.2.2. Digital Image Correlation (DIC) Methods

Main working principle of this method is detecting the template with minimum difference to the target on a specific investigated area. It utilizes random textures on a surface as targets. Detection of these targets, which consists of great number of small dots in the form of speckles in consecutive video frames, yields the overall displacement measurements. These targets are generally sprinkled over the area of interest and the pattern of these speckles are random. This randomness creates unique targets all over the painted area, and thus, these targets are recognized in each image frame. Since the number of followed target and geometries are large, the process duration with this method is considerably long. This method suits better for continuous models and provide displacement and strain values over an entire area. In addition to structural dynamics, this method is used in material tests on crack propagation and temperature changes (McCormick and Lord, 2010).

1.2.3. Targetless Methods

In lieu of mounting an optical target on a tested structure or if the specimen is slender, where the application of such target may alter the dynamic charactersitics, the only option left for the measurement of dynamic response is the targetless methods. These methods consist of edge detection, pattern matching and cross correlation. Among these three methods, edge detection and pattern matching techniques are widely used methods in dynamic structural tests. Edge detection method uses edge detection algorithms to first identify the physical boundaries of testing objects, then track these boundaries to obtain the structural response (Baqersad *et al.*, 2017). On the other hand, pattern recognition method seeks for the similarity of a certain area which corresponds to part of the specimen between consecutive frames and match the certain areas from them. Researchers (Baqersad *et al.*, 2017) noted that, even the computational demand is not too high for edge detection algorithms, the robustness of the pattern recognition methods is quite satisfactory.

1.3. Literature Review

Extracting useful data from the images is a concept which dates back to even before the invention of basic cameras, the Renaissance Age. Leonardo da Vinci in 1480, implied that vision could be used as a very powerful measurement tool in the following quotation: “Perspective is nothing else than the seeing of an object behind a sheet of glass, smooth and quite transparent, on the surface of which all the things may be marked that are behind this glass. All things transmit their images to the eye by pyramidal lines, and these pyramids are cut by the said glass. The nearer to the eye these are intersected, the smaller the image of their cause will appear” (Doyle, 1964).

With the development of first cameras, gathering information by the use of this brand-new tool became quite instrumental. As in the case of many different inventions, the first use of extracting information from images was conducted for military purposes. During the World War I, it was tried to gather intelligence behind the enemy lines from aerial images.

Widely usage of the photogrammetry in civil life has started in 1920’s to identify the borders and creating well-developed topographic maps. However, utilization of the image-based measurements in the area of civil and structural engineering has started only in 1980’s.

Main interest of early applications of image-based methods was about determining the mechanical strains in structures (Peters and Ranson, 1982). Among other methods, which perform optimal strain measurements, DIC method was used in these early studies (Chu, Ranson andSutton, 1985). Over the years, these methods expanded their capacities as the qualities and capabilities of camera recorders were drastically improved.

Chang and Ji, (2007) presented a method to monitor 3D structural vibration responses with the images obtained by two recorders. To increase the accuracy, geometrical calibration methods were utilized. Three experiments were carried out for different models under different circumstances such as sinusoidal movement of a single point, wind tunnel test of a bridge model and an earthquake vibration for a 3-storey small-scaled structure. Results showed that as the vibration frequency increased, measurement errors had higher values.

Morlier *et al.* (2007) used high-speed cameras to record a bridge structure and investigated the dynamic characteristics via using OpenCV-based software. The software that was used in this study was based on Lukas-Kanade optical flow algorithm. The primary objective of this study was to determine the location of the damage. However, it was observed that in the field tests noise became a significant issue to overcome.

Nogueria *et al.* (2009) stated that most of the design codes expect engineers to complete their designs within certain frequency limits in order to satisfy the serviceability limit states criteria. Based on this fact, researchers proposed a methodology that initially determines the spatial displacement signals from the video records and then evaluates the natural frequencies of the structures. They considered a black dot over a white background as a target and found the centroid of this target for each frame. The results of this study were satisfactory for a specific frequency interval due to the sampling rate of the recorder. Also, it was noted that the measurement methodology was applicable for only in plane displacements. The recording phase of the experiment was vulnerable to certain distortions such as insufficient illumination and reflections of nearby objects on the image.

Choi *et al.* (2010) introduced the Dynamic Displacement Vision System (DDVS) which concentrated on a specific target called Range of Interest (ROI) and kept track of this specific area. The presented system resized captured frames in each step and re-evaluated the coefficient which defined the ratio between the pixel and the real size of the specified distance which is marked by signatures on ROI.

Jurjo *et al.* (2010) investigated the performance of digital image acquisition system in observing the dynamic behavior of the slender columns. There were two different experiments conducted; one, in order to evaluate the vision-based system, while the other, for the dynamic behavior. Adhesive markers were mounted on column specimens and tracked frame by frame. Results of the analyses indicated a strong correlation between theoretical calculations and experimental data. It was also mentioned that conventional measurement devices caused troublesome differences in structural response of the model.

Park *et al.* (2010) underlined the significance of the horizontal displacements to understand the behavior of flexible high-rise structures. They presented various obstacles to conduct the measurement of these displacements by contact methods due to the greater sizes of these structures. Researchers introduced a system to obtain displacements of particular points on a flexible column structure by using the video records of two web-cams installed on testing structure. These web-cam recordings targeted points from different angles. Horizontal displacements extracted by using both spatial variation of position and rotation values that were obtained from the records. The results compared with the laser displacement sensor measurements and the difference was found less than 0.5

Nayyerloo *et al.* (2011) investigated the validity of a method developed to track displacements which uses records by high speed line-scan cameras in seismic experiments. The method proposed detection of edges on a line and identified the position of a certain target. It was stated that the method could obtain displacements of the target regardless of the magnitude of the motions. In addition, researchers suggested a calibration method that reduces the error notably. Kim and Kim, (2011) proposed a method to acquire the displacement data of multiple points through digital image processing technique called “Digital Image Correlation” (DIC). In order to increase the accuracy, Image Transform Function (ITF) was used in the study. A shaking table test and a set of field tests took place as the experimental validations of the research. Also, natural frequencies and tension forces occurred on tested structures were estimated with this methodology. Results yielded negligible errors in comparison with the contact-type sensors.

Alemdar *et al.* (2011) employed a video-based measurement method in their experimentswith the ultimate purpose of observing the deformations of columns on large-scale reinforced concrete (RC) bridge structure. Dynamic tests were conducted on a shaking table. Plastic hinging regions of columns were recorded and different dynamic responses were investigated. Results of the experiments implied that the video-based measurement method accomplished to identify lateral and vertical displacements, as well as overall deformation configurations. However, the system was relatively powerless in secondary calculations such as rotations of the columns.

Hoult *et al.* (2012) conducted tension tests on steel specimens and tried to achieve extracting strain data from video recordings. They tracked certain regions of the specimens, which are differentiated by painting in a certain way, and used DIC method. The results of the study underlined the distortive effect of out of plain motions. Researchers examined different solution techniques, such as expanding the distance between specimen and camera and recording the strain on different surfaces to overcome such problems.

Ribeiro *et al.* (2013) developed a system to measure dynamic displacements of structures and examined the versatility of image-based measurement system at both laboratory and field. Their system consisted of a high-speed video camera, a lens, lamps for lighting purposes and a precision target as an object to follow. The unstable position of the camera and varying illumination conditions were considered as significant reasons of reduced precision in long range recordings. Other miscellaneous equipment was used to provide a sufficient and consistent amount of light to illuminate the target. Chen *et al.* (2014) performed a series of experiments that had the main objective of executing the modal analysis and detecting the mode shapes of the specimen from video recordings. A recently-developed motion magnification technique was utilized to visually observe various modes of vibrations of the specimens under dynamic loads. Results compared with the data received from accelerometers and laser vibrometers and it was concluded that the video-based measurements were in good correlation with those measured by conventional methods.

McCarthy *et al.* (2013) stated that photogrammetric measurement methods yielded satisfactory results under static loads. They conducted a research to evaluate whether the same methods were applicable for dynamic structural tests. The study presented a method that eliminated disadvantages of low sampling rate by blurring the images. Fundamental benefit of the blurring process was to receive data in sub-pixel level, which lead to achieve higher accuracy. The test results showed that the method used in the study had a capability of achieving an accuracy of 0.25 mm in model structures.

Wu *et al.* (2014) monitored planar 2D vibrations by a vision system in their research. LED stickers were selected as targets and mounted on critical points on the model. The study also presented two different calibration schemes to deal with the errors due to the scale factor approach, which were called registration and direct linear transformation. The interesting application in the study was that the researchers used image reconstruction techniques in order to increase the accuracy. The proposed monitoring structure was achieved to measure displacements of specimens up to the frequency of 20 Hz. As for the future work, 3D experiments using spontaneous recorders would be used.

Another experimental study that selected image-based methods as the measurement technique was performed by Lu *et al.* (2014). They tested collapse phases of various types of structures involving three RC frame-and-wall model specimens; single wall and destruction glass columns model, single wall and destruction glass wall model, and cross wall and destruction glass wall model. Elements of the recording system presented in the study were two high-speed Complementary Metal-Oxide-Semiconductor (CMOS) cameras, a synchronous controller, a host computer and two illumination sources. The study contained important evidences indicating the abilities of the photogrammetric measurement systems in collapse state. The placement of the recorders allowed researchers to track displacements in 3D. Results of the experiments showed that remote measuring system is able to track displacement, velocity and acceleration values of the tested models.

Feng *et al.* (2015) introduced another video-based sensing method that measured the displacement of different structures. They used a template matching algorithm which increases the accuracy in sub-pixel level. Adjustment of the parameter called ?upsampling factor? provided better results in their experiments. They performed both laboratory and field tests to validate their measurement system. Both existing (bolts and joints) and artificial targets (special templates) used in their laboratory tests as targets. The results were satisfactory for laboratory tests. Validation of field tests was completed by frequency spectrum analysis.

Marrugo *et al.* (2015) conducted experiments to test the displacement measurement of a target consisting of a black background and two white dots. The algorithm followed in this study was based on tracking correlation of an image frame with the template images (targets). The researchers concluded that the image processing successfully performs with maximum of 5% error.

Baqarsad *et al.* (2016) conducted a quite comprehensive study that evaluated the different methods and trends in the area of measurements of dynamic structural responses via photogrammetry and optical methods. According to the authors, methods could be divided into three main categories: Point tracking, DIC and targetless methods. It was also indicated that, with continuously developing technology, the capacities of these methods increase their abilities to monitor dynamic behaviors. When computer vision is combined with the photogrammetry techniques, researchers might go beyond many limits of conventional methods.

In the experimental studies of Li *et al.* (2016) image processing methods were utilized to assess the structural responses of a 3-story RC frame from an elastic phase to plastic state and finally to collapse stage. Due to the limitations of the accelerometers and LVDTs in non-linear and collapse states, displacements of targets positioned at the joints of the frame could only be extracted from video recordings. Researchers used an image-based measurement system named "Binocular Stereo Vision" (BSV), which consisted of the records of two high resolution and high-speed cameras with the purpose of increasing the accuracy of the system.

Another interesting study which involved video-based measurement conducted by Tosun *et al.* (2017) in the area of fluid mechanics. Objective of the Researchers was tracking the free surface of a liquid and evaluating the sloshing force at the base of a tank which contained fluid. The comparison of the results of image processing method and conventional measurement method coincide fairly in low amplitude sloshing motion around the same fundamental frequencies.

Researchers in the past proposed various methods in the usage of image-based methods and developed considerably accurate measurement systems. Numerous studies presented noteworthy findings to measure various static or dynamic structural testing with these methods. The main contributions of this study would be the analysis, comparison and evaluation of various cases and methods in image-based measurements. Within the scope of this study; experiments were conducted to investigate the effects of two different image-based methods, recording characteristics in terms of resolution and sampling rate, and investigation of different structural models and cases (scaled models of SDOF and MDOF, and full scale MDOF structure). Survey of strengths and deficiencies of these methods under different conditions could provide valuable contributions to the literature. Additionally, many of the experimental video records utilized in this study were recorded by commercial cameras and mobile phones. This study presents the measurement capabilities of these inexpensive and commonly available devices.

1.4. Research Rational

Even if the current mechanical measurement devices (strain gages, LVDTs, LPTs, accelerometers, lasermeters, etc...) could be very sensitive as their costs increase, they are exposed to many adverse effects that could reduce their capabilities over time. They need careful and regular maintenance, as well as demand frequent calibration. In addition, these devices require high frequency data acquisition systems, expensive cabling network and other special equipment to receive and transmit measurement signals. They are also very expensive as their data capturing rate gets higher. To receive the measurement data from these devices, researchers need to perform tedious works such as installation of cables and control the environmental conditions to filter the distorted data. Image-based techniques, on the other hand, require nothing more than placing the recorder and target(s). Since the signal from the recorder is within the video itself, there is no need for complex and variety of equipment such as data logger and cables networking. Developing an image-based system as a measurement tool could tremendously reduce costs and time spent in the evaluation of data.

Another reason to prefer image-based techniques is the large range of measurement capability. It is not easy to use LVDT and LPT when the dynamic displacements are quite large due to their limited strokes. Strain gauges also have specific limits which could easily be gone beyond their range in an ordinary dynamic experiment. However, the measurement range of a video recorder is not only limited, but also changes with the relative position of the recorder with respect to the specimen. In a typical seismic experiment with large displacements, researcher could compensate the range of motion with some reduction in real displacement/pixel ratio.

In a crowded and large environment such as structural laboratory, some of the image processing techniques such as DIC and edge detection based methods could not be used. There are many changes and distortions on the background which could disturb significantly the signal retrieved. Therefore, there is a need for development of a method and an algorithm which could meet the needs of the crowded and unstable environmental conditions exist in typical structural laboratories.

1.5. Objective and Scope of the Study

The first and fundamental objective of this study is to propose a method which could extract the dynamic responses of Single degree of freedom (SDOF) and multi degree of freedom (MDOF) test specimens. Responses of each story are measured by both accelerometer and different image-based methods. Detection of modal frequencies of MDOF specimens is also among the objectives of this study.

In order to achieve these goals, an algorithm based on statistical approach using the contrast between the target and non-target points was developed. It was one of the fundamental methods followed in previous studies and intended for most suitable framework under an uncontrolled environment in terms of light. The algorithm which was based upon this framework also contained different filters that could drastically reduce the distortion. This method was based on using the LED light sources as a target. However, brightness of the sunlight and the reflection of it on different surfaces had the same effect as the targets. Thus, another objective was to make sure that the proposed method considered the effect of different light sources and recognize the different between target and other false positives.

An algorithm, developed by Kanade-Lucas-Tomasi (KLT) to capture motion was also utilized in this study. Performance of this method for extracting displacements of structures under dynamic excitation was evaluated. Success of the KLT algorithm in different stages and applicability of it were investigated.

The structural responses aimed to be extracted were mainly relative and absolute displacements, velocity and acceleration of the discrete model. In case of MDOF model, responses of each story level were evaluated. The relative response data also revealed the natural frequency of the structure, which plays a critical role in the earthquake resistant design.

Measuring strains from video records and evaluating the performance of this experiment were also within the interest of this study. It was not quite easy for image processing methods to take place of this well-developed, yet tedious mechanical measurement device in shake table experiments. Yet, this study presented a validation of this goal within a reasonable success.

An important aspect of this study was the verification of the proposed method and evaluation of the performance by comparison with conventional measurement devices. Different responses obtained from video records were compared with different devices and the capabilities some image processing techniques were evaluated.

Another evaluation within the scope of this research was the effect of various recording criteria such as sampling rate and resolution. The response data from experiments recorded by different devices with different recording characteristics were studied and evaluated.

1.6. Organization of the Thesis

This thesis consists of six chapters. First chapter includes general information about the image-based methods, different categories they divided into, literature review, and motivation and scope of the thesis. Second chapter describes two different image-based algorithms that were utilized, their methodology and applications. Third chapter presents the mathematical methodologies and computer software developed for this study. Fourth chapter briefly explains the experimental setup and procedures, and the fifth chapter presents results of shake table experiments. Finally, sixth chapter contains conclusions out of this research and suggestions for future studies.

2. ALGORITHMS AND METHODS UTILIZED TO EXTRACT DISPLACEMENT

2.1. Statistical Threshold Method

2.1.1. Algorithm

The algorithm proposed below requires a target which creates a high contrast from the area around itself. This high contrast value leads to better threshold values, less false positives and more accurate results. In the experiments included in this study, as it provided the maximum light intensity among all possibilities, LED targets were used to tag center of mass and base of column. Light intensity difference between LED target and an ordinary marker could be observed as seen in Figure 2.1 and Figure 2.2.

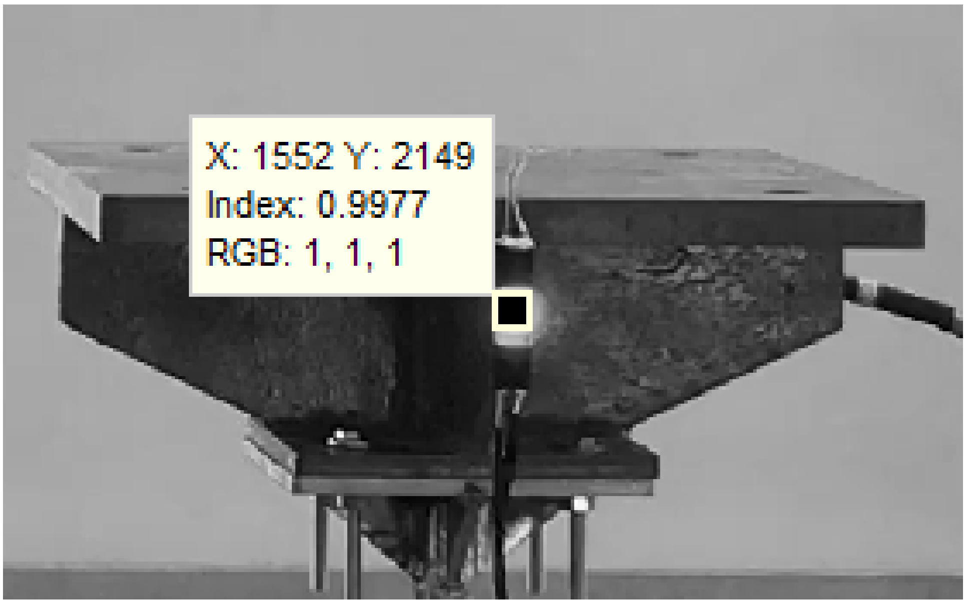

Figure 2.1. LED Color Intensity Values.

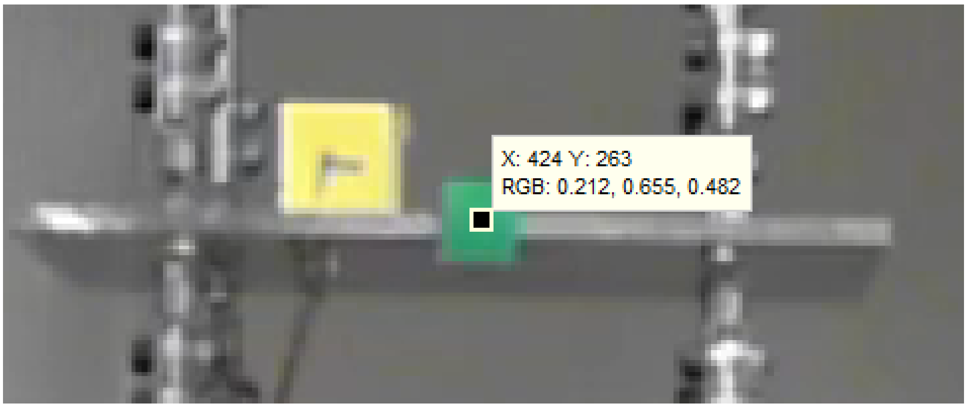

Figure 2.2. Ordinary Marker Color Intensity Values.

The algorithm is based on statistical approach. Grey values of LED markers are either quite close or equal to maximum value of the greyscale. A threshold value close to maximum would extract the pixels of light source and exclude the other (McAndrew, 2004). After this simple thresholding, indices of remaining pixels in the binary matrix yield the centroid of the light source, thus, the lumped mass and/or base.

Limiting the area of interest with probable pixels, which target possibly exist during the excitation period, reduces the process time. In this algorithm possible range of vertical and horizontal motion are also required. Equation 2.1 to Equation 2.4 describes the algorithm of this method.

$$G_v\left(i_v, j_v, n\right) = G\left(i, j, n\right) => G\left(i, j, n\right) > TH \tag{2.1}$$

$$\mathrm{y}_p\left(\mathrm{n}\right) = \overline{i_v}, \mathrm{x}_p\left(\mathrm{n}\right) = \overline{j_v} \tag{2.2}$$

$$\overrightarrow{x_d} = \overrightarrow{x_p} - x_p\left(1\right) \tag{2.3}$$

$$\overrightarrow{y_d} = \overrightarrow{y_p} - y_p\left(1\right) \tag{2.4}$$

where, TH refers to threshold value and G refers to any pixel grayscale value that depends on the variables i (row index), j (column index) and n (number of frame); G_v refers to the valid pixels of grayscale value, which is above the threshold value, and i_v and j_v are representing the row and column indexes of these pixels; y_p and x_p are the averages of these indices in a particular frame, and vectors x_d and y_d are the differences of these vectors from the initial values ($x_p(1)$ and $y_p(1)$).

This process was applied for each lumped-mass in addition to the base of the column. After tracking each of them separately, relative motion was obtained by subtracting them.

2.1.2. Solution Against Sunlight Distortion

An important problem in structural laboratories is the unstable background conditions and frequent interferences in a crowded area. During the study, sunlight or other illuminations constantly distorted the records causing false positives in binary matrices that were mentioned above. In order to overcome this problem, a control mechanism was added to the algorithm. Distortion of the sunlight and how this distortion created false positives are presented in Figure 2.3 to Figure 2.5, which show the detection of correct centroid in case of sun light distortion.

Figure 2.3. Gray Scale Range of Interest.

Figure 2.4. Binary Matrix of Range of Interest Distorted by Sunlight.

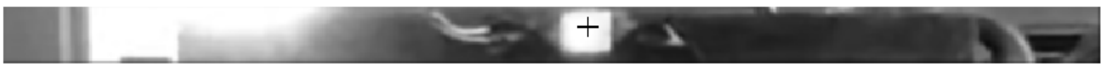

Figure 2.5. Detected Centroid in Case of Distortion.

As the frame recognized by program, both column and row indices of all valid points, which had higher gray values than the threshold, were re-arranged in an ascending order. Then, differentiation with respect to the row or column index was obtained. A differentiation value greater than 1.0 implied the discontinuity among valid points. In the region of interest, there was one continuous target, which indicated the position of the lumped mass. When the index coordinate vector was separated from the points of discontinuity, several groups of continuous points were obtained, and one of them became the real target. Equation 2.5 to Equation 2.7 briefly present the algorithm of this prevention method.

$$x_{cr}\left(m\right) = x\left(n\right) => x\left(n\right) - x\left(n-1\right) > 1.0 \tag{2.5}$$

$$x_{pr}\left(m\right) = \bar{x} => x_{cr}\left(m\right) < x < x_{cr}\left(m+1\right) \tag{2.6}$$

$$\min\left(\left|x_{pr} - x_{p}\left(t-1\right)\right|\right) = x_{p}\left(t\right) \tag{2.7}$$

where, x_{cr} is the pixels representing boundaries of discrete pixel groups above threshold value, x is the vector that indicates horizontal positions of all pixels above threshold and n is the index of this vector; x_{pr} represents the centroid of each discrete pixel groups; x_p is the centroid of the above threshold values and t refers to index of the consecutive frames.

Mean values of these discrete groups were subtracted from the position recorded in the previous frame, or the initially located position, if the process was on the first frame. The group which had the absolute minimum of these subtracted values was selected and considered as a real target.

After position vectors were obtained, derivatives of these vectors were then taken with respect to time. Frame rate data was received from the recorded video and Savitzky-Golay (1964) derivation process was applied. Scaling with a known distance provided the transformation of unit from pixel to millimeter unit.

A natural frequency of a structure could also be found from a free vibration displacement response. After the ground excitation, the specimen experiences free vibration and the data within this interval provides the natural frequency of the system. Fast Fourier Transformation (FFT) mathematical method is used for this purpose. The damping ratio of the system could then be found from this free vibration displacement data using logarithmic decrement method. This damping ratio is regarded as the characteristic of the system after the excitation.

These characteristics are the requirements to calculate the mass-normalized energy terms of the motion. In other words, input energy which occurs due to the motion, and kinetic, damping and strain energies that are produced due to this motion. Therefore, all energy terms could be calculated using these characteristics (natural frequency and damping) and the responses (displacement, velocity and acceleration) of system.

2.2. Kanade Lucas Tomasi (KLT) Optical Flow Tracker

2.2.1. Theory

Computer vision techniques are fairly powerful tools when it comes to tracking an object in a particular video recording. One of these techniques was developed by Kanade, Lukas and Tomasi in 1994 and it is called Kanade Lukas Tomasi (KLT) optical tracker. It is an efficient technique in estimating the position of a moving pixel within frames. It utilizes the relation between consecutive frames. When a pixel on a frame is considered, it would have the same intensity in the next frame. This assumption is also valid for the intensity function over an area. The intensity function would remain same, but a shift in the function is occurred. In ideal conditions, the difference between these shifted functions of two consecutive frame must be equal to zero. However due to the noise and other distortive effects some amount of error exists in this equality

(Birchfield, (1997)). The error could be defined as shown in Equation 2.8.

$$\in = \iint_{\mathrm{W}} \left[\mathrm{J}\left(\mathrm{x} + \frac{\mathrm{d}}{2}\right) - \mathrm{I}\left(\mathrm{x} - \frac{\mathrm{d}}{2}\right) \right]^2 \mathrm{w}\left(\mathrm{x}\right) \mathrm{dx} \tag{2.8}$$

where x and d could be defined as $x = [x, y]^T$, x and y are original positions in horizontal and vertical direction; $d = [dx, dy]^T$ and dx and dy are the changes in horizontal and vertical direction and w(x) is a weight function which generally considered equal to 1.0.

Equality of intensity values of two consecutive frames is shown in Equation 2.9 as:

$$I_1\left(x_1, y_1\right) = I_2\left(x_1 + u, y_1 + v\right) \tag{2.9}$$

where u is defined as the horizontal shift and v is the vertical shifts. Taylor expansion of I_2 on $x_1 + u$ is equal as shown in Equation 2.10:

$$\begin{aligned} & I_2\left(x_1 + u, y_1 + v\right) = I_2\left(x_1, y_1\right) + u\tfrac{\partial I_2}{\partial x}\left(x_1, y_1\right) \\ & + v\tfrac{\partial I_2}{\partial y}\left(x_1, y_1\right) \end{aligned} \tag{2.10}$$

That yields an expression with two unknowns, as shown in Equation 2.11:

$$I_{diff} = I_1 - I_2 = u\frac{\partial I_2}{\partial x}\left(x_1, y_1\right) + v\frac{\partial I_2}{\partial y}\left(x_1, y_1\right) \tag{2.11}$$

when this expression is defined over an area it yields the linear system in 2.12:

$$\begin{bmatrix} u \\ v \end{bmatrix} = \begin{bmatrix} \frac{\partial I_2}{\partial x}^2 & \frac{\partial I_2}{\partial y}\frac{\partial I_2}{\partial x} \\ \frac{\partial I_2}{\partial y}\frac{\partial I_2}{\partial x} & \frac{\partial I_2}{\partial y}^2 \end{bmatrix}^{-1} \begin{bmatrix} I_{diff}\frac{\partial I_2}{\partial x} \\ I_{diff}\frac{\partial I_2}{\partial y} \end{bmatrix} \tag{2.12}$$

when this linear equation is solved displacements u and v can be determined. The matrix in this linear equation is called gradient matrix (Birchfield, (1997)).

2.2.2. Detected Features

In order a matrix to be invertible its determinant should not be zero. Practically, as the determinant reaches a value higher than zero, the results obtained by KLT algorithm becomes more reliable. Determinants closer to zero produces meaningless matrices. One of the greatest advantages of the KLT Tracker algorithm is that it presents its own feature detection method which complies with itself.

The gradient matrix has the dimensions of 2 by 2 and its determinant depends on two eigenvalues. Larger eigenvalues present greater opportunity to track features. Physically, it corresponds to two different strong gradients on image in different directions. If there is only one gradient, it means that the presented feature is part of an edge. This concept is called "barber pole illusion" due to the fact that it has only one detected strong gradient feature like a barber pole. Only the direction orthogonal to the edge could be clearly selected. This notion was named as "Aperture Problem" as explained in Figure 2.6.

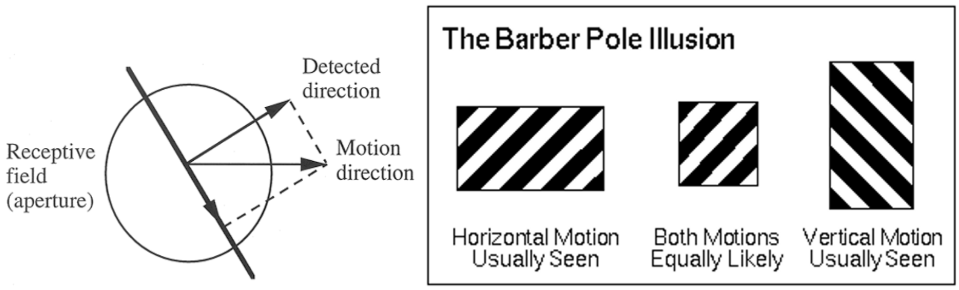

Figure 2.6. Aperture Problem and Barber Pole Illusion.

Two strong gradients correspond to a corner. In 1994, Shi and Tomasi presented a method to find most convenient features to use in KLT Tracking algorithm. The method is basically selecting a threshold value (which might be an eigenvalue of a plain area in the frame) and finding a window which has a matrix with larger minimum eigenvalue than this threshold. This guarantees the "texturedness" of the window and provides an ability to be tracked in any direction.

2.2.3. Pyramids of Image

Regular KLT algorithm cannot deal with large displacements. The reason is the linear Taylor expansion considered in the algorithm. This linear approximation is only true when the displacements are small. As a solution to this problem, recreating the same image with lower resolutions was proposed by Tomasi and Kanade in 1991. As the original image recreated with lower resolutions, pixel displacements in those images get smaller. Calculating the displacement in those different levels and minimizing the error between them provides a solution with much less error. Since the initial resolution is highest and it gets lower towards the end, the system combines all these images are called Image Pyramids. Visual representation of these pyramids is seen in Figure 2.7.

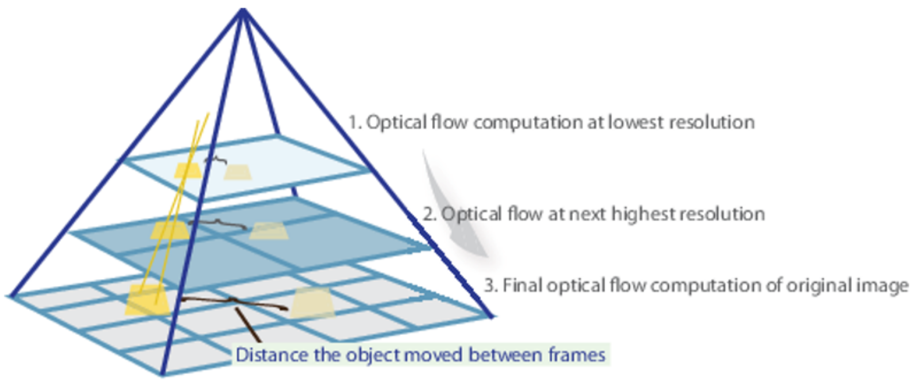

Figure 2.7. Aperture Problem and Barber Pole.

2.2.4. Iterations

It is convenient to perform iterations to obtain more accurate displacement vectors. Since the gradient matrix does not change, computational effort of these iterations are just calculating the difference matrices between the target window and the window considered in the specific iteration.

2.2.5. Bi-directional Error

As a control mechanism one could perform a bi-directional error analysis (Kalal *et al.*, 2010). It corresponds to calculating the error between a forward and backward step. After the tracking occurs from previous to current frame, they are tracked again from current to previous frame. If the difference between the original position of a pixel and calculated one is above a certain threshold, this specific pixel is considered an error and it should be eliminated.

In this study KLT Tacker code was used with the inputs of 4 pyramids, 5 iterations and infinite bi-directional error and block size of 31x31 matrix.

2.3. Evaluation and Comparison of KLT and Statistical Threshold Method

When it comes to motion tracking, two algorithms have different advantages and disadvantages over each other. When necessary conditions exist, accuracy of the KLT Tracker algorithm is better the Statistical Threshold algorithm. However, these conditions might not present always, especially in a structural laboratory with varying environmental conditions. Provisions of a stable and textureless background, which make structure visible and distinctive, might not be possible, especially for relatively large and high structures.

3. NUMERICAL ANALYSIS AND USER INTERFACES

3.1. Time History Analysis

Experiments were conducted with calibrated testing equipment and their resulting experimental data showing the real responses of structures. Also, a simple numerical study was conducted to evaluate the responses and compared with experimental results. A software evaluating Time History analysis using Newmark-β method (Newmark, 1959) for SDOF systems was developed in MATLAB programming language. Elastic-Perfectly Plastic (EPP) material model was considered in this software.

One of the comparison methods considered in this study was to compare with the relative displacement indirectly obtained by the strain gauge data. The method that used by Güllü *et al.* (2018) was based on the relation between the strain distribution and moment at the base. This method is only valid for elastic cases. In the following Equation 3.1 to Equation 3.5 describe the methodology. Figure 3.1 symbolizes a SDOF system and explains the variables used in the derivation of formulas for relative displacement from strain gauge readings, and Figure 3.2 presents the flowchart of this derivation.

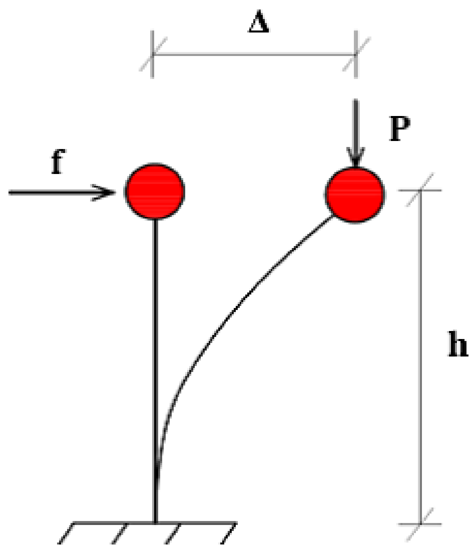

Figure 3.1. Representation of SDOF system.

Relation between strain and displacement could be explained as following:

$$M_b = P.\Delta + k.\Delta.\mathrm{h} \tag{3.1}$$

$$M_b = \int \sigma.e.dA \tag{3.2}$$

$$\sigma = E.\epsilon \tag{3.3}$$

where M_b is the moment created on the base, P is the weight exerted by the mass, h is the height of this mass, σ is the stress on infinitely small areas on cross-section of the specimen, and e is the fiber distance from the neutral axis; E is the modulus of elasticity and ϵ is the strain.

Following Equation 3.4 and Equation 3.5 describes the derivation for displacement.

$$k = \left(\frac{3EI}{h^3}\right) \tag{3.4}$$

$$\Delta = \frac{M_b}{P + \left(3E\frac{I}{h^2}\right)} \tag{3.5}$$

where k is the stiffness of the system, I is the moment of inertia of the cross section and Δ is the relative displacement of the mass.

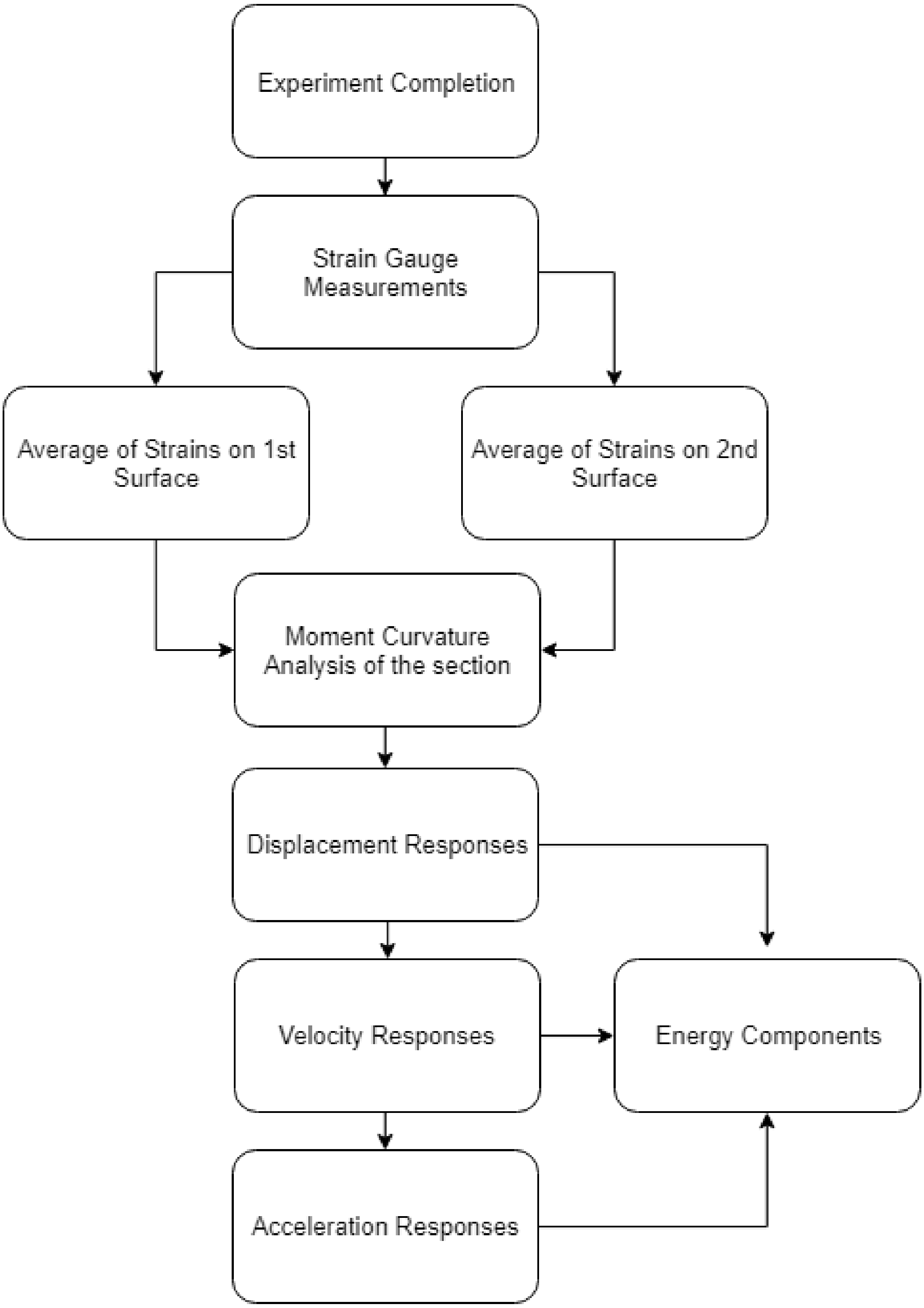

Figure 3.2. Flowchart of the Displacement Algorithm.

3.2. Energy Terms

As part of the numerical analysis, final step of the algorithm was the calculation of terms of relative energy equation. These terms are introduced by Bertero and Uang (1990). The energy equation is determined by multiplying each term of the equation of motion by its instantaneous displacement and then integrating it. The resulting input energy contains parts of other energies such as kinetic, damping and strain energies, and considers both ground motion and relative motion (Equation 3.6 to Equation 3.9). This energy term, gives a good base to compare different data and asses the success of the method. The Input energy term, which is an integration of the product of relative velocity and ground acceleration, contains both relative and ground motion. Comparison of input energy values, achieved by different methods, reveals the combined difference between compared measurement data. Input energy represents the energy exerted by ground motion on the fixed base system.

$$m\ddot{u}\left(t\right) + c\dot{u}\left(t\right) + f_s = -m\ddot{u}_g\left(t\right) \tag{3.6}$$

$$\int m\ddot{u}\left(t\right) du + \int c\dot{u}\left(t\right) du + \int f_s du = -\int m\ddot{u}_g\left(t\right) du \tag{3.7}$$

$$\int m\ddot{u} du + \int c\dot{u}\left(t\right) du + \int f_s du = -\int m\ddot{u}_g\left(t\right) du \tag{3.8}$$

$$E_k + E_d + E_s = E_I \tag{3.9}$$

where m is the mass; $\ddot{u}(t), \dot{u}(t)$ and $\ddot{u}_g(t)$ are, the relative acceleration, relative velocity and ground acceleration, respectively, and f_s is the spring force exerted on the system. The energy terms of E_k, E_d, E_s and E_I are the kinetic, damping, strain and input energies, respectively. Actually, hysteretic and damping are combined if the structural specimen experience inelastic behavior. The strain and kinetic energy terms diminish at the end of the motion. Only hysteretic and damping energies remain, and they are related to level of damage of the system. This is also called plastic energy.

3.3. User Interfaces

3.3.1. Motivation to Development of User Interfaces

Various experiments were conducted, and different measurement devices were used to collect data. To compare these data for each response, noise filtering was done and most appropriate data to be used in the calculation of responses were selected. Five different user interfaces were generated in MATLAB user interface creation program called "Guide".

3.3.2. Acceleration to Responses Interface

Accelerometer was one of the measurement devices used during the experiments. Different accelerometers were placed on each mass center symbolizing the degree of freedom. Acceleration data reflected the absolute acceleration of each free mass and the ground acceleration.

Interface serves the purpose of obtaining responses of velocity and displacement terms using acceleration input. Acceleration data obtained from accelerometers, as well as time data are selected from the relevant document by the Import command. After clicking the "push" button, two integrations are performed. First is the absolute velocity and second is the absolute displacement. User than saves these new data in the workspace to be used at a later time. Figure 3.3 is a screenshot taken from this interface.

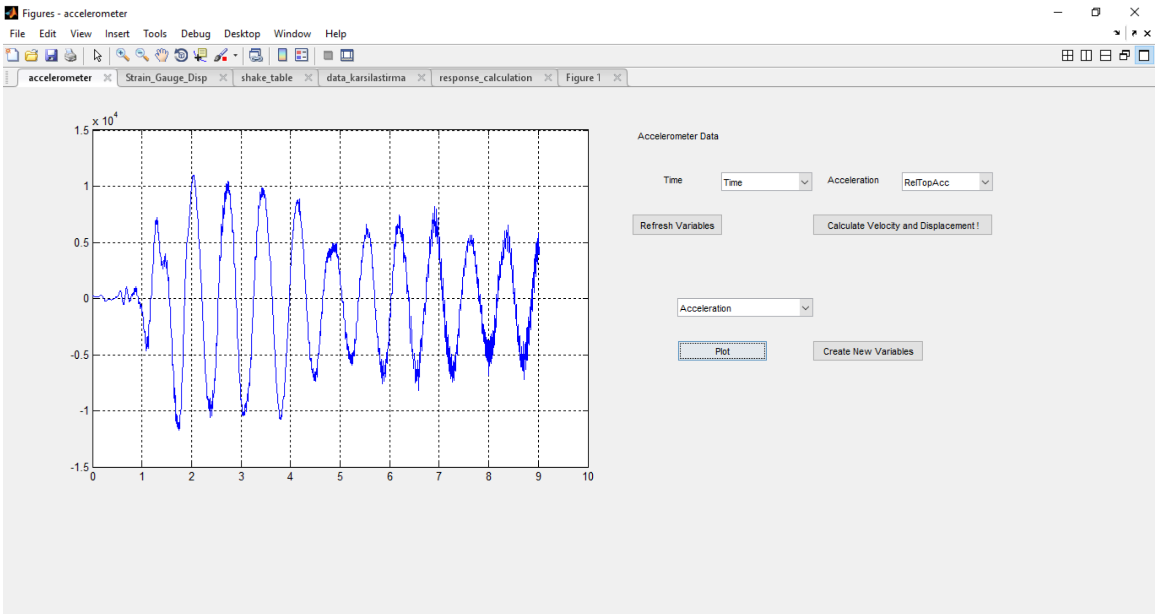

Figure 3.3. Acceleration to Responses Interface.

3.3.3. Strain to Responses Interface

As mentioned above, mathematical relation between strain and relative displacement was used to determine relative response between ground and other masses. The methodology of obtaining relative displacement from this value was explained in Chapter 3.1. The methodology used in this algorithm is only valid for SDOF systems. The task of this interface was to calculate the relative displacement and other derivatives such as relative velocity and acceleration responses. However, to perform this operation, user should provide inputs of the terms exist in Equation 3.1 to Equation 3.5.

These inputs are corner coordinates of the cross section, amount of the mass on the top, modulus of elasticity, effective height of the specimen, the strain gauge data and time vector. Strain gauge data requires the strain input of both surfaces of column cross section. Figure 3.4 shows a screenshot taken from this interface.

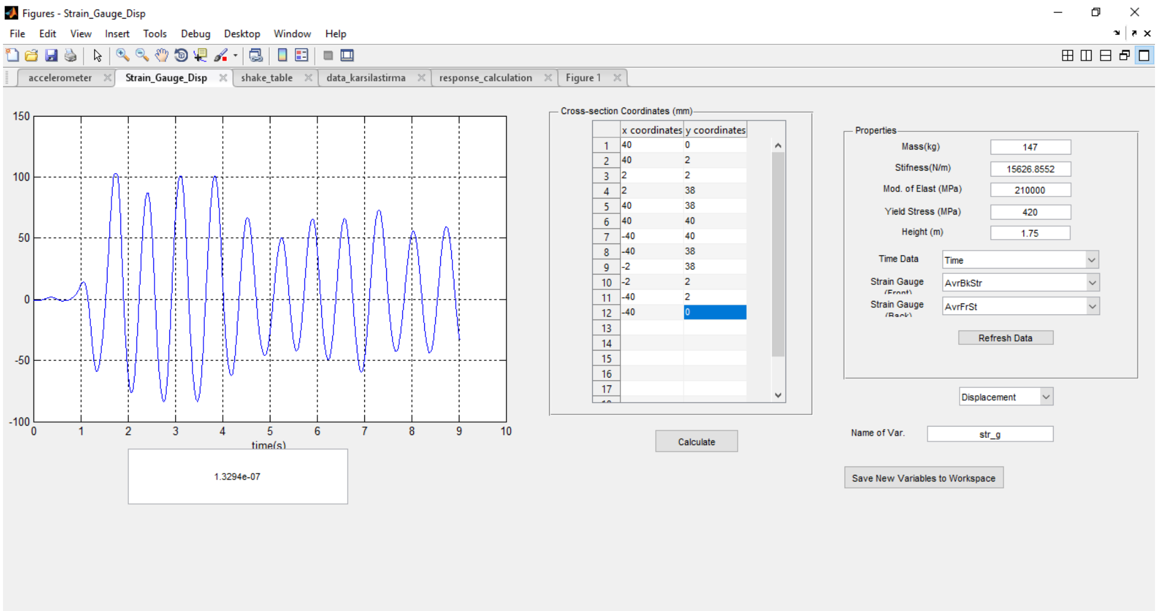

Figure 3.4. Strain to Responses Interface.

3.3.4. Image-Based Response Calculation Interface

This interface contains the software of Statistical Threshold algorithm to perform tracing of specified points. Five different types of input required for the analysis to take place and these types are considered as different steps in the interface. These five steps are: Video, Indices of Targets on matrix of first frame, Margin of Motion, Scaling and Characteristics of the structure.

Video input requires the beginning and the end of the experiment record in the video. Initial or the final part of the video may contain some scenes unrelated to the experiment. To eliminate these scenes user should provide the first and last timing of the video. Then, user could select the video record from the related file.

In the second step user must enter the x and y coordinates of the centroids of both targets. First target represents the target on the mass while the second is related to the ground. This order is required for the next steps in the calculation process. Third step has the purpose of narrowing down the range of interest. Predicted limits of the motion is required from user in the unit of millimeter. Then, this unit turns into pixel by dividing it with a scale factor. The advantage of this step provides elimination of any unnecessary areas on the video frame and shortens the computation time significantly.

Fourth step is the scaling step, which provides the conversion of pixel distances to real distances. Vertical and horizontal coordinates of two points and the distance between them are required for this step.

Fifth step is the entering dynamic characteristics of the specimen, which affects the dynamic motion of the lumped mass. These characteristics are the mass, damping ratio and natural period of the system. These are required for the energy calculation process which takes place after the extraction of displacements.

After completing these entries, user clicks the push button of “Start Processing” and a function that contains the Statistical Threshold algorithm starts to process the video. Once this processing is over, user may switch graphs and saves the variables of response in a MATLAB workspace or an Excel spreadsheet created by the program. Additionally, user could select the free vibration data by the help of “brush tool” and calculate the period of the motion using Fast Fourier Transform, FFT and the damping ratio using Logarithmic Decrement. Figure 3.5 is a screenshot taken from this interface.

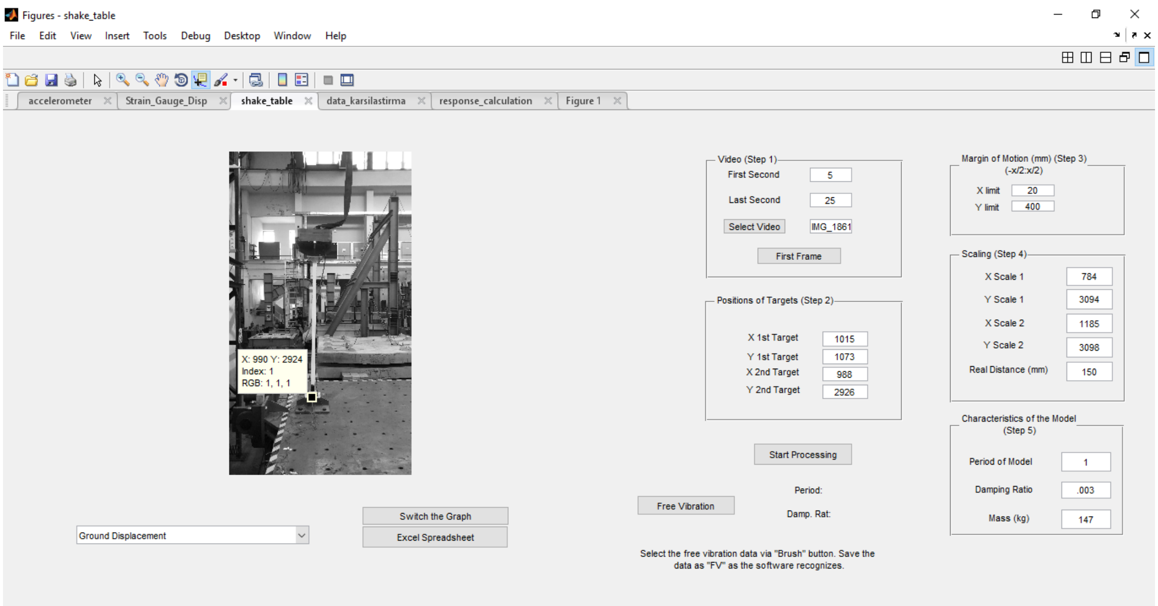

Figure 3.5. Image Based Response Calculation Interface.

3.3.5. Data Comparison Interface

This interface is one of the most crucial among all interfaces. It identifies overlapping different data and eliminating the phase difference. Other than that, data obtained from both conventional and image-based sensors in various cases need to be filtered. User compares 3 different data sets and these data should also contain time variables. These comparisons could be made in both time domain and frequency domain. High pass or low pass filter may also be applied to a selected data. Comparing data with different sampling rate is not an easy task when the process is delicate. Resampling the existing data may help this situation and minimize the phase shift between two sets of data. Last function of the interface is resampling the data and increasing the accuracy of phase shift minimization process. Figure 3.6 is a screenshot taken from this interface.

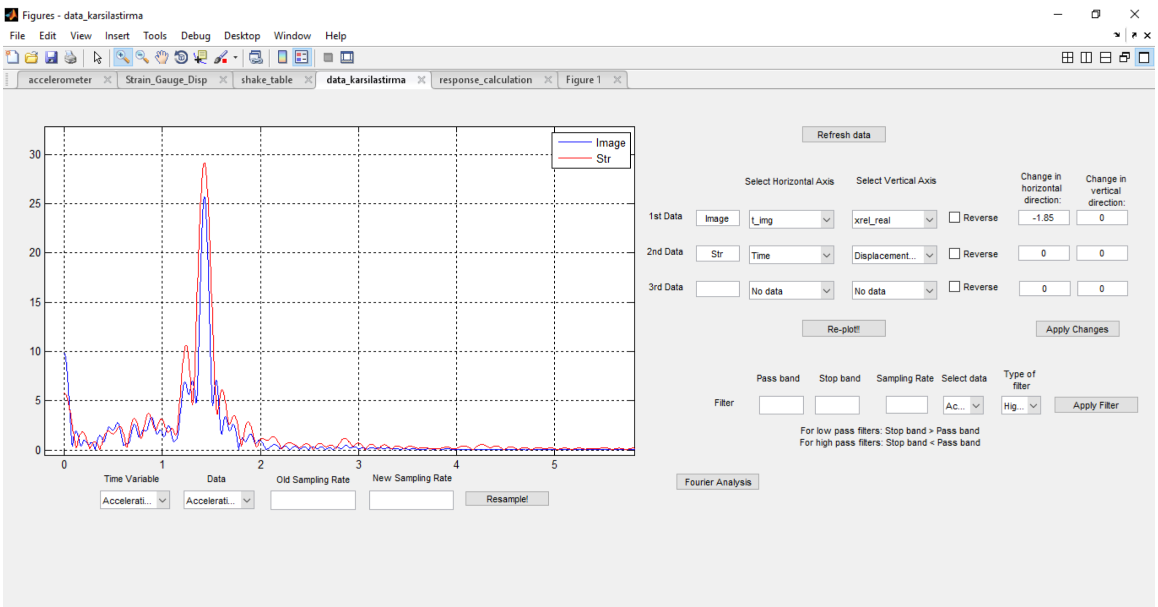

Figure 3.6. Data Comparison Interface.

3.3.6. Final Response Selection

The variables obtained from other programs could be used finally to determine the energy responses. Time data selected by the user determines the sampling rate of the rest of the data. All terms required for energy balance equation are selected by the user. Damping ratio is considered constant and required from the user. Figure 3.7 is a screenshot taken from this interface.

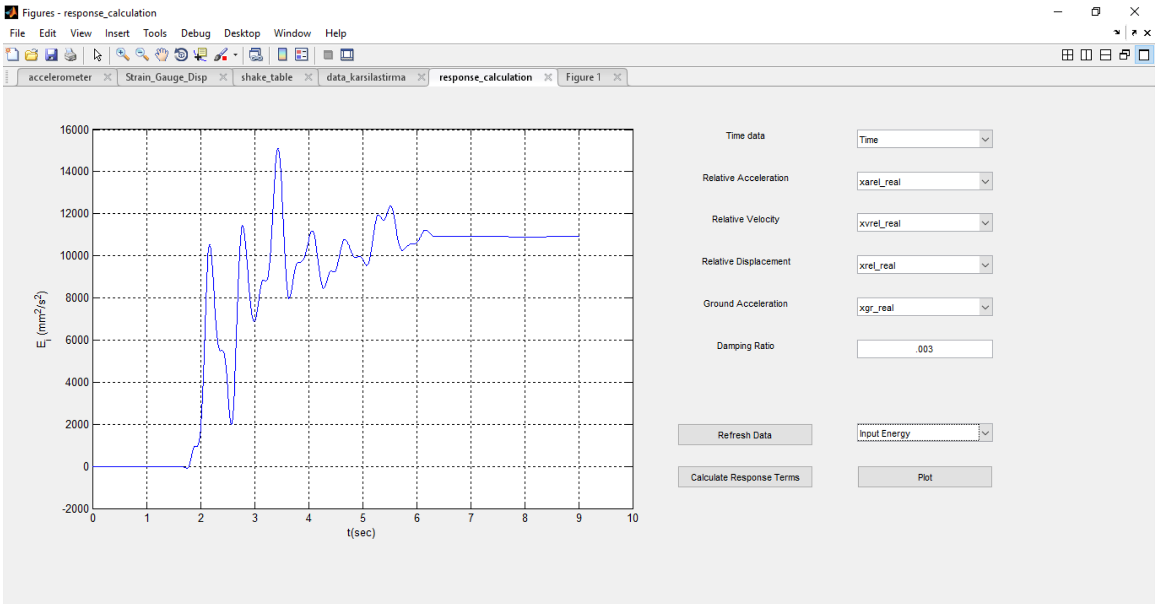

Figure 3.7. Final Response Selection.

4. EXPERIMENTAL SETUP AND PROCEDURE

4.1. Experimental Setup and Equipment

The main objective of this study was to measure displacements of specimens fixed on a shake table under simulated dynamic earthquake motion through image-based algorithms.

Therefore, the setup was designed to avoid accidental out of plane motions, to simulate idealized structural model by providing correct boundary conditions and select right locations of instrumentations. Characteristics of each experiment are given in the Table 4.1.

SDOF and MDOF systems were exposed to different real earthquake records on the ARI-1 shake table of STEELab at Istanbul Technical University. Important features and limitations of this shake table are given as following:

- Capacity of Displacement = 32.5 cm (from the rest)
- Capacity of Velocity =100 cm/sec.
- Capacity of Acceleration= 2g.

Table 4.1. Characteristics of Experiments.

	Trial	**SDOF Elastic**	**SDOF (1080p vs 4K)**	**SDOF Plastic**	**MDOF Elastic**	**MDOF Plastic**	**Strain**	**MDOF Full-Scale**
Ground Motion	Sinusoidal	San Salvador /Erzincan/ Loma Prieta	Chi Chi	San Salvador	San Salvador-HAD-165	San Salvador	None (Free Vibration)	Northridge earthquake
Scale Factor	-	0.2	0.2	0.75 / 1	0.2 / 0.1	0.75 / 1 / 1.5	-	1
Degree of Freedom	- (Ground Motion is measured)	1	1	1	3	3	1	7
Compared Data	Shake Table Input	Strain Gauges	Strain Gauges	Accelerometers and Strain Gauge	Accelerometers/ LVDT	Accelerometers	Strain Gauge	Accelerometers
Tracking Method	KLT and Statistical Threshold	Statistical Threshold	Statistical Threshold	Statistical Threshold	KLT	KLT	KLT	KLT

4.1.1. SDOF Experimental Setup

Specimens had varied characteristics such as mass, material, height and cross section. The specimens were produced with height of 750 mm. Cross-sectional dimensions of the specimens had 20 mm x 40 mm x 1 mm. The additional masses were tuned in order to obtain varying natural frequencies of 1.0, 1.5 and 2.0 Hz. Typical shake table setup with a SDOF specimen having LED targets attached is shown in Figure 4.1, and connection plates of columns to base and the mass with strain gauges mounted are shown in Figure 4.2. These test samples were tested as part of the master thesis of Seyhan Okuyan (2017) and doctoral thesis of Güllü (Thesis under preparation).

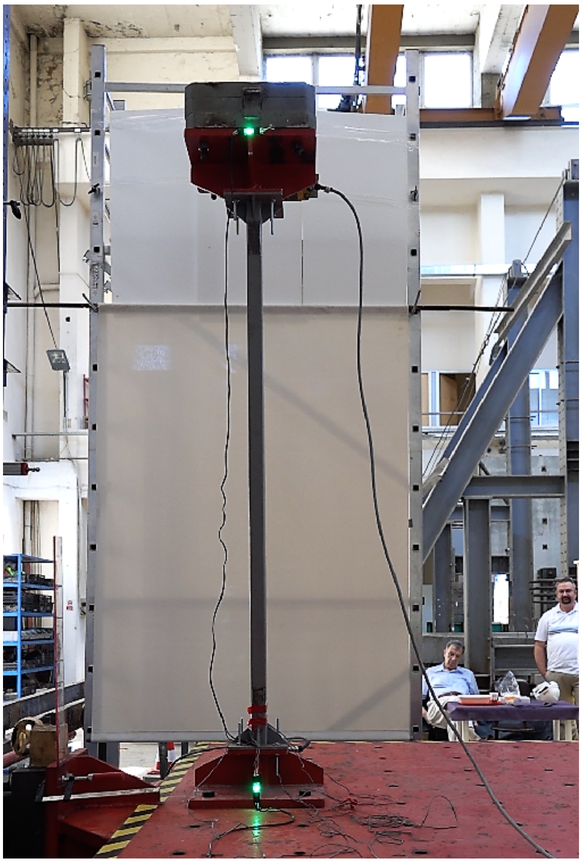

Figure 4.1. Experimental SDOF specimen instrumented with LEDs and strain gauges.

Figure 4.2. Connections of Specimens.

4.1.2. MDOF Experimental Setup

MDOF Systems with 3 degrees of freedom, namely, 3 story displacements are examined. Masses of 920 kg were attached at each story level. The conventional accelerometer measurement devices were compared with the image-based methods in these experiments. Derivatives of each displacement were calculated to obtain responses of each degrees of freedom. Excitation applied to the shake table was the San Salvador acceleration ground motion with scale factors of 0.1 and 0.2 in plastic experiments, and 0.75 and 1.0 in plastic experiments. Figure 4.3 shows the MDOF test specimen and Figure 4.4 indicates the target features detected by KLT algorithm. These test specimens were tested as part of the doctoral thesis of Güllü (Thesis under preparation).

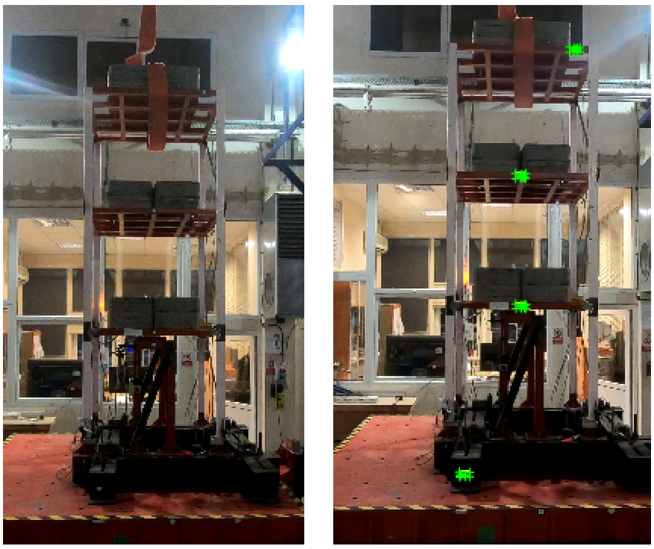

Figure 4.3. Experimental MDOF Specimen.

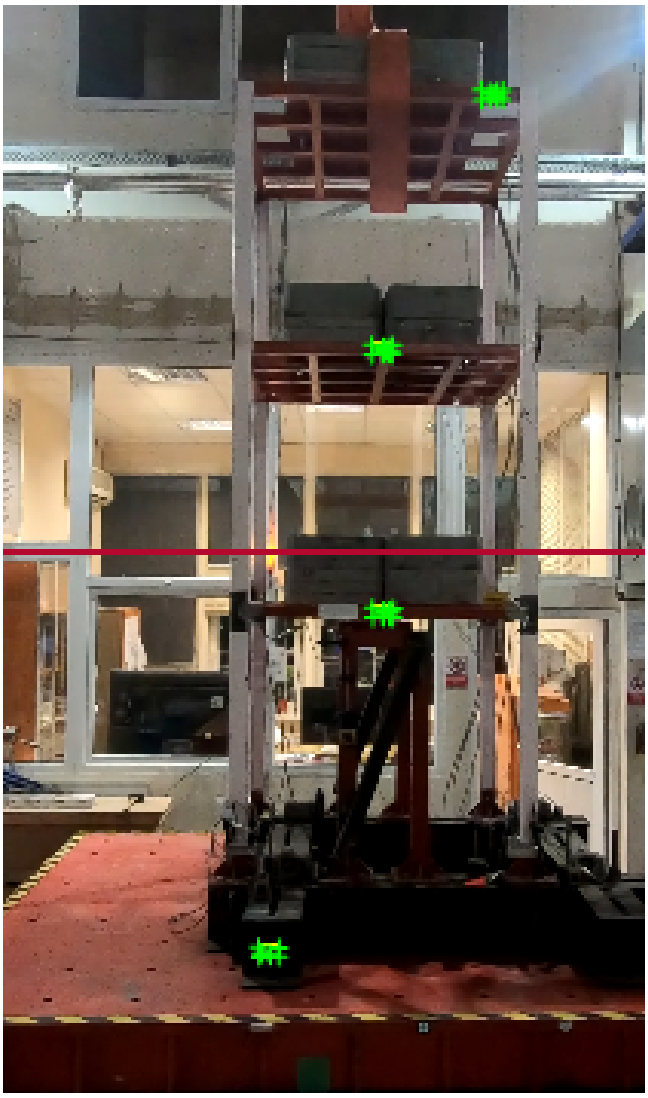

Figure 4.4. Detected features at targets mounted on MDOF Specimen.

4.1.3. Experimental Setup of the Strain Measurements

As mentioned before, one of the objectives of this study was to investigate the measurement of strains on each face of the column cross section. Four markers with 5 mm radius were placed on the base of the column specimen in order to conduct these measurements. Horizontal displacements of these markers were determined with KLT Tracking method. Two markers on the left were utilized to measure strains on the one surface and two markers on the right to the other surface, as shown in in Figure 4.5. Strain gauges were instrumented on both of these surfaces as conventional measurement devices.

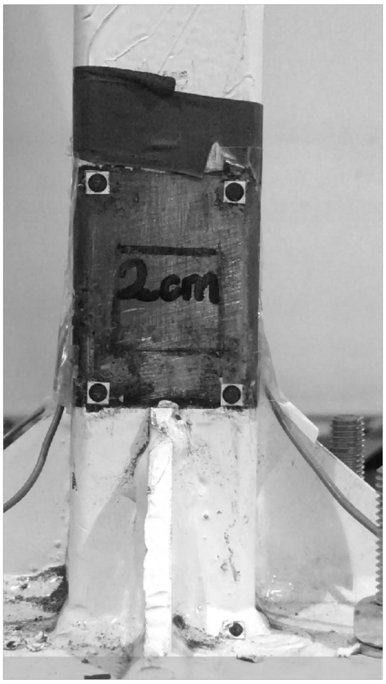

Figure 4.5. Screenshot from strain measurements.

4.1.4. Full Scale MDOF (UCSD) Experimental Setup

The full-scale measurement tests that were conducted at the University of California San Diego in 2007 were also taken into consideration. These experiments were conducted on Large High Performance Outdoor Shake Table. All video records of tests and accelerometer data at each floor level are available in public domain. The specimen had 7 floors. The height and floor dimensions were 2.54m and 4.29m x 8.13m, respectively. This 7-storey full-scale building model was subjected to a seismic ground motion of Northridge EQ (1994). The video recordings were analyzed using KLT method. Natural targets such as edges or connections were used to identify and track each story. Figure 4.6 shows the test building and Figure 4.7 shows the dimensions of the test structure. Important features and limitations of the shake table are given as following:

- Size: 7.6 m x 12.2 m
- Peak acceleration bare table: 400 ton payload 4.2g / 1.2g
- Peak velocity: 1.8 m/s
- Stroke: ±0.75 m
- Maximum gravity (vertical) payload: 20 MN
- Force capacity of actuators: 6.8 MN
- Maximum overturning moment (bare table,400 tons specimen): 35 MN-m, 50 MN-m
- Frequency bandwidth: 0 - 33 Hz

Figure 4.6. View of the Full-Scale Specimen from side.

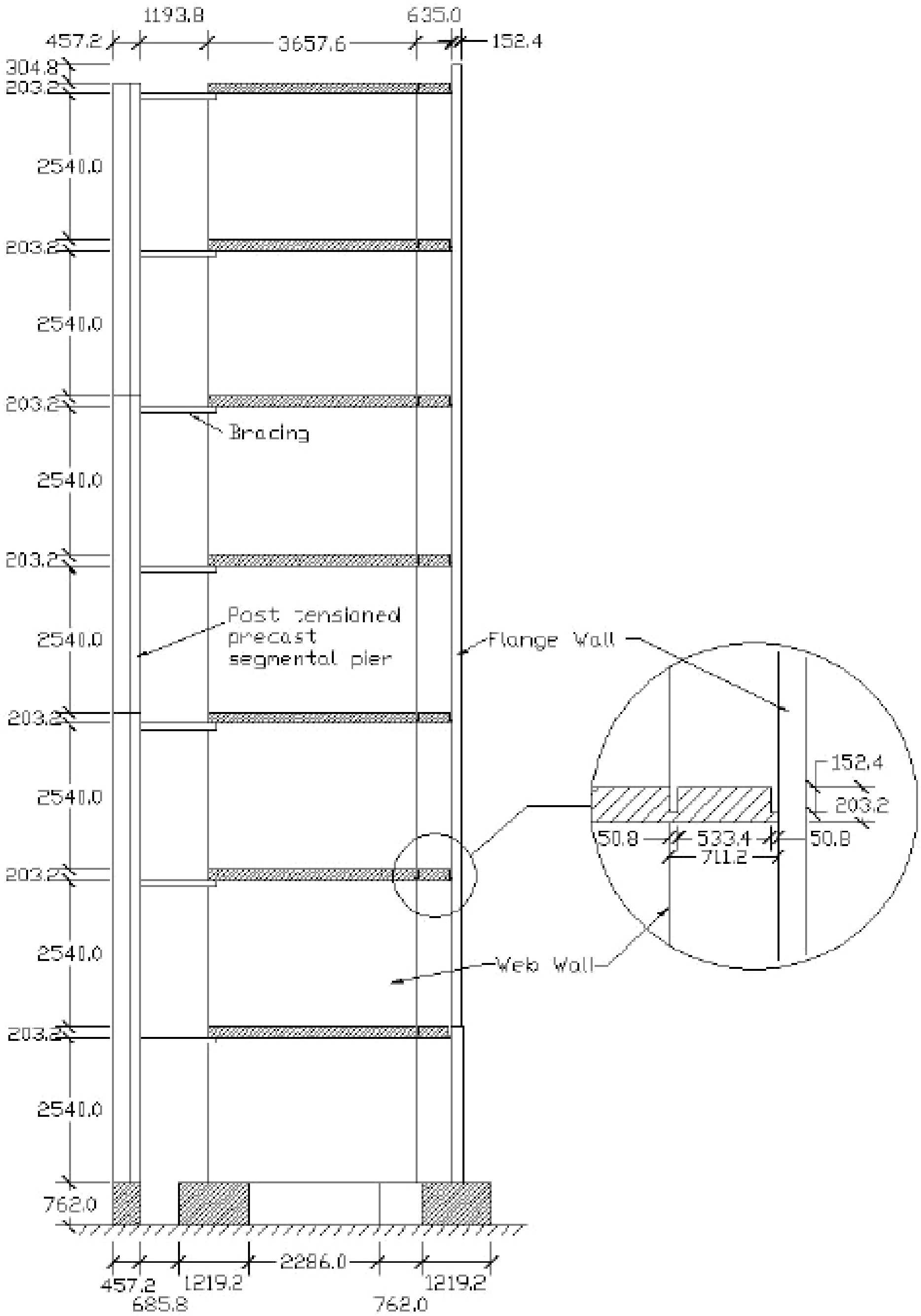

Figure 4.7. Dimensions of the Full-Scale Specimen from side.

4.2. Hardware Properties of Image Based Measurement

Different recording devices were used in experiments. List of devices, their technical features and type of experiments they were utilized are given in the Table 4.2.

Table 4.2. Technical features of recording devices used in experiments.

Camera	**Effective Photo Resolution**	**Frame Rate**	**Resolution**	**Experiments**
I Phone 7	12.0 MP (CMOS)	30	4K	Elastic SDOF Experiments
I Phone 8	12.0 MP (CMOS)	60	4K	Plastic SDOF Experiments
Go Pro HERO6	12.0 MP (CMOS)	60	2.7 K	MDOF Experiments (Elastic + Plastic)
Basler ace	3.0 MP (CMOS)	100	2045x1520	Strain Experiments

5. EXPERIMENTAL RESULTS

In this study, a wide variety of experiments were conducted. These experiments could basically be divided into 7 categories:

(i) Preliminary tests
(ii) SDOF Elastic tests
(iii) SDOF Plastic tests
(iv) MDOF Elastic tests
(v) MDOF Plastic tests
(vi) MDOF Full scale tests
(vii) Strain measurement trial tests

5.1. Results of Preliminary Tests

In order to determine the effectiveness of KLT and LED-based Statistical Threshold methods under different conditions, preliminary tests were conducted. From Figure 5.1 and Figure 5.2 results of these tests were presented.

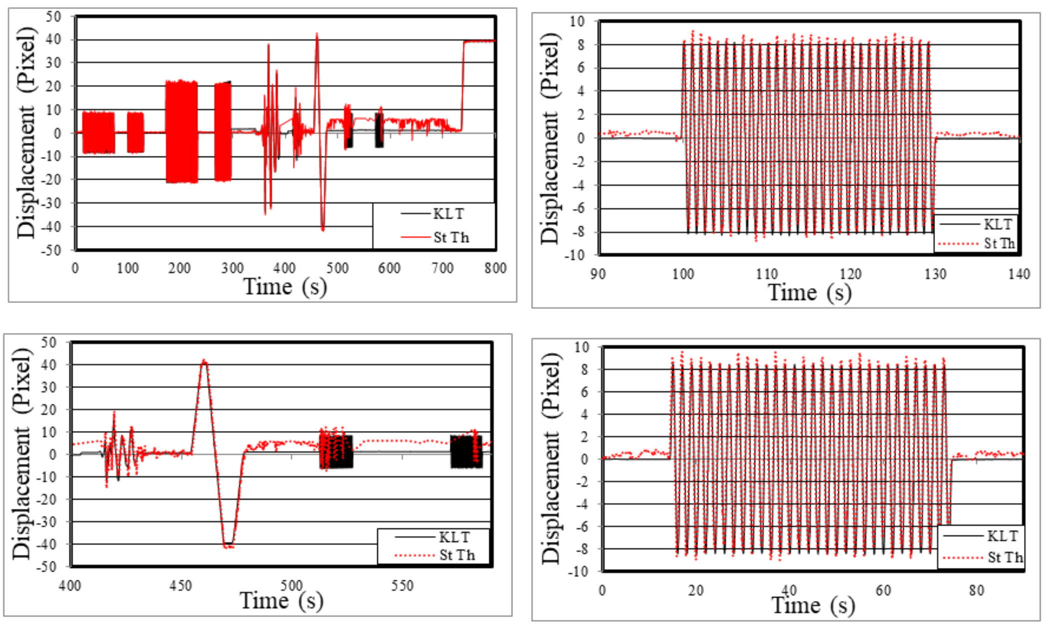

Figure 5.1. Comparison KLT vs TH Traction (640p, 30 fps).

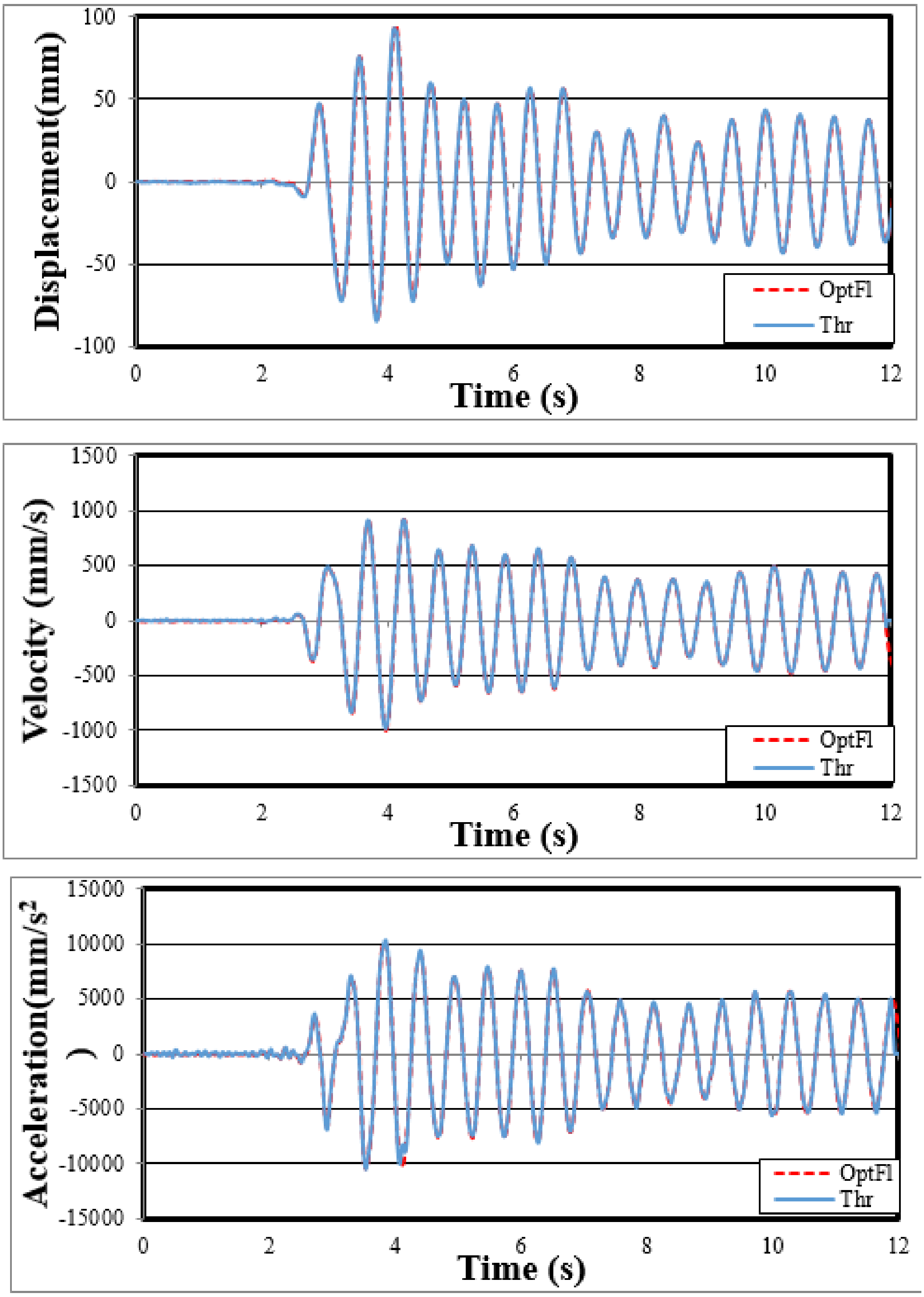

Figure 5.2. Comparison KLT vs TH Traction (4K 30 fps).

In videos with lower resolution, KLT Tracker outperformed the Statistical Threshold method during the entire excitation. KLT Tracker provided less than a pixel of accuracy and it tracked the geometric features captured by an algorithm appropriate for itself. On the other hand, accuracy of the Statistical Threshold method depends on the number of the pixels over this specific threshold value. Therefore, for this method, since the resolution was relatively low, measured values did not represent the actual displacements. When the comparisons in high resolution videos were observed, the overlap of two different methods could be readily seen. This overlap was directly related to the increased number of the pixels above the threshold. Consequently, as the resolution got higher, displacement measurements of both methods converged, hence the difference was vanished.

5.2. Results of Single Degree of Freedom Elastic Experiments

In these experiments, three different earthquake records representing different soil types were used. These records were San Salvador Earthquake, Erzincan Earthquake and Loma Prieta Earthquake acceleration ground motion records with a scale factor of 0.2 in order not to exceed the limitations of the shake table.

These experiments were the first actual tests conducted within the scope of this thesis. The responses in these experiments were found by the threshold method explained above.

Steel columns with different masses corresponding to three different periods were tested, and periods of 0.5 second, 0.667 second and 1.0 second were determined. From Figure 5.3 to Figure 5.11 comparative results between image-based and strain gauge measurements are presented.

Experimental comparison of strain gauge results and the displacements obtained from the video records are presented in the graphs below. Sampling rate of the strain gauge was 200 Hz while video records had the sampling rate of 30 Hz. Velocity and Acceleration were obtained via Savitzky-Golay 1^{st} derivation filter with window size of 9.

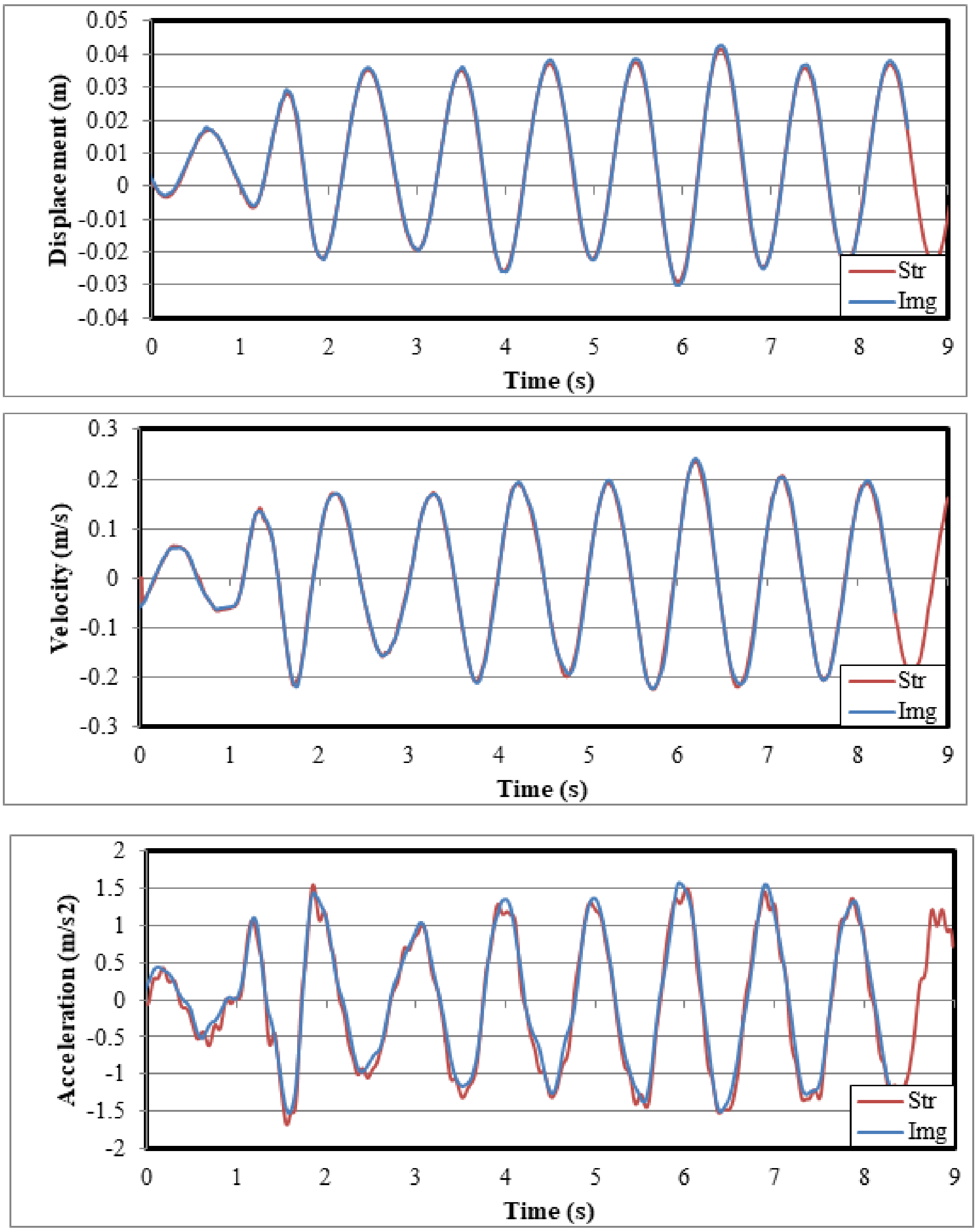

Figure 5.3. Acceleration comparison graphic of strain gauges (Str) and high resolution record (4K, 30 fps). EQ Record: San Salvador, Scale Factor: 0.2, T=1.

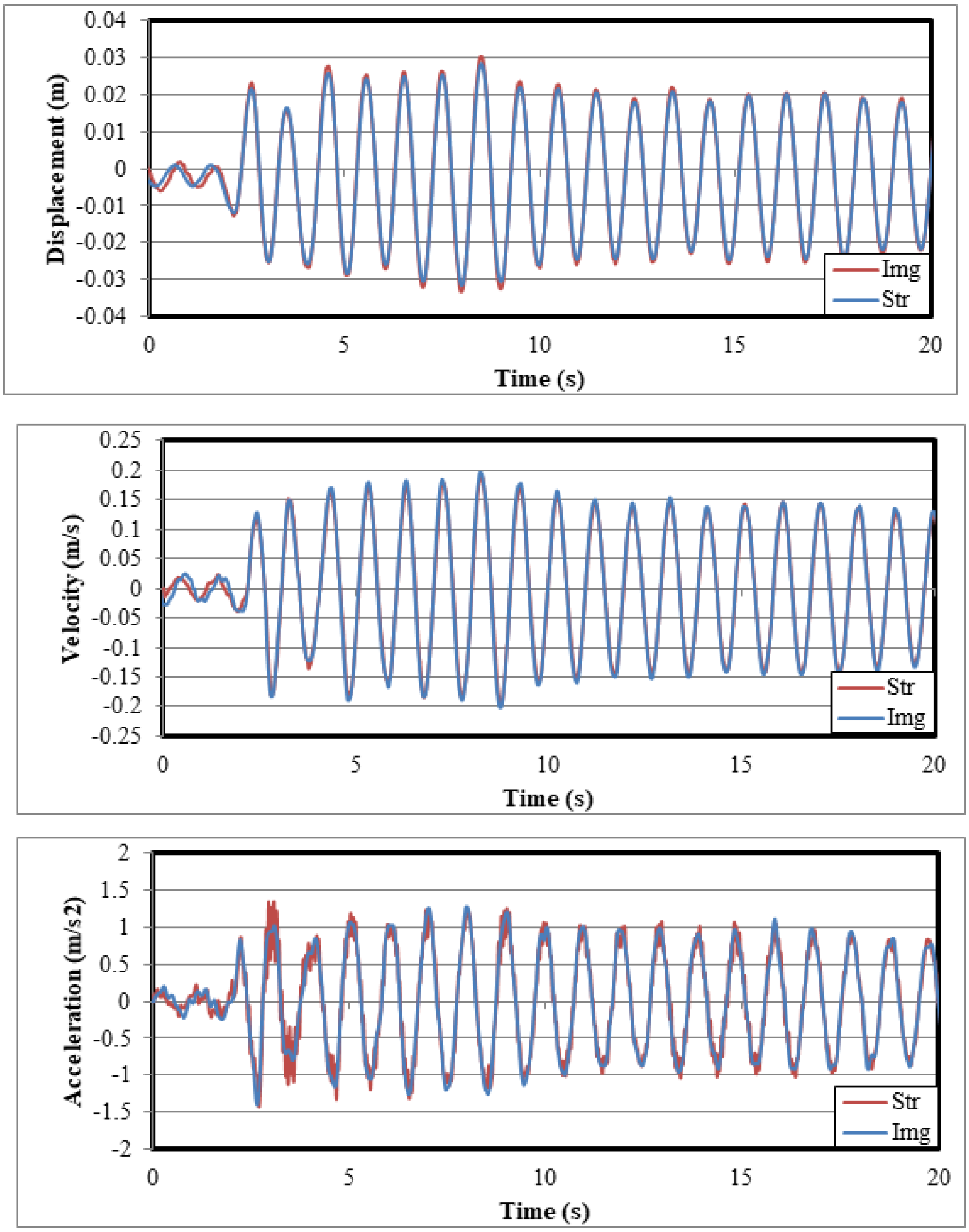

Figure 5.4. Response comparison graphic of strain gauges (Str) and high resolution record (4K, 30 fps). EQ Record: Erzincan, Scale Factor: 0.2, T=1.

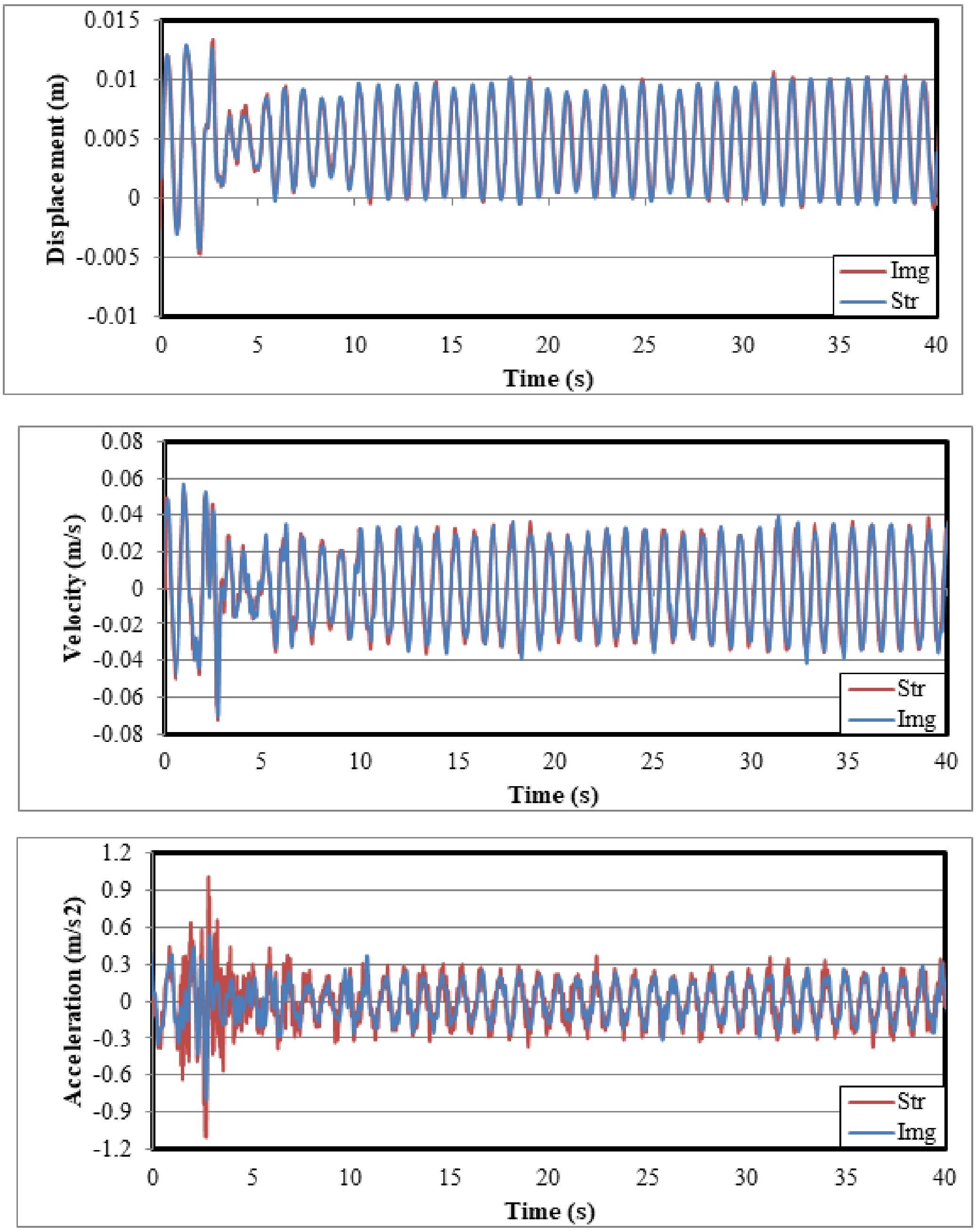

Figure 5.5. Response comparison graphic of strain gauges (Str) and high resolution record (4K, 30 fps). EQ Record: Loma Prieta, Scale Factor: 0.2, T=1.

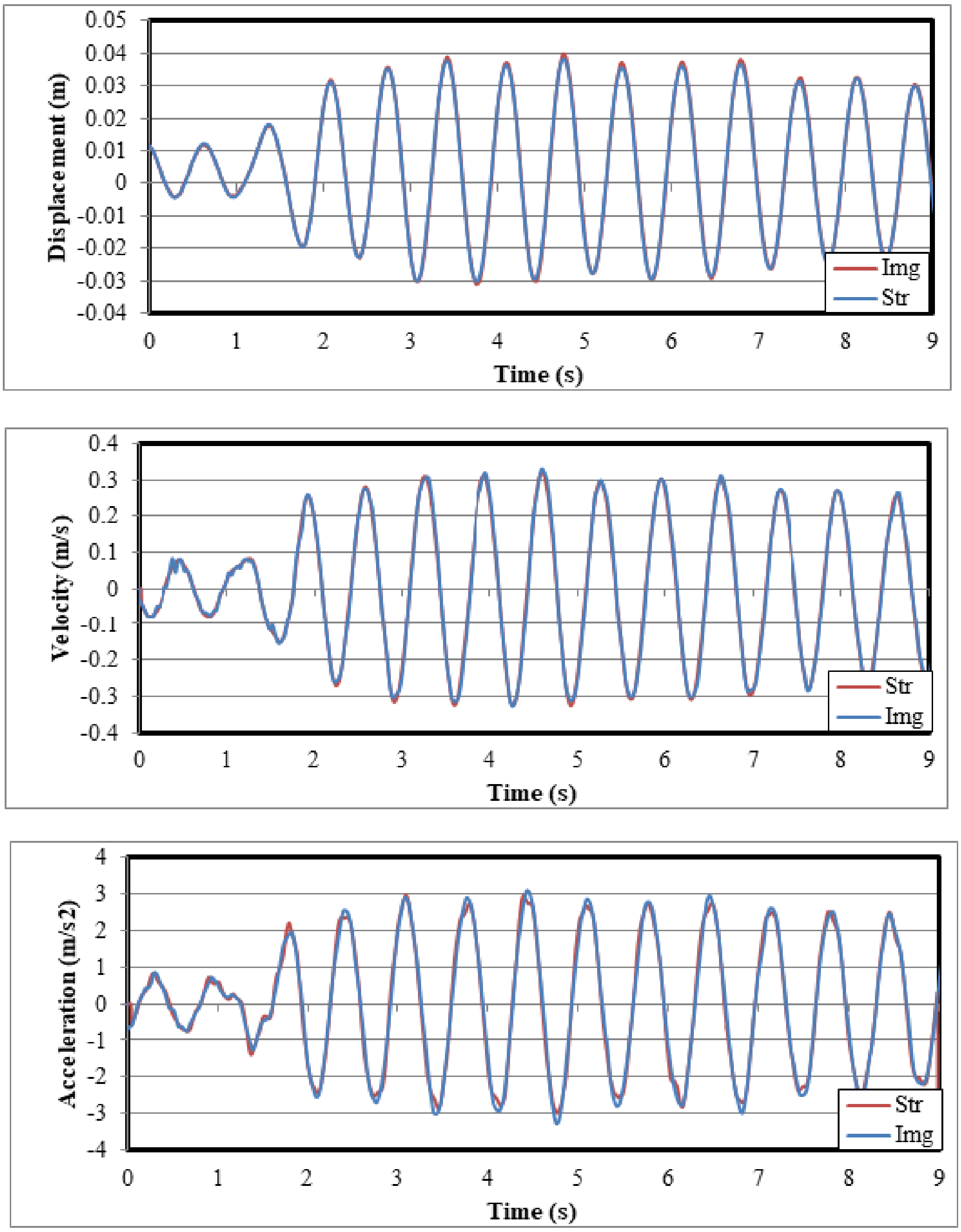

Figure 5.6. Response comparison graphic of strain gauges (Str) and high resolution record (4K, 30 fps). EQ Record: San Salvador, Scale Factor: 0.2, T=0.667.

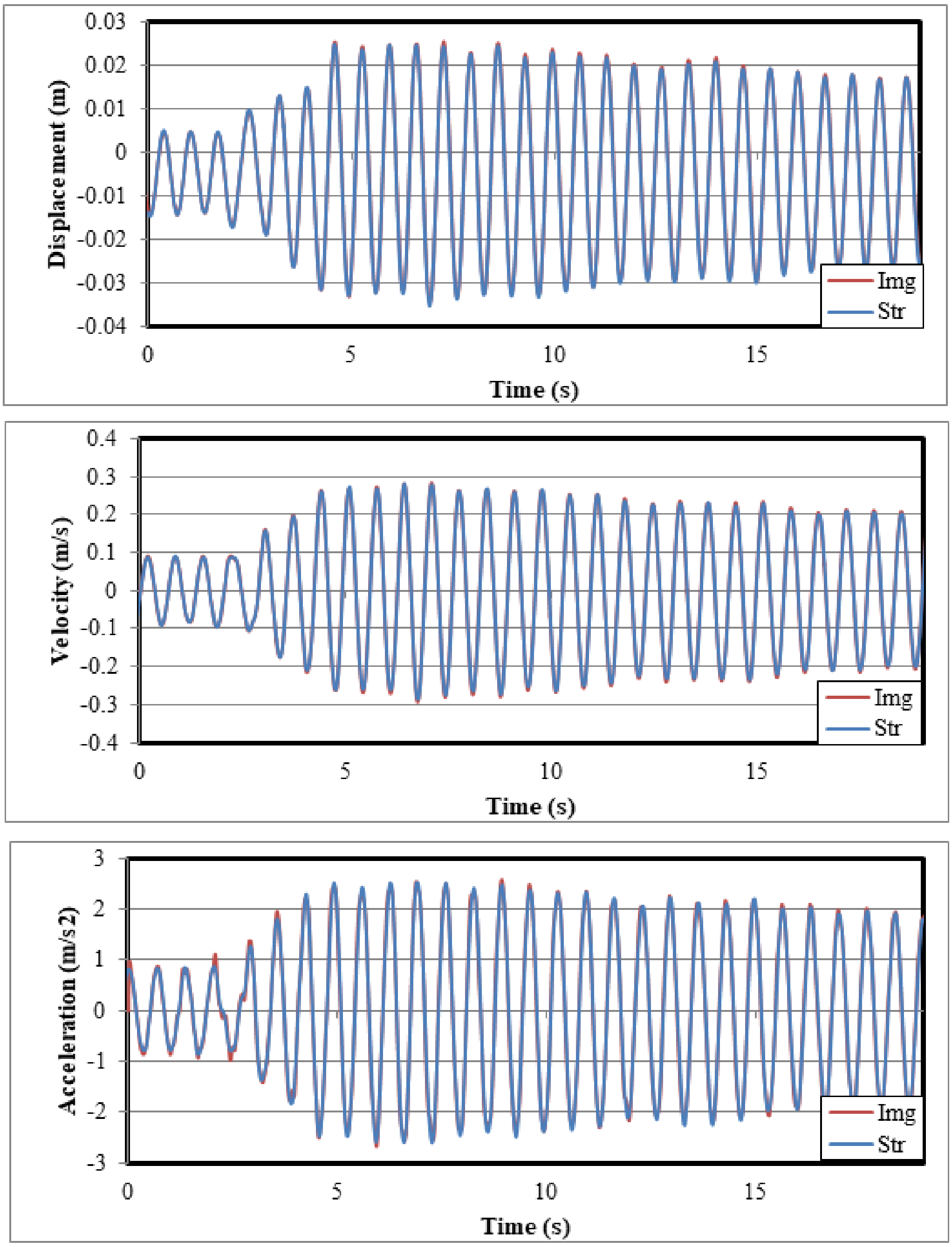

Figure 5.7. Response comparison graphic of strain gauges (Str) and high resolution record (4K, 30 fps). EQ Record: Erzincan, Scale Factor: 0.2, T=0.667.

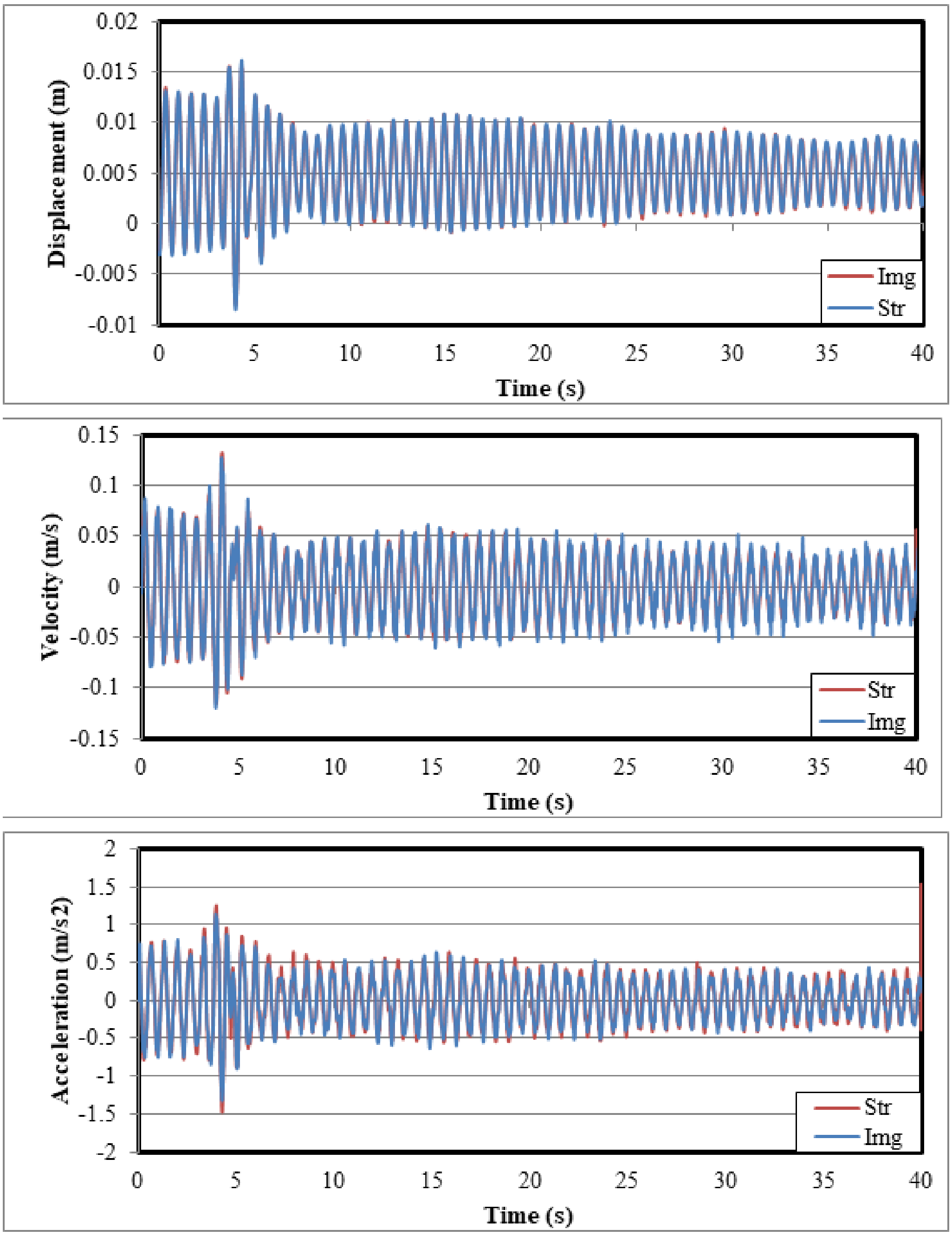

Figure 5.8. Response comparison graphic of strain gauges (Str) and high resolution record (4K, 30 fps). EQ Record: Loma Prieta, Scale Factor: 0.2, T=0.667.

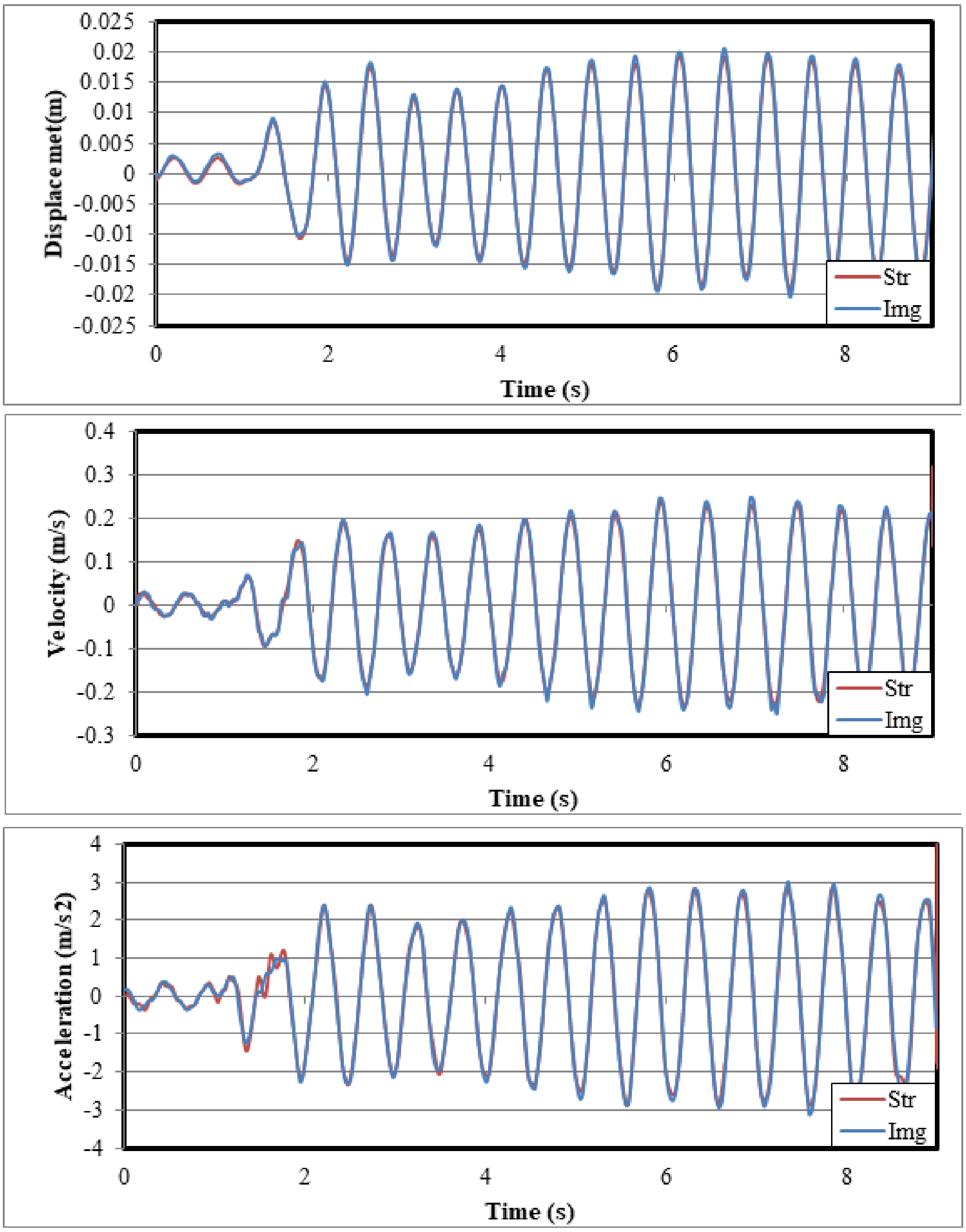

Figure 5.9. Response comparison graphic of strain gauges (Str) and high resolution record (4K, 30 fps). EQ Record: San Salvador, Scale Factor: 0.2, T=0.5.

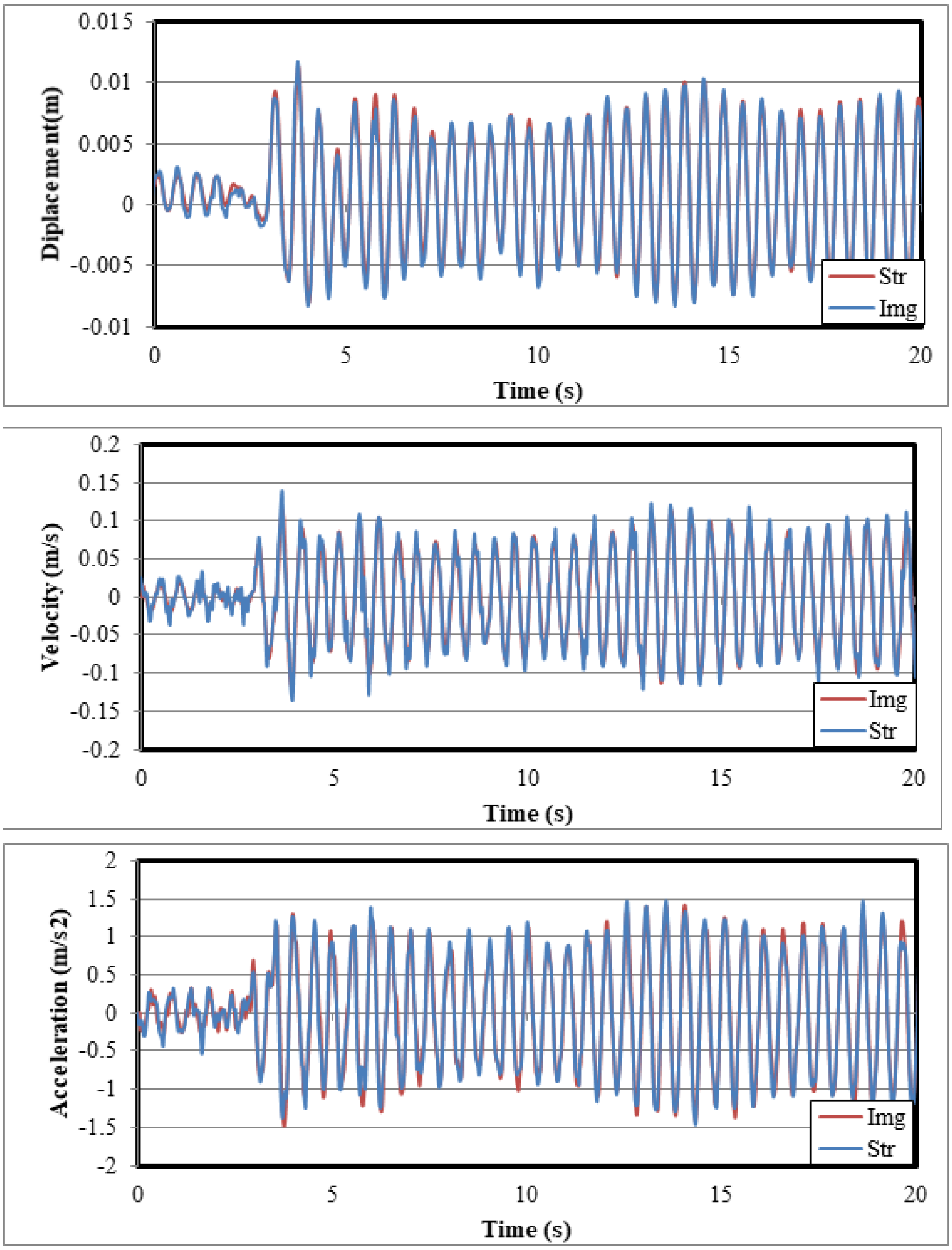

Figure 5.10. Response comparison graphic of strain gauges (Str) and high resolution record (4K, 30 fps). EQ Record: Erzincan, Scale Factor: 0.2, T=0.5.

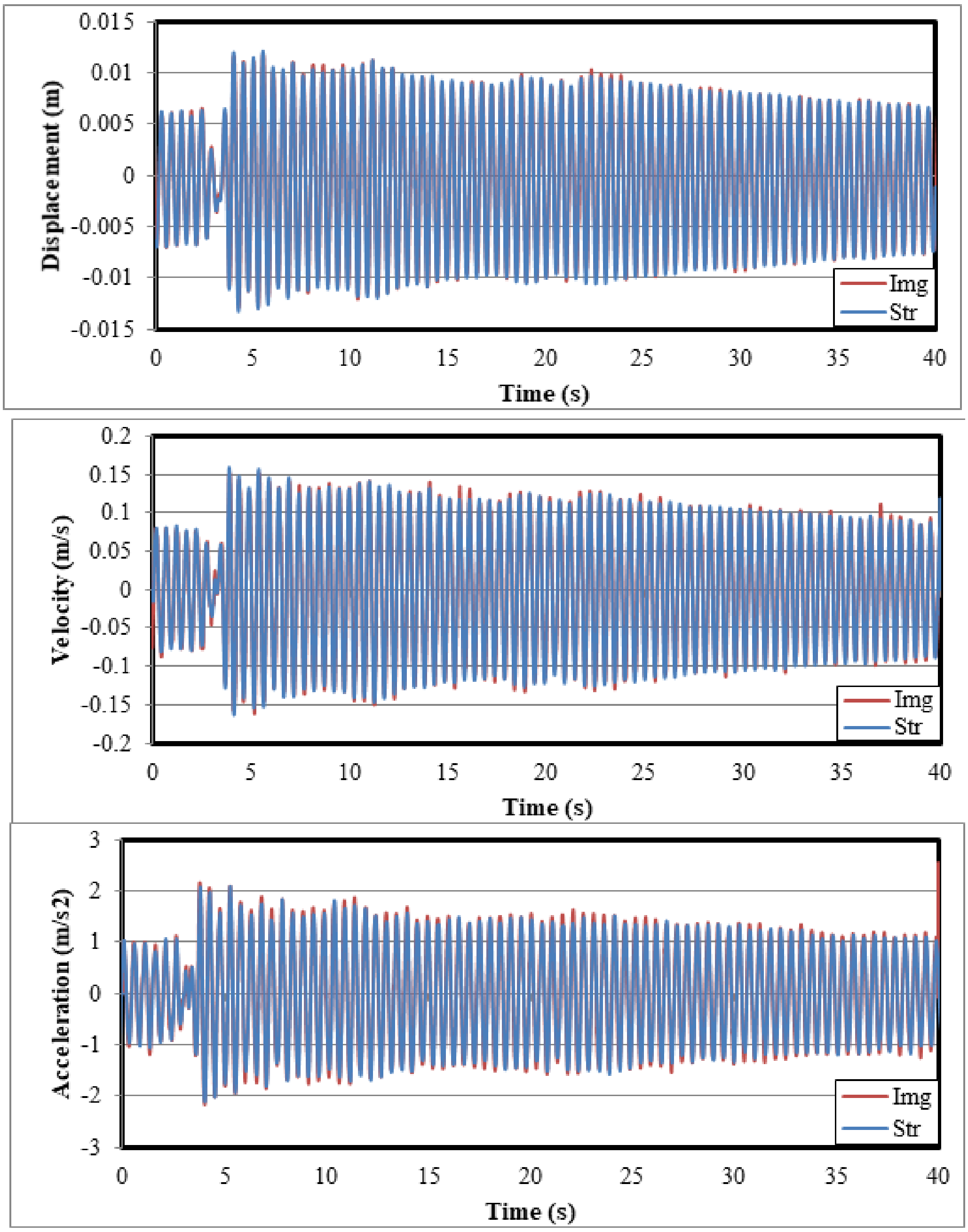

Figure 5.11. Response comparison graphic of strain gauges (Str) and high resolution record (4K, 30 fps). EQ Record: Loma Prieta, Scale Factor: 0.2, T=0.5.

As seen in the figures, compared response data, especially displacements, were not significantly different. These comparisons for all three cases with different natural frequencies were yielded accurate results. However, distortion of the environmental effects could also be observed in the acceleration responses. As an example, in Figure 5.5., it could be seen that the mismatch between image-based data and traditional acceleration data occurred due to the contamination of noise in the first five seconds. The source of this noise might be due to a flaw in the hydraulic system of the shake table or any other vibratory activity took place in the laboratory at that moment.

In general, responses of structures within 1.0 Hz and 2.0 Hz of natural frequency band could be easily detected by video cameras with resolution of 4K and sampling rate of 30 fps. Exact matchings in peak values could not be obtained in some cases but the difference was not too significant to indicate a systematic error in measurement methods.

Another set of experimental results provided the comparison between two different cases of recordings. Two different record of the same experiment provided a chance to analyze the effects of resolution and sampling rates of video records in Statistical Threshold method. One had the higher resolution and lower sampling rate (4K, 30 fps), while the other had the lower resolution and higher sampling rate (1080p, 60 fps). In this experiment, period of the specimen was 0.667 second. Results of these experiments are presented in Figure 5.12 to Figure 5.19.

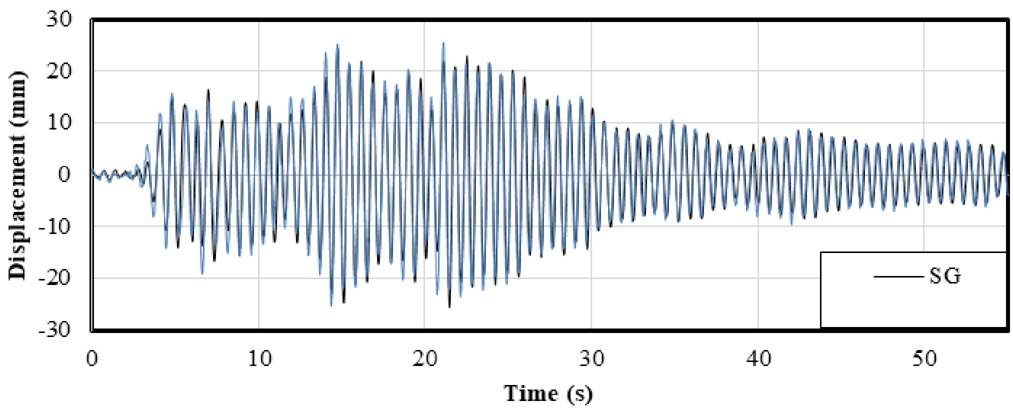

Figure 5.12. Displacement comparison graphic of strain gauges (Str) and high resolution record (4K, 30 fps). EQ Record: ChiChi Scale Factor: 0.2.

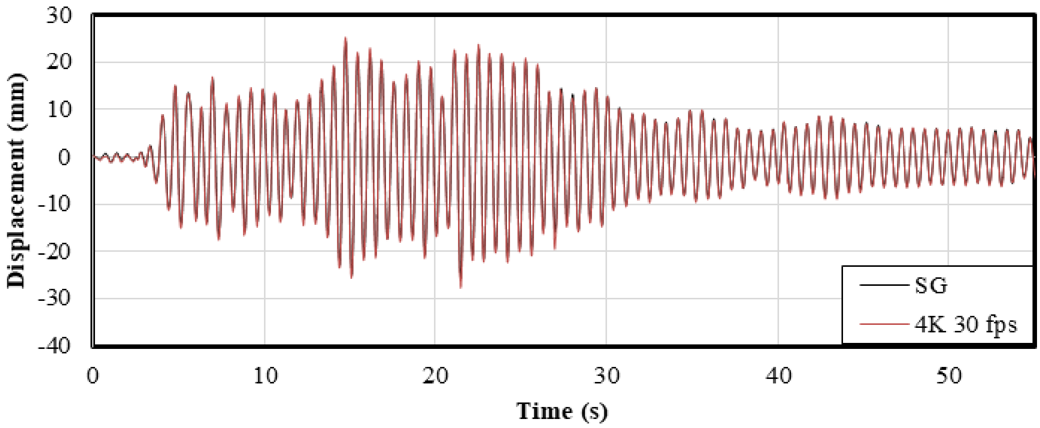

Figure 5.13. Displacement comparison graphic of strain gauges (Str) and low resolution record (1080p, 60 fps). EQ Record: ChiChi Scale Factor: 0.2.

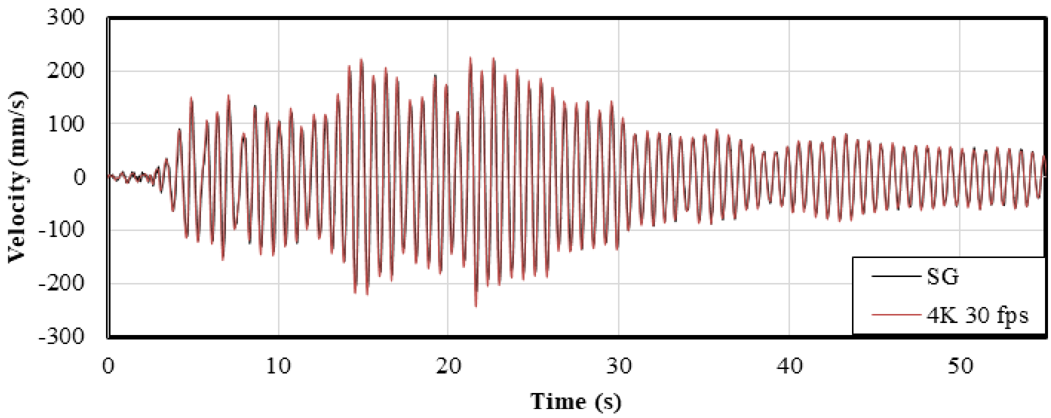

Figure 5.14. Velocity comparison graphic of strain gauges (Str) and high resolution record (4K, 30 fps). EQ Record: ChiChi Scale Factor: 0.2.

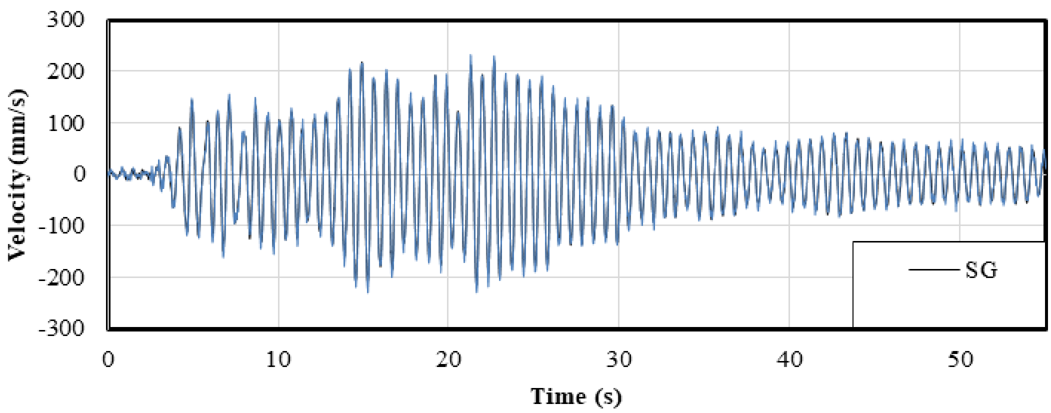

Figure 5.15. Velocity comparison graphic of strain gauges (Str) and low resolution record (1080p, 60 fps). EQ Record: ChiChi Scale Factor: 0.2.

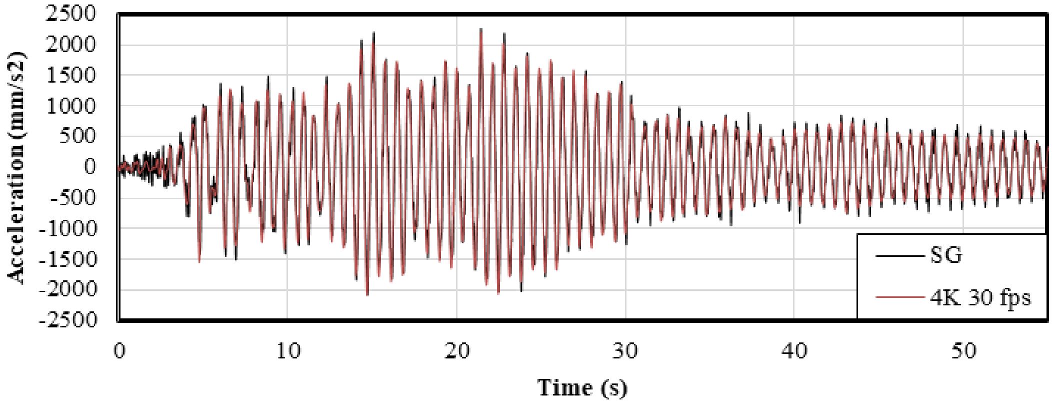

Figure 5.16. Response comparison graphic of strain gauges (Str) and high resolution record (4K, 30 fps). EQ Record: ChiChi Scale Factor: 0.2.

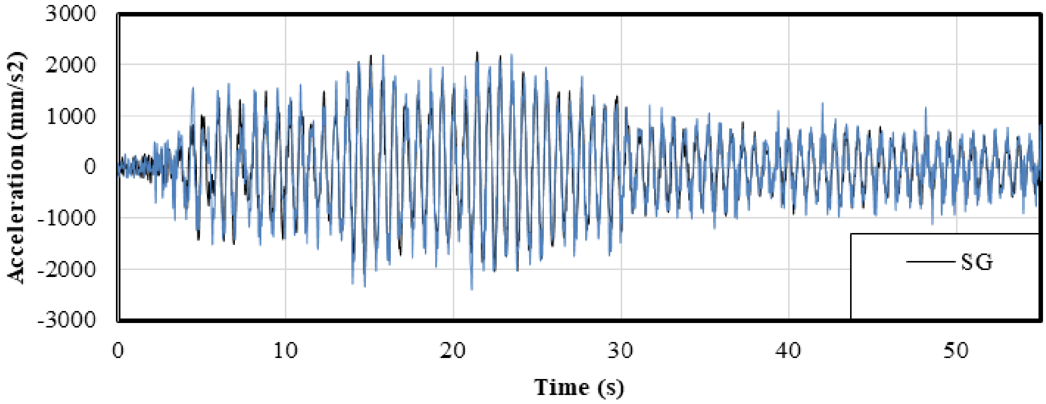

Figure 5.17. Response comparison graphic of strain gauges (Str) and low resolution record (1080p, 60 fps). EQ Record: ChiChi Scale Factor: 0.2.

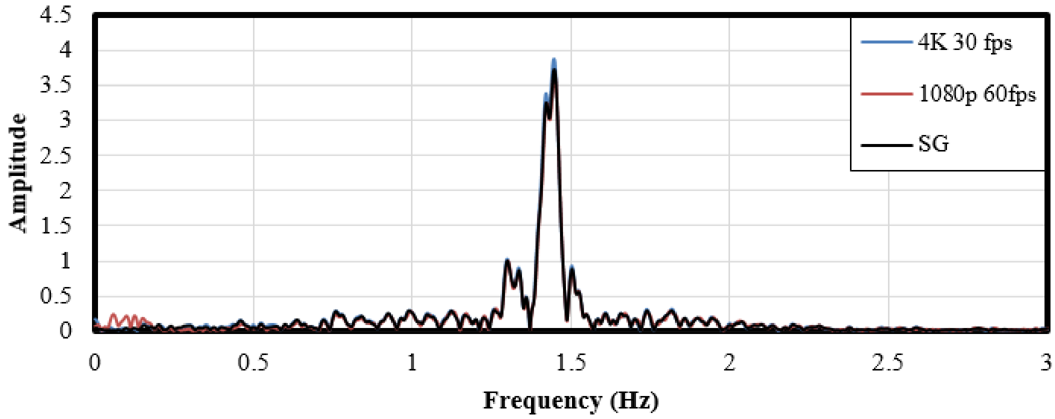

Figure 5.18. Frequency domain comparison graphic of strain gauges (Str) high resolution (4K, 30 fps) and low resolution record (1080p, 60 fps). EQ Record: ChiChi Scale Factor: 0.2.

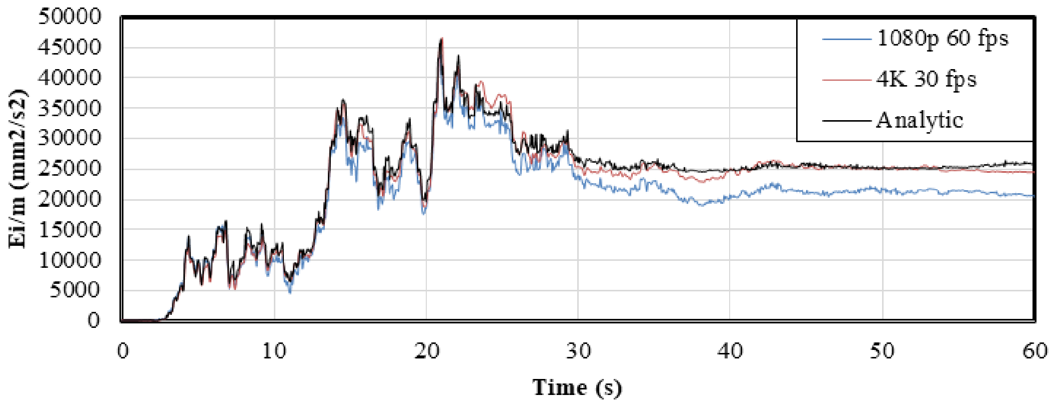

Figure 5.19. Input Energy comparison of high resolution (4K, 30 fps) and low resolution (1080p, 60 fps) records with respect to analytical results. EQ Record: ChiChi Scale Factor: 0.2.

In the results of these set of experiments, effects of sampling rate and resolution in LED-Based Statistical Threshold method could be observed. Displacement, velocity and acceleration responses, as before, significantly concurred. Inconsequential errors existed in some peaks, especially in the measurements of lower resolution records. As mentioned before, comparison of input energy terms could be regarded as a solid indicator of combined error. Especially in Figure 5.19, the significance of the resolution for LED-Based Statistical Threshold method was revealed. Cumulative error observed in the measurements of video records with 4K resolution was considerably less than of video records with 1080p resolution. When the role of the sampling rate was questioned, it could be observed that 30 fps sampling rate yielded results quite similar to both strain gauge data and video record of 60 fps. The video with sampling rate of 30 fps did not generated a significant problem in this case.

5.3. Results of Single Degree of Freedom Plastic Experiments

In these experiments, San Salvador Ground motion was applied to the shake table with specimens having different natural vibration periods. Five different masses were used to obtain five different periods. Two accelerometers were placed on bottom and top of the specimen to measure ground and absolute accelerations. In these results, displacements obtained from strain gauge measurements. Results of these experiments are presented in Figure 5.20 to Figure 5.24.

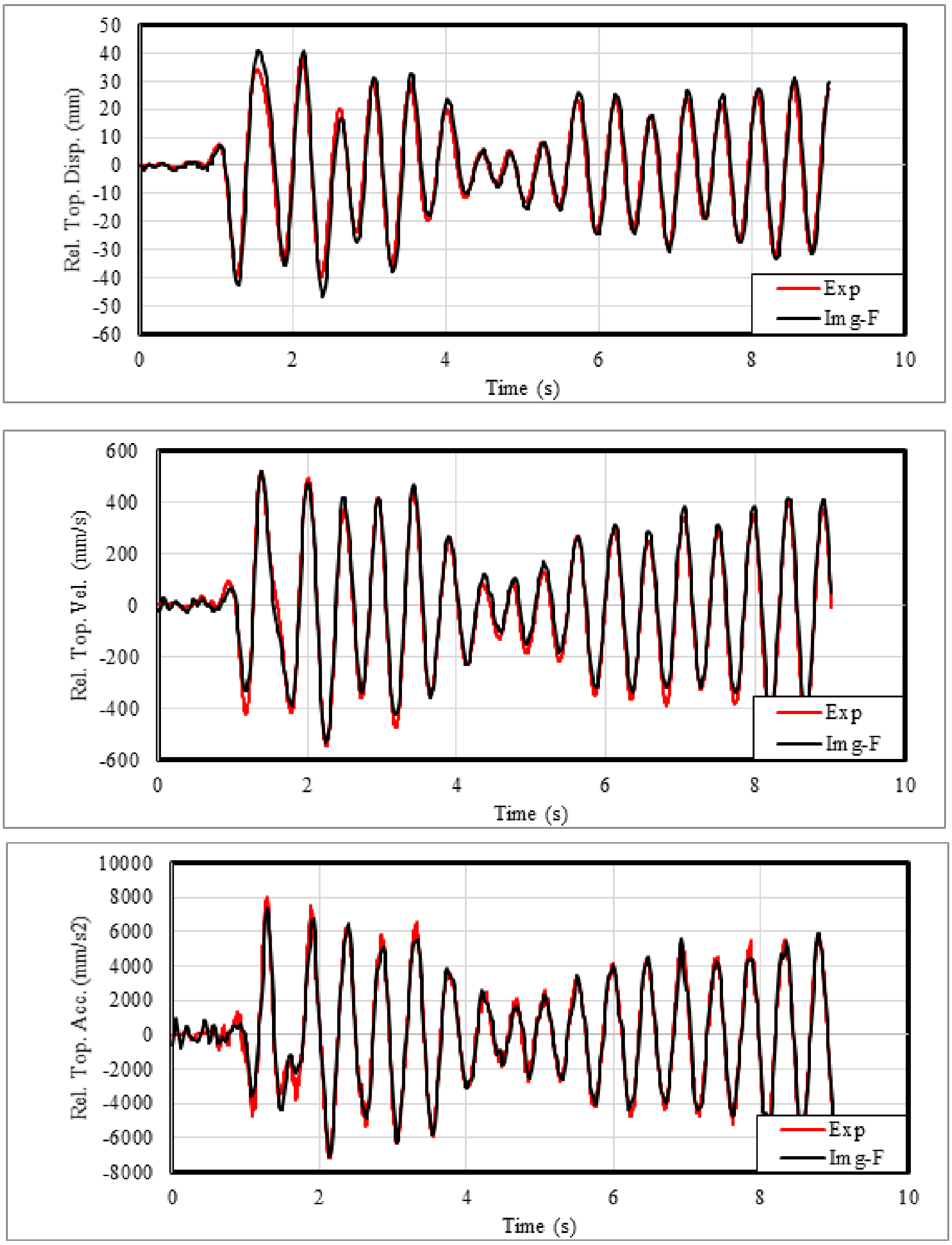

Figure 5.20. Response comparison graphic of conventional method (Exp) and video record (Img-F) 4K, 60 fps EQ Record: San Salvador, Scale Factor: 1.0 m=71.3 kg.

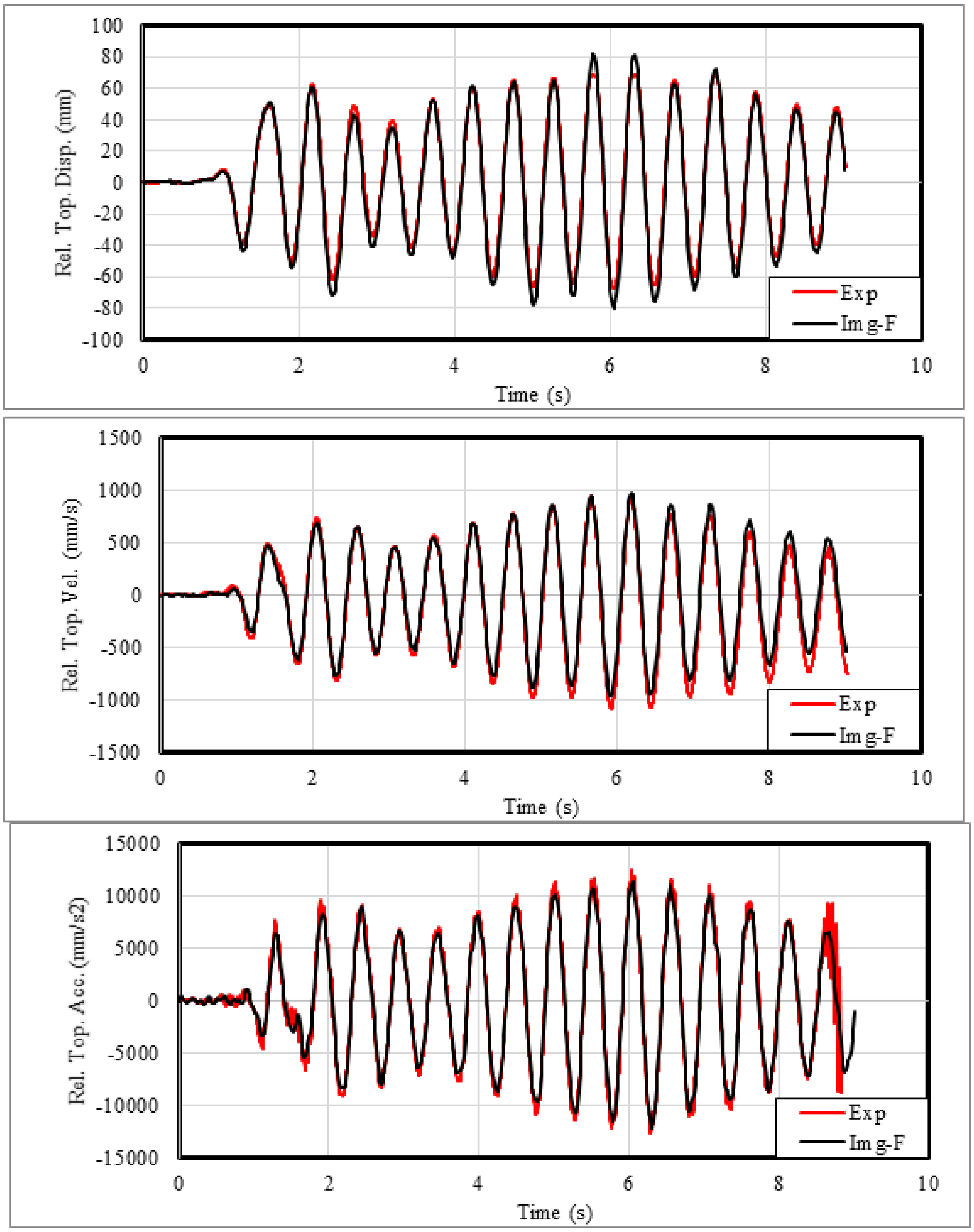

Figure 5.21. Response comparison graphic of conventional method (Exp) and video record (Img-F) 4K, 60 fps EQ Record: San Salvador, Scale Factor: 1.0 m=81.5 kg.

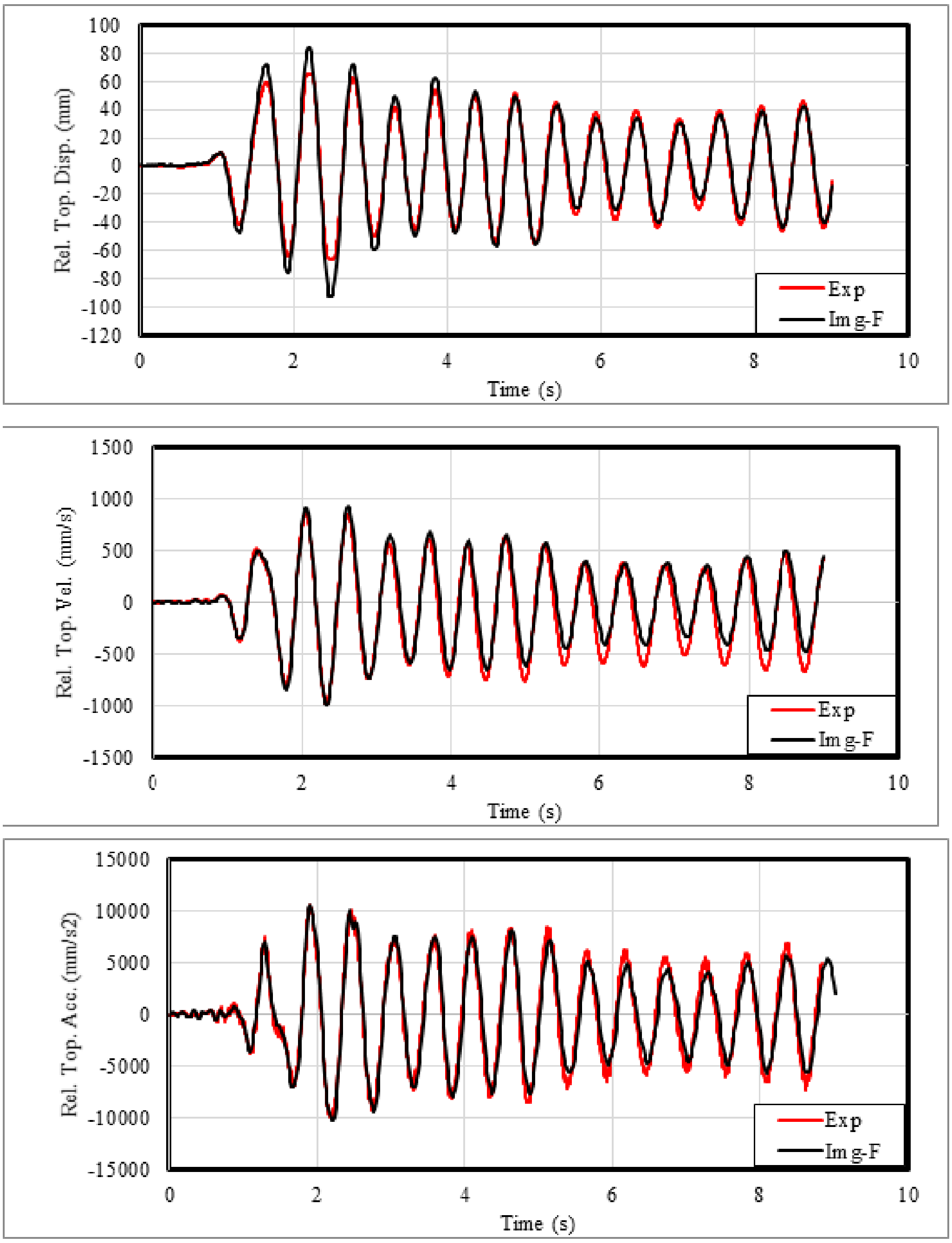

Figure 5.22. Response comparison graphic of conventional method (Exp) and video record (Img-F) 4K, 60 fps EQ Record: San Salvador, Scale Factor: 1.0 m=94.4 kg.

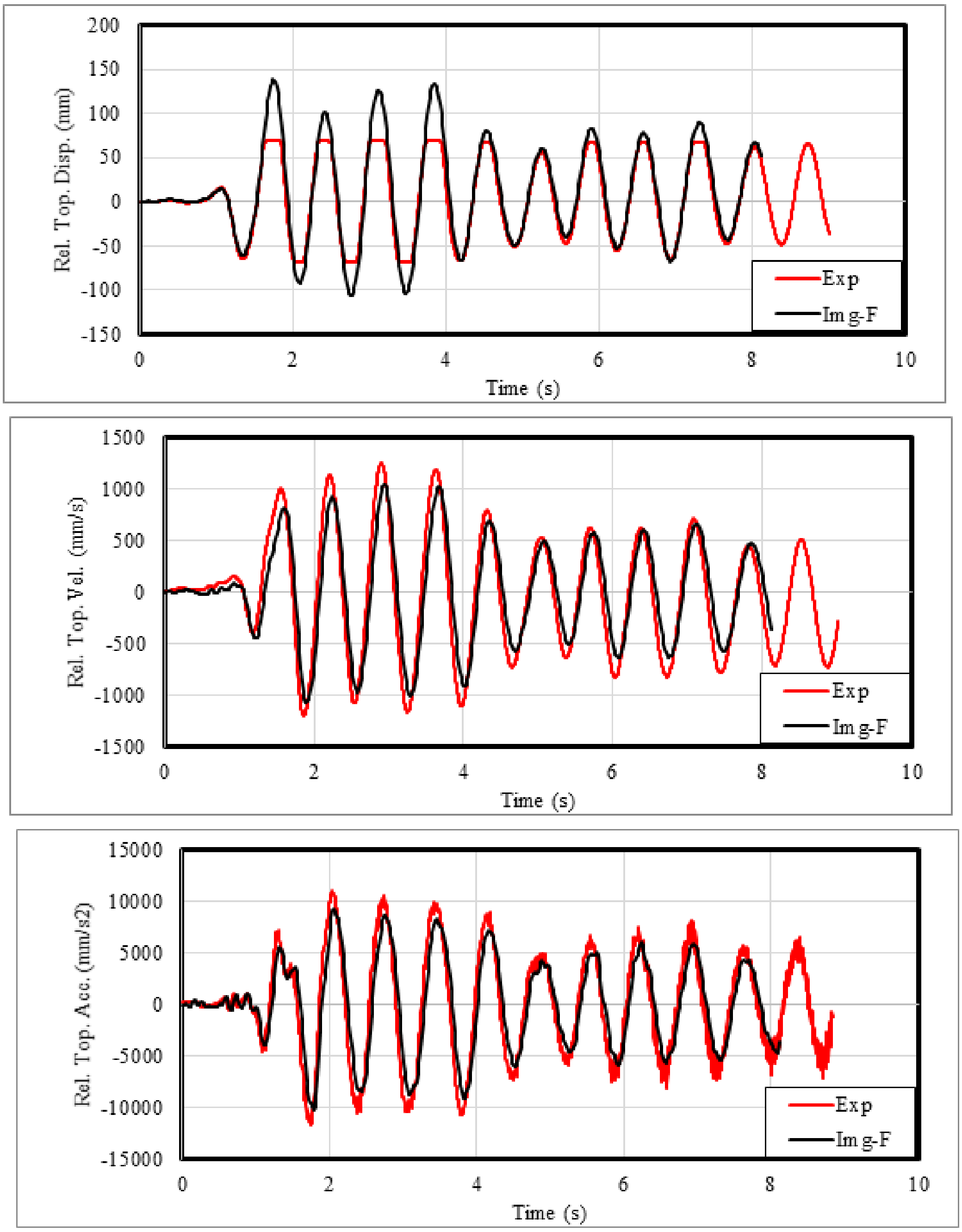

Figure 5.23. Acceleration comparison graphic of accelerometer (Exp) and video record (Img-F) 4K, 60 fps EQ Record: San Salvador, Scale Factor: 1.0 m=147 kg.

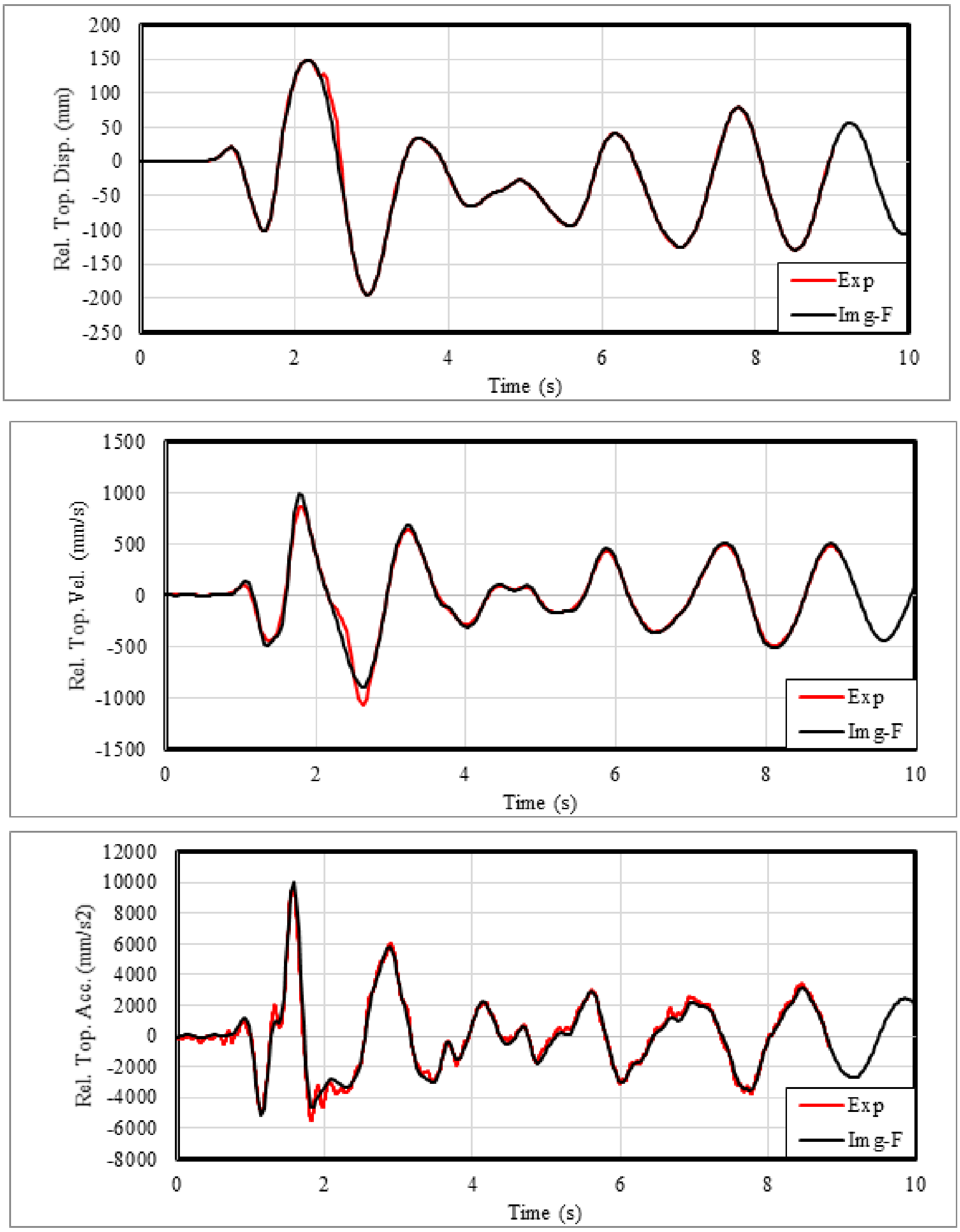

Figure 5.24. Response comparison graphic of conventional method (Exp) and video record (Img-F) 4K, 60 fps EQ Record: San Salvador, Scale Factor: 1.0 m=376 kg.

Results of these experiments indicated the performance of image-based methods in relatively high displacements. At that point, as the resulting strains were above the limits of the strain gauge, the method calculating displacement from the strain gauge was considered as invalid. Accelerations, however, were within the limits of accelerometers placed on the mass and the ground. Therefore, comparison of acceleration data could be more accurate. Acceleration responses in figures presented coinciding acceleration data with both conventional and image-based methods. The high frequency signal existed in the accelerometer data was also considered as unexpected noise. These high frequency noises had not been observed in image-based measurement data during these experiments.

5.4. Results of Multi Degree of Freedom Elastic Experiments

San Salvador and HAD-165 records were induced to the shake table and three-story model was tested. Accelerometers on each story and an LVDT on the base were used as base measurement devices. Comparisons were made between these reference devices and to image-based methods. In these experiments, scale factor of ground motions was selected rather low in order to stay within the elastic range. Results of these experiments are presented in Figure 5.25 to Figure 5.34.

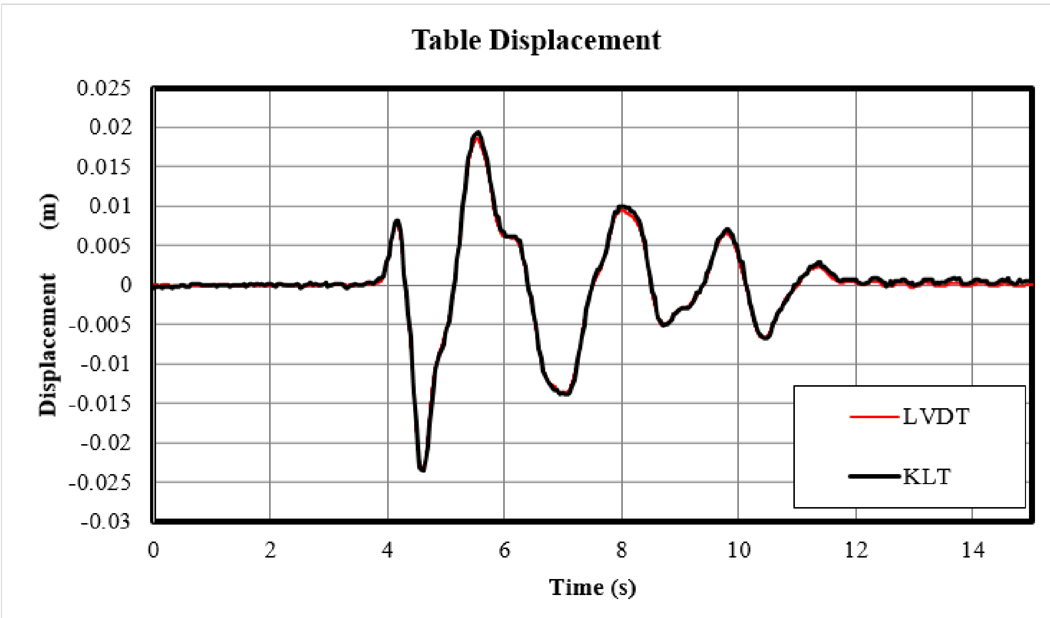

Figure 5.25. Ground Displacement comparison graphic of conventional method (LVDT) and video record (KLT) 2.7K, 30 fps EQ Record: San Salvador, Scale Factor: 0.2.

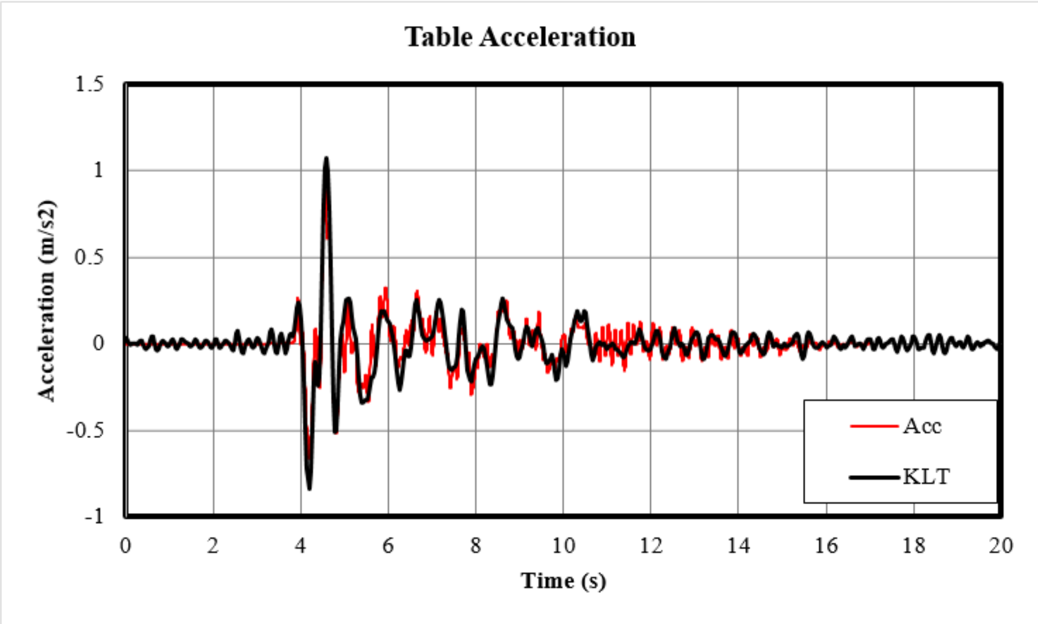

Figure 5.26. Ground Acceleration comparison graphic of accelerometer (Acc) and video record (KLT) 2.7K, 30 fps EQ Record: San Salvador, Scale Factor: 0.2.

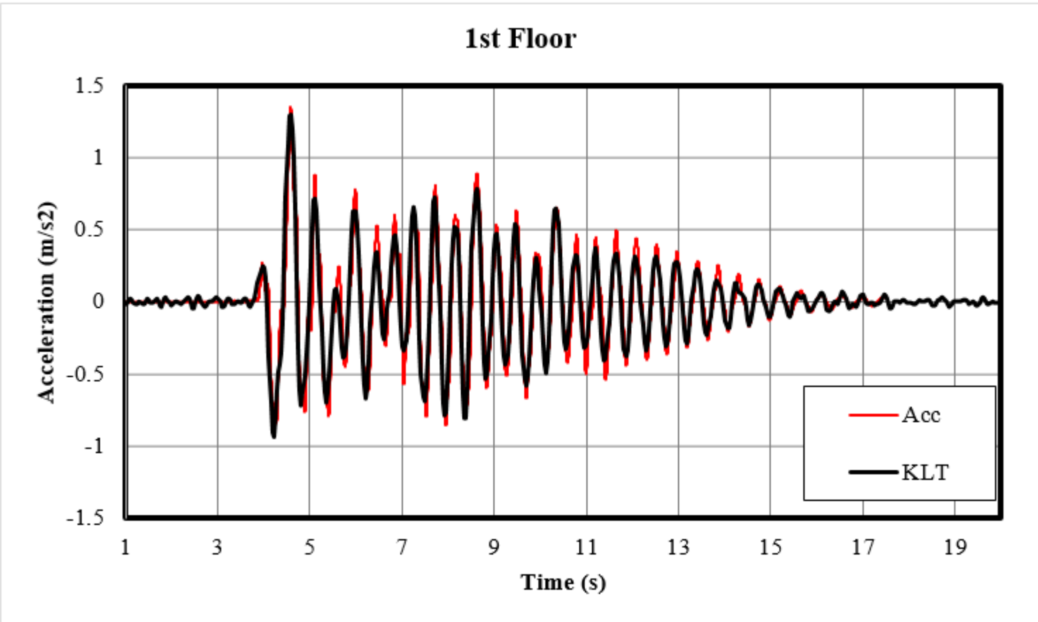

Figure 5.27. 1^{st} Floor Acceleration comparison graphic of accelerometer (Acc) and video record (KLT) 2.7K, 30 fps EQ Record: San Salvador, Scale Factor: 0.2.

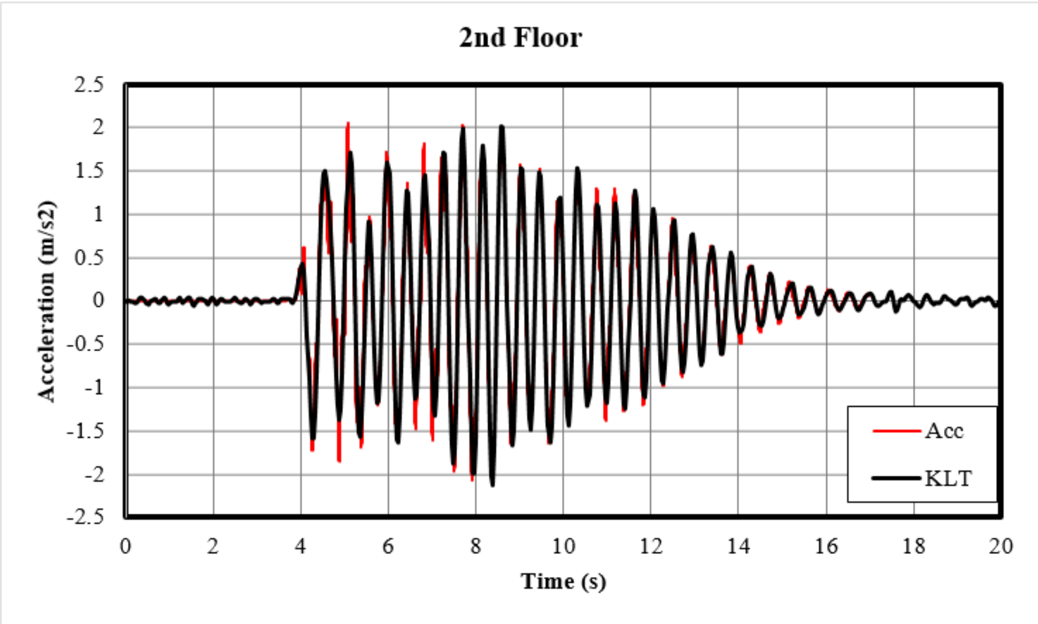

Figure 5.28. 2^{nd} Floor Acceleration comparison graphic of accelerometer (Acc) and video record (KLT) 2.7K, 30 fps EQ Record: San Salvador, Scale Factor: 0.2.

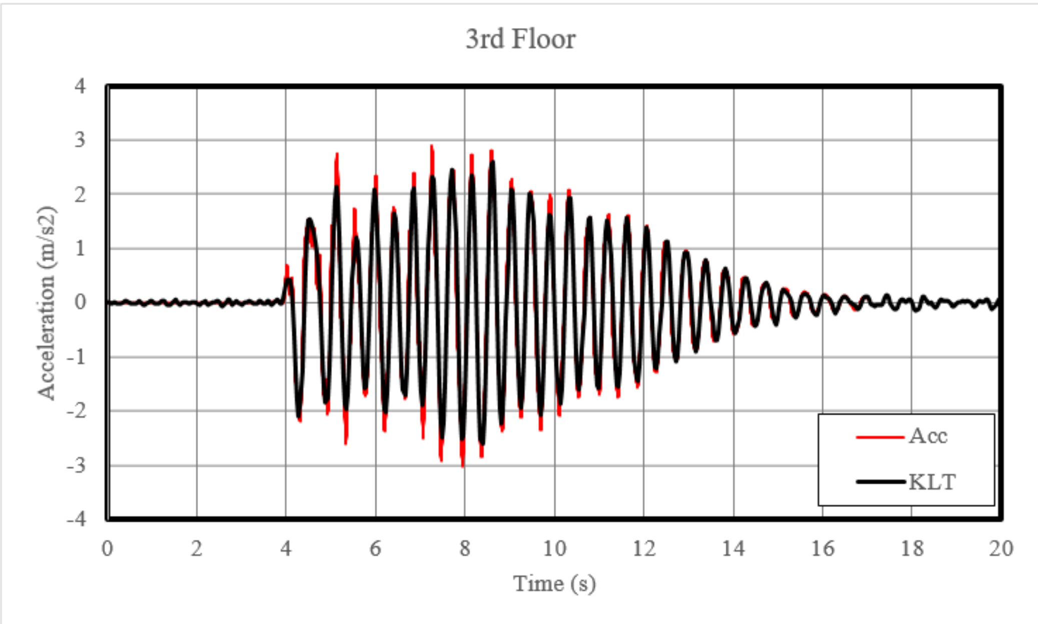

Figure 5.29. 3^{rd} Floor Acceleration comparison graphic of accelerometer (Acc) and video record (KLT) 2.7K, 30 fps EQ Record: San Salvador, Scale Factor: 0.2.

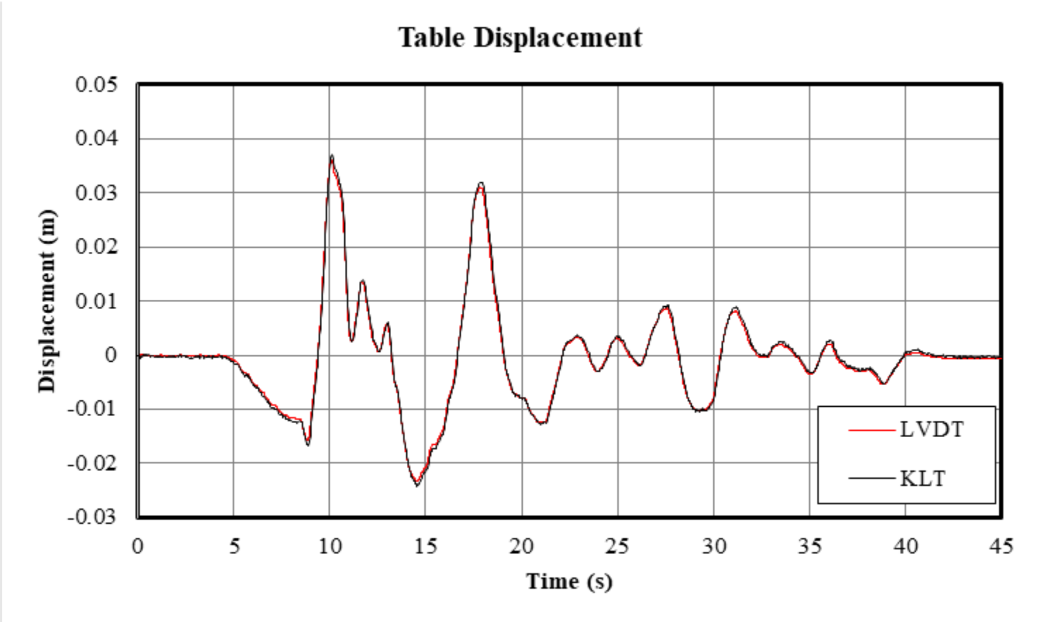

Figure 5.30. Ground Displacement comparison graphic of conventional method (LVDT) and video record (KLT) 2.7K, 30 fps EQ Record: HDA165, Scale Factor: 0.2.

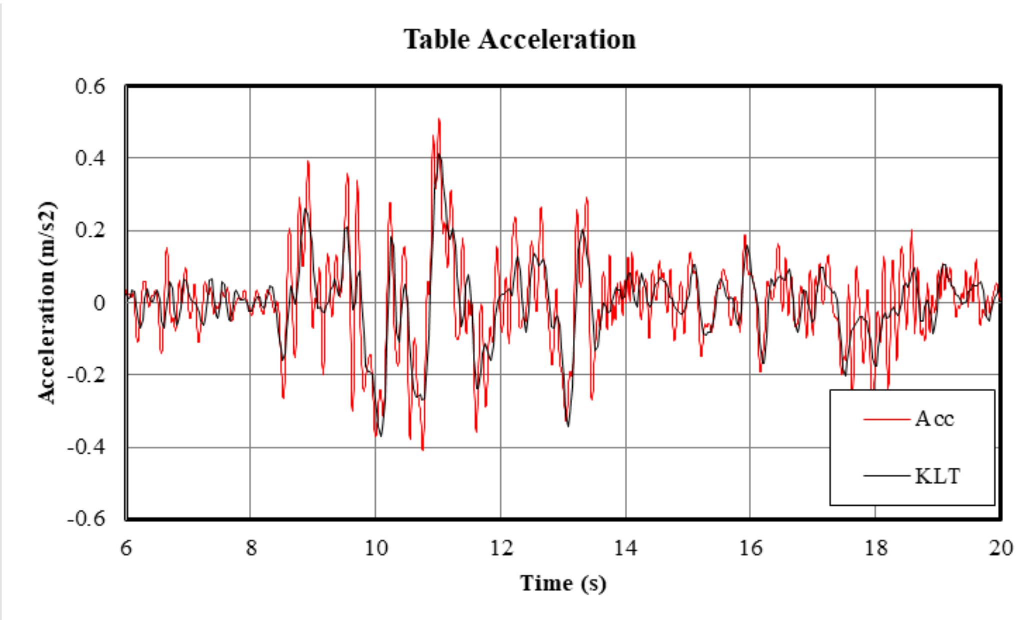

Figure 5.31. Ground Acceleration comparison graphic of Accelerometer (Acc) and video record (KLT) 2.7K, 30 fps EQ Record: HDA165, Scale Factor: 0.2.

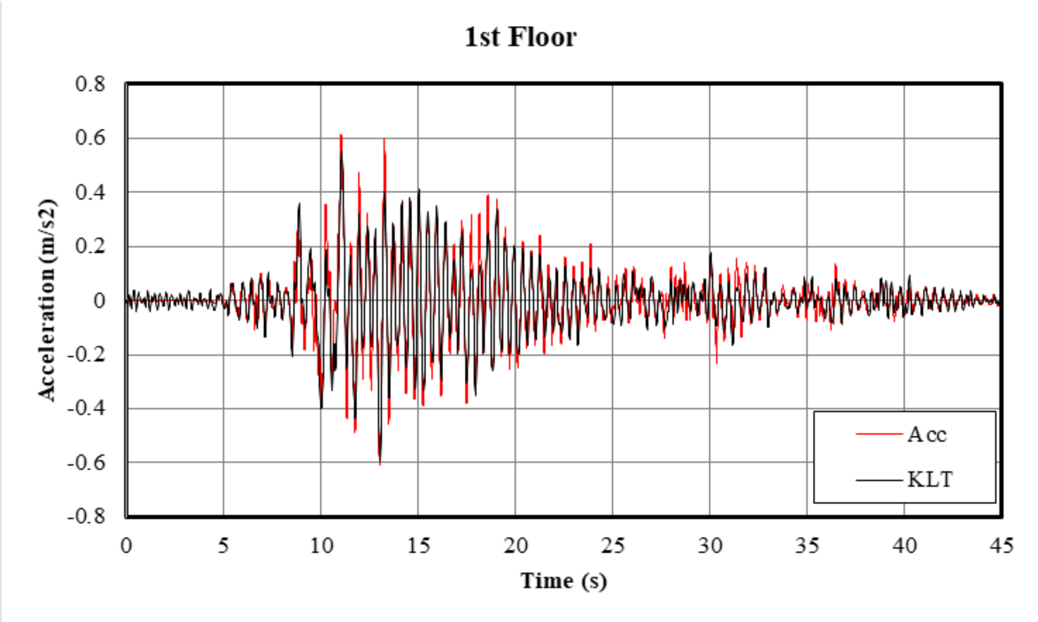

Figure 5.32. 1^{st} Floor Acceleration comparison graphic of accelerometer (Acc) and video record (KLT) 2.7K, 30 fps EQ Record: HDA165, Scale Factor: 0.2.

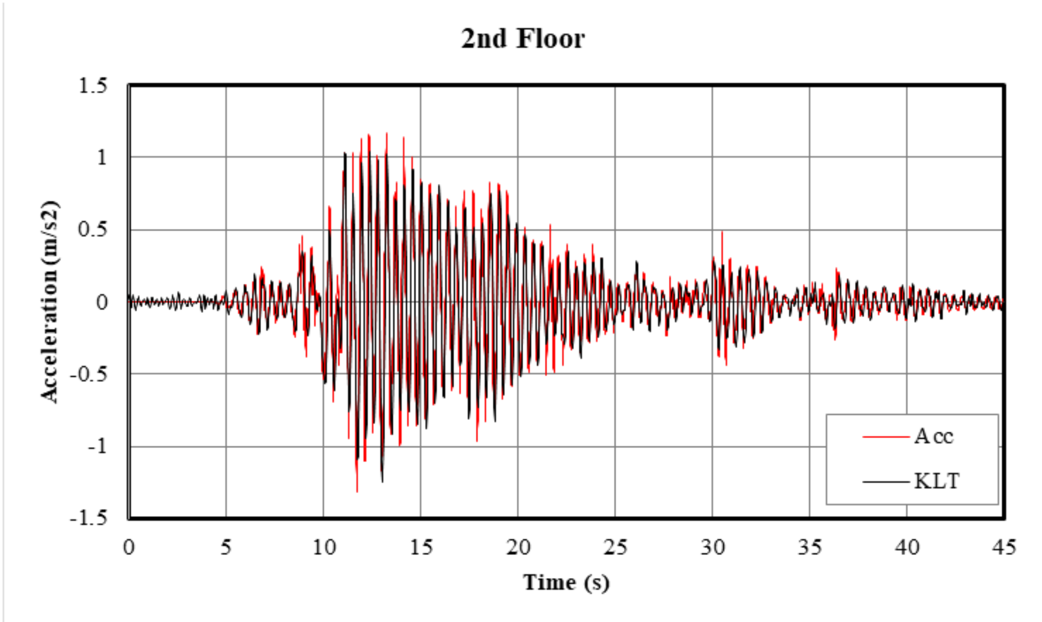

Figure 5.33. 2^{nd} Floor Acceleration comparison graphic of accelerometer (Acc) and video record (KLT) 2.7K, 30 fps EQ Record: HDA165, Scale Factor: 0.2.

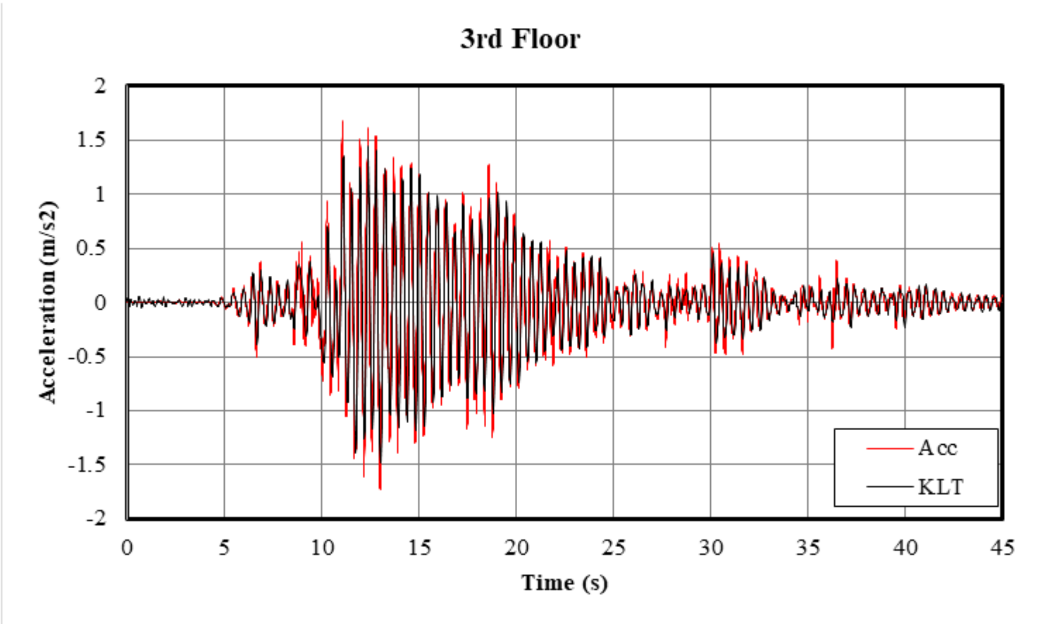

Figure 5.34. 3^{rd} Floor Acceleration comparison graphic of accelerometer (Acc) and video record (KLT) 2.7K, 30 fps EQ Record: HDA165, Scale Factor: 0.2.

In results of these experiments, it could be observed that the ground displacement comparisons were in good agreement, however, the high frequency signals in the ground acceleration data could not be detected by the image-based measurements. The mismatch in the comparison of ground acceleration data, revealed the necessity of the higher sampling rate. In order to understand the reasons of this mismatch, compared data needed to be sampled in the same rate, at least, with closer sampling rates. However, results of floor acceleration comparisons presented quite satisfying results. The high contribution of the first natural period, which was 0.42 second and within the limits of video camera sampling rate, considered as the main reason of these overlapping data.

5.5. Results of Multi Degree of Freedom Plastic Experiments

In these experiments San Salvador Earthquake records with larger scale factors were used. These larger scale factors resulted in the plasticization of the structural model on the shake table. Acceleration of each story and displacement of the base were also measured and compared with the image-based measurements. Results of these experiments are presented in figures from Figure 5.35 to Figure 5.49.

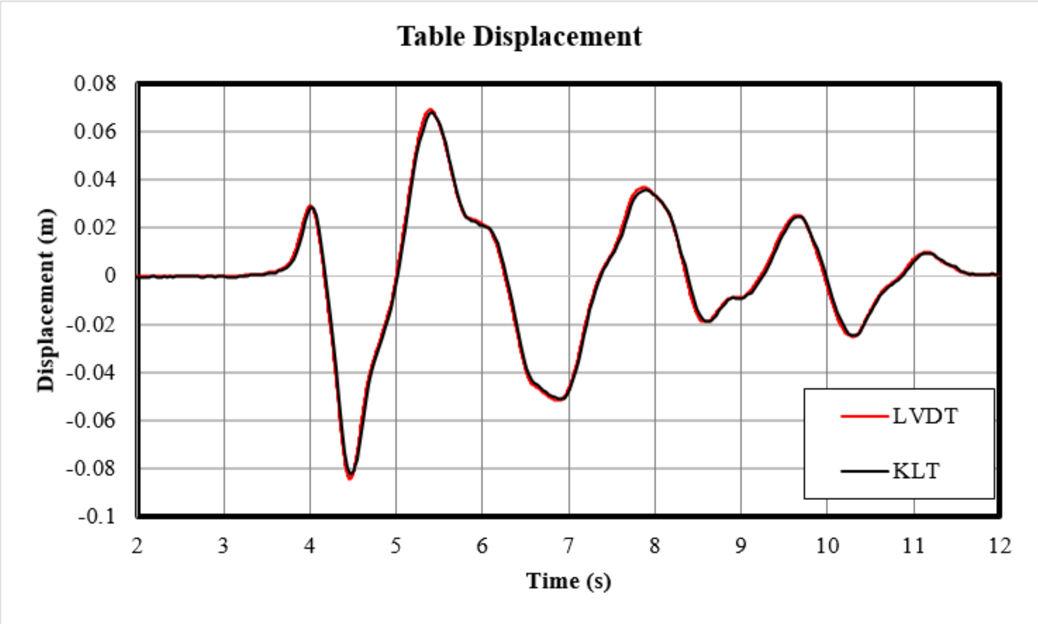

Figure 5.35. Ground Displacement comparison graphic of conventional method (LVDT) and video record (KLT) 2.7K, 30 fps EQ Record: San Salvador, Scale Factor: 0.75.

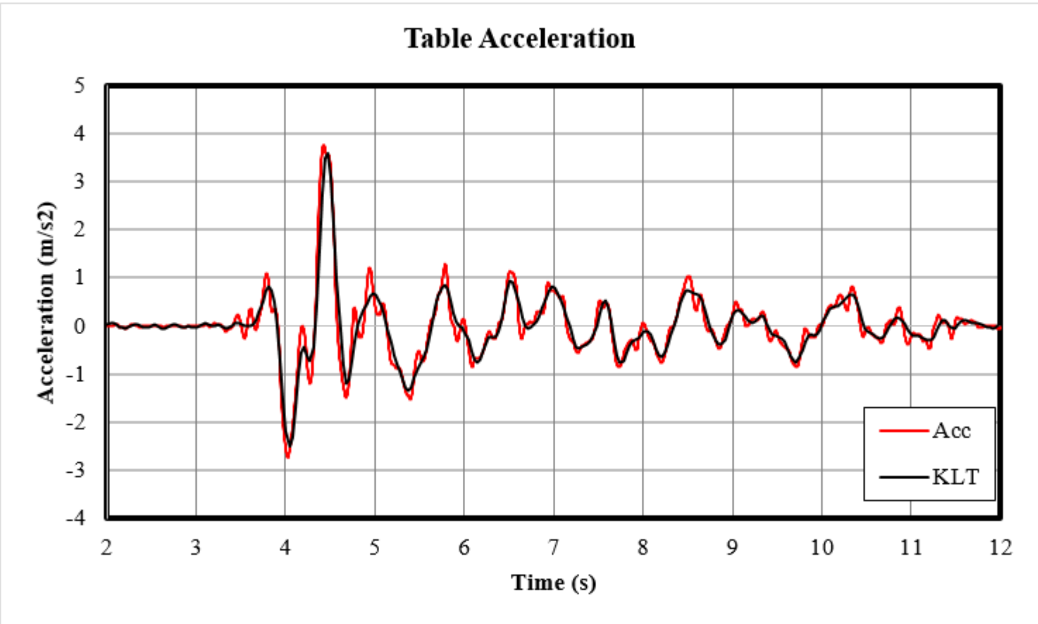

Figure 5.36. Ground Acceleration comparison graphic of accelerometer (Acc) and video record (KLT) 2.7K, 30 fps EQ Record: San Salvador, Scale Factor: 0.75.

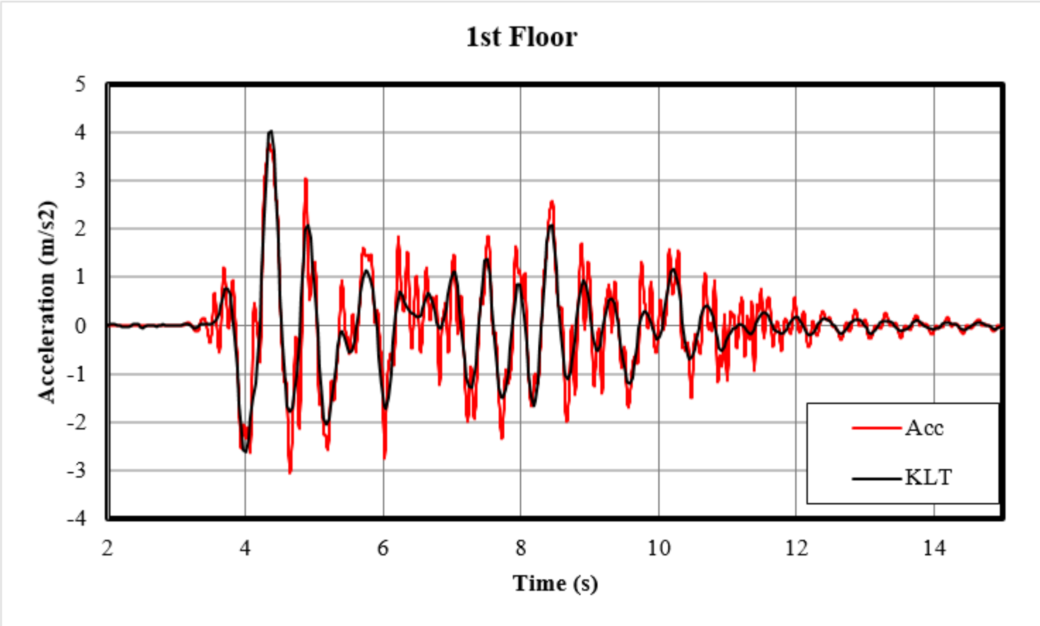

Figure 5.37. 1^{st} Floor Acceleration comparison graphic of accelerometer (Acc) and video record (KLT) 2.7K, 30 fps EQ Record: San Salvador, Scale Factor: 0.75.

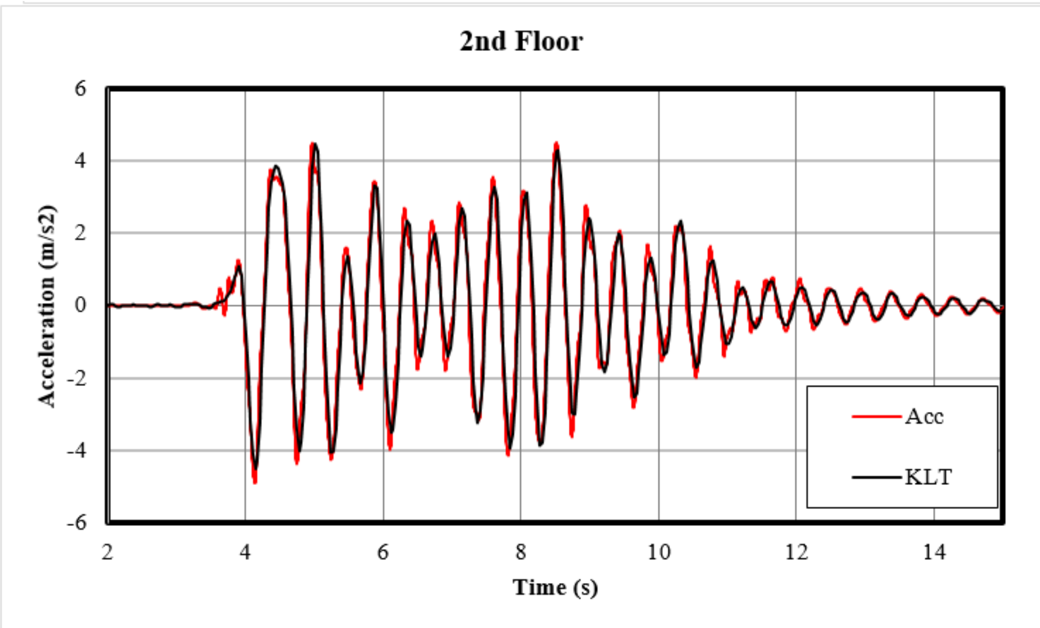

Figure 5.38. 2^{nd} Floor Acceleration comparison graphic of accelerometer (Acc) and video record (KLT) 2.7K, 30 fps EQ Record: San Salvador, Scale Factor: 0.75.

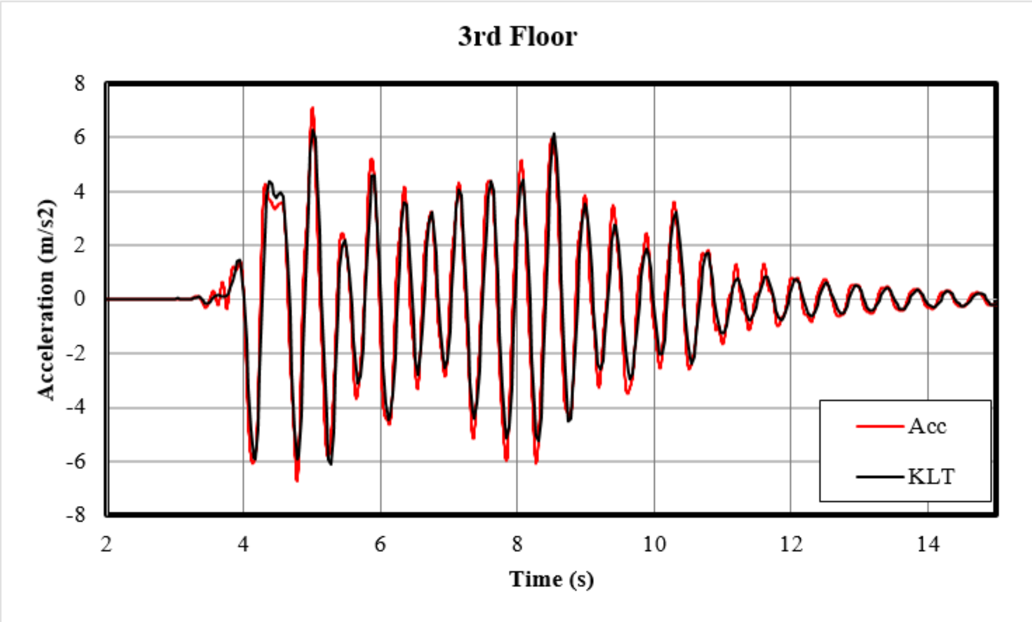

Figure 5.39. 3^{rd} Floor Acceleration comparison graphic of accelerometer (Acc) and video record (KLT) 2.7K, 30 fps EQ Record: San Salvador, Scale Factor: 0.75.

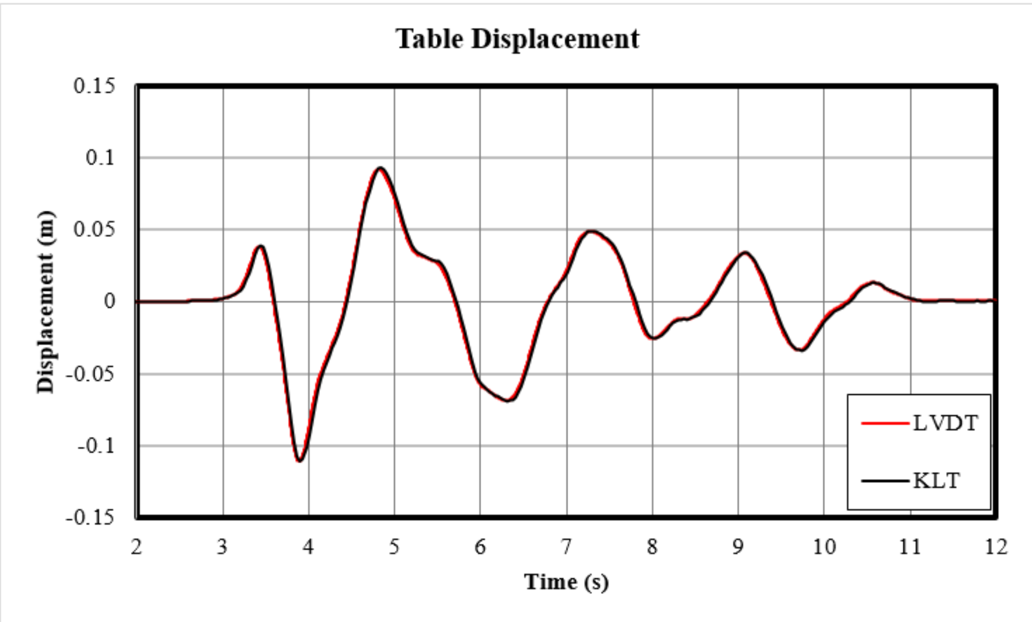

Figure 5.40. Ground Displacement comparison graphic of conventional methods (LVDT) and video record (KLT) 2.7K, 30 fps EQ Record: San Salvador, Scale Factor: 1.0.

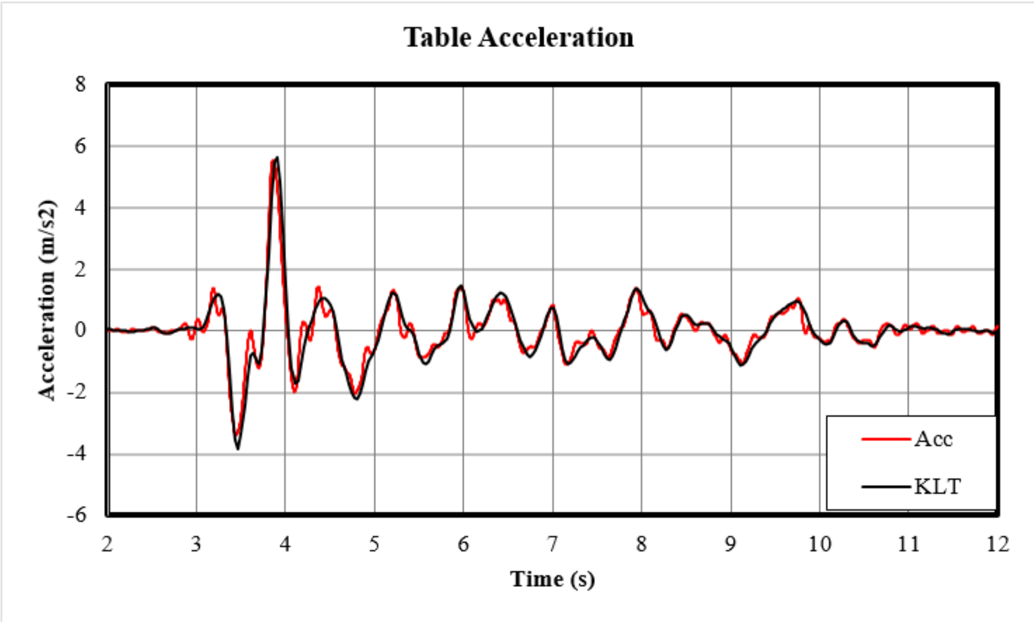

Figure 5.41. Ground Acceleration comparison graphic of accelerometer (Acc) and video record (KLT) 2.7K, 30 fps EQ Record: San Salvador, Scale Factor: 1.0.

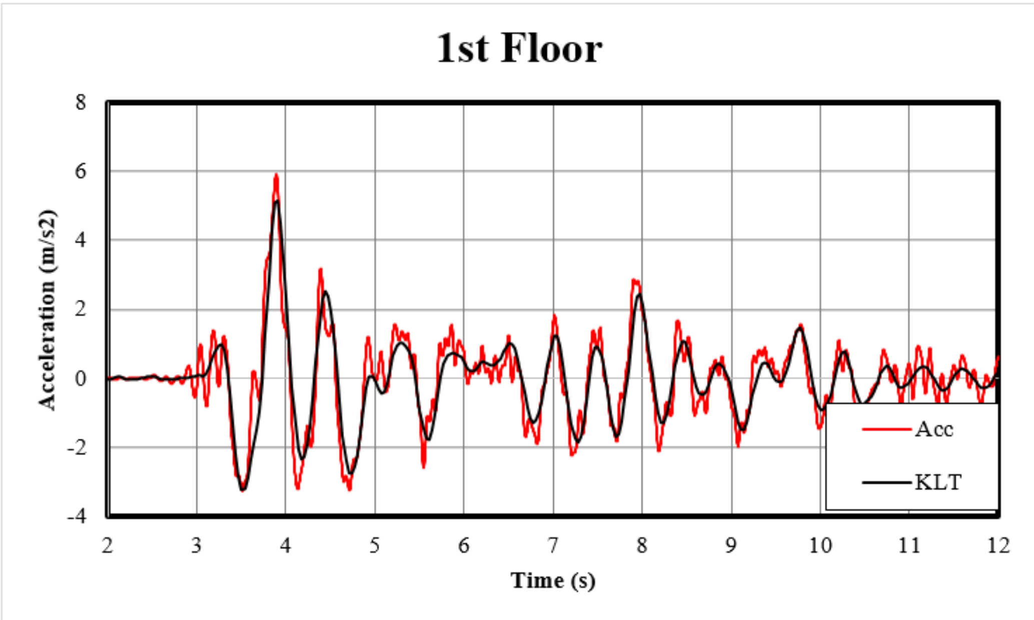

Figure 5.42. 1^{st} Floor Acceleration comparison graphic of accelerometer (Acc) and video record (KLT) 2.7K, 30 fps EQ Record: San Salvador, Scale Factor: 1.0.

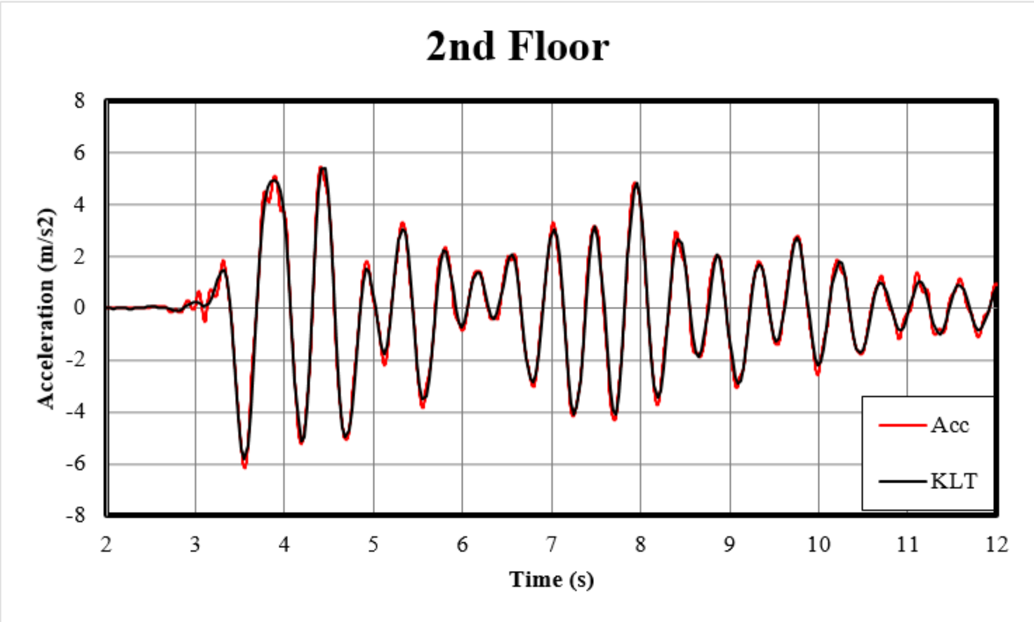

Figure 5.43. 2^{nd} Floor Acceleration comparison graphic of accelerometer (Acc) and video record (KLT) 2.7K, 30 fps EQ Record: San Salvador, Scale Factor: 1.0.

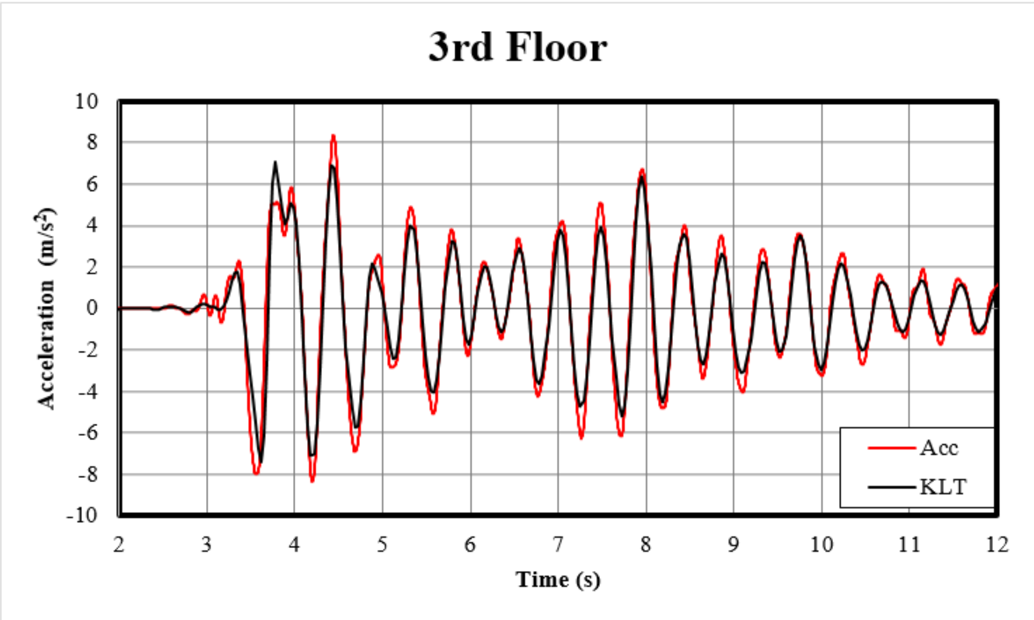

Figure 5.44. 3^{rd} Floor Acceleration comparison graphic of accelerometer (Acc) and video record (KLT) 2.7K, 30 fps EQ Record: San Salvador, Scale Factor: 1.0.

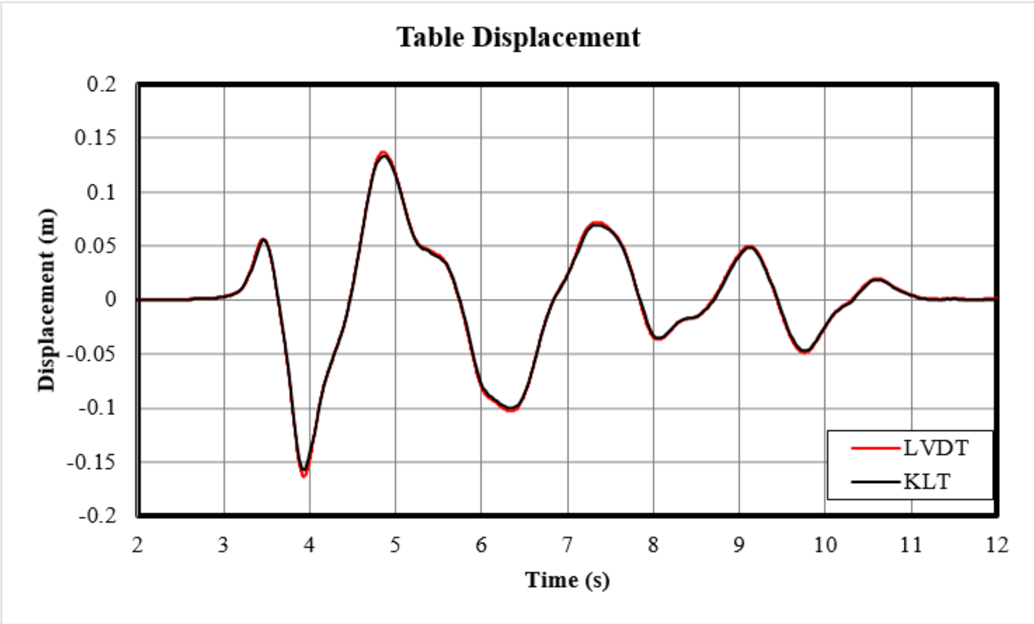

Figure 5.45. Ground Displacement comparison graphic of displacement (LVDT) and video record (KLT) 2.7K, 30 fps EQ Record: San Salvador, Scale Factor: 1.5.

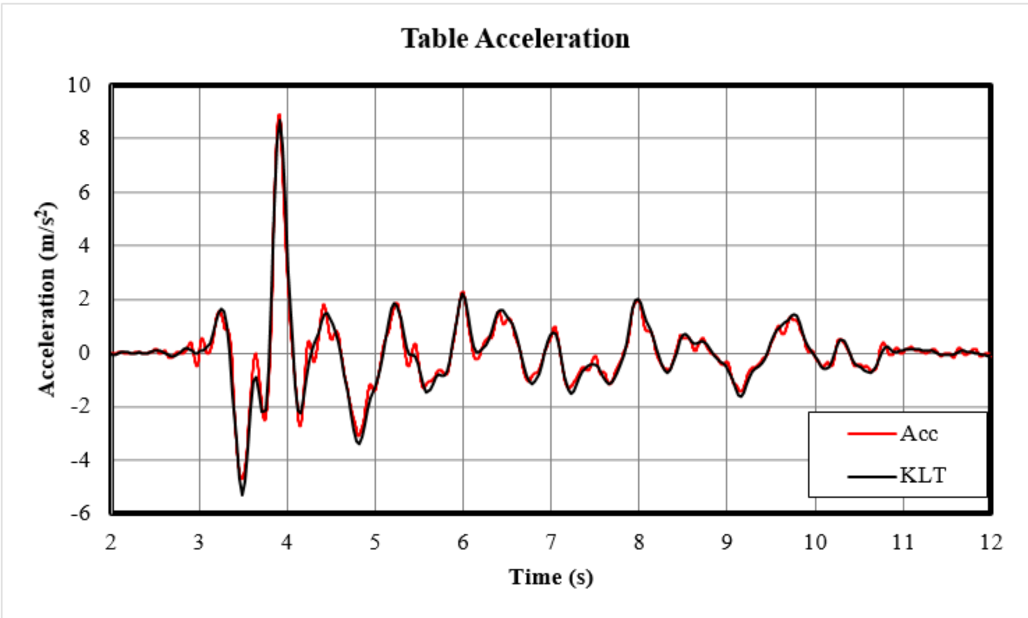

Figure 5.46. Ground Acceleration comparison graphic of accelerometer (Acc) and video record (KLT) 2.7K, 30 fps EQ Record: San Salvador, Scale Factor: 1.5.

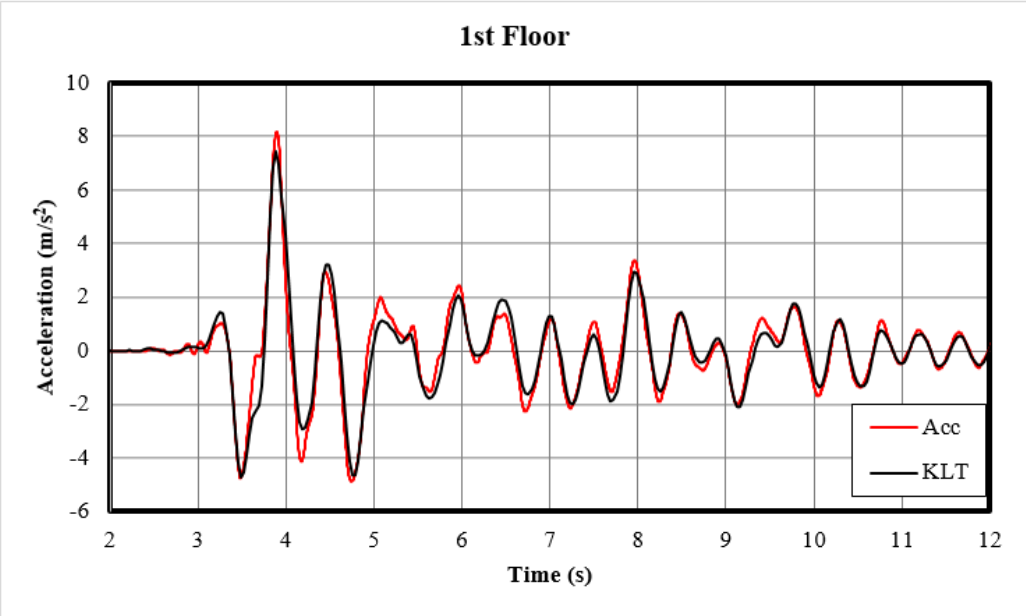

Figure 5.47. 1^{st} Floor Acceleration comparison graphic of displacement (Acc) and video record (KLT) 2.7K, 30 fps EQ Record: San Salvador, Scale Factor: 1.5.

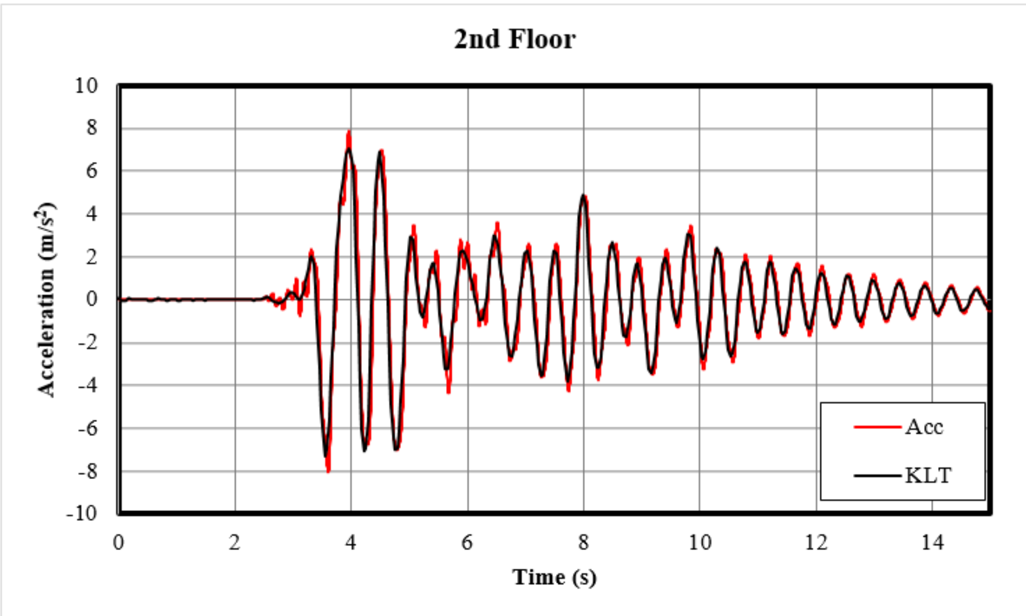

Figure 5.48. 2^{nd} Floor Acceleration comparison graphic of accelerometer (Acc) and video record (KLT) 2.7K, 30 fps EQ Record: San Salvador, Scale Factor: 1.5.

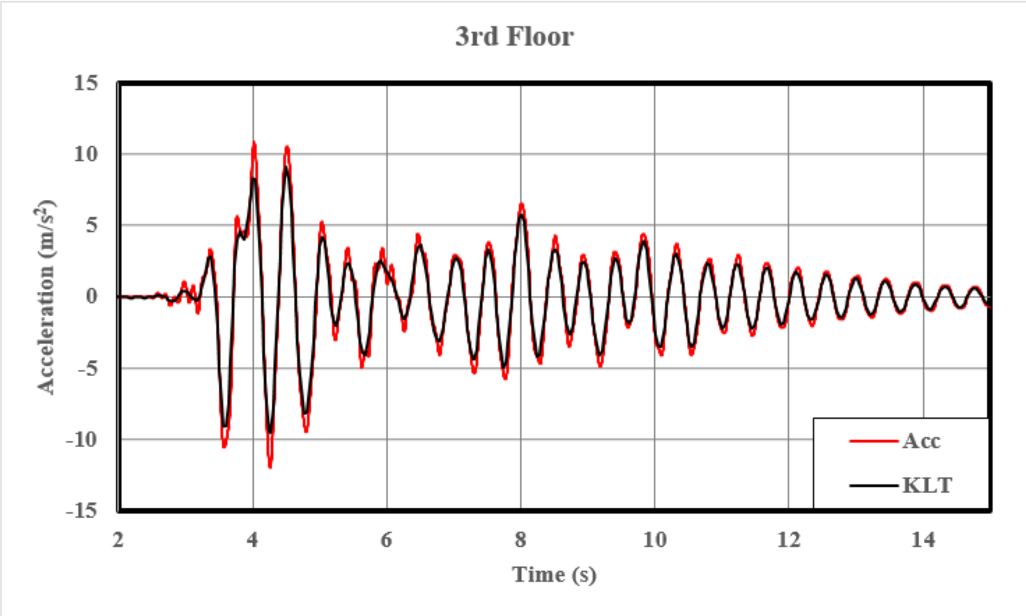

Figure 5.49. 3^{rd} Floor Acceleration comparison graphic of accelerometer (Acc) and video record (KLT) 2.7K, 30 fps EQ Record: San Salvador, Scale Factor: 1.5.

The results and observations of these experiments were similar to elastic MDOF experiments. A successful comparison was observed in displacement data and high frequency signals were missed in the image-based measurements. Ground acceleration comparison presented superior matching than that of the elastic experiments due to the differences in the frequency contents of San Salvador and HDA165 ground motions.

5.6. Results of Strain Measurements

In these experiments, free vibration and San Salvador ground motion records were used. Camera was placed close to the surface. High pass and low pass filters were used to eliminate noise due to the vibration of the recorder during dynamic experiments. Especially low frequency contamination distorted the data. Figure 5.50 presented the comparison between strain gauge and image-based measurements after the application of filters. Figure 5.51 is the graphical representation of the unfiltered data. Low frequency contamination can be observed in this figure.

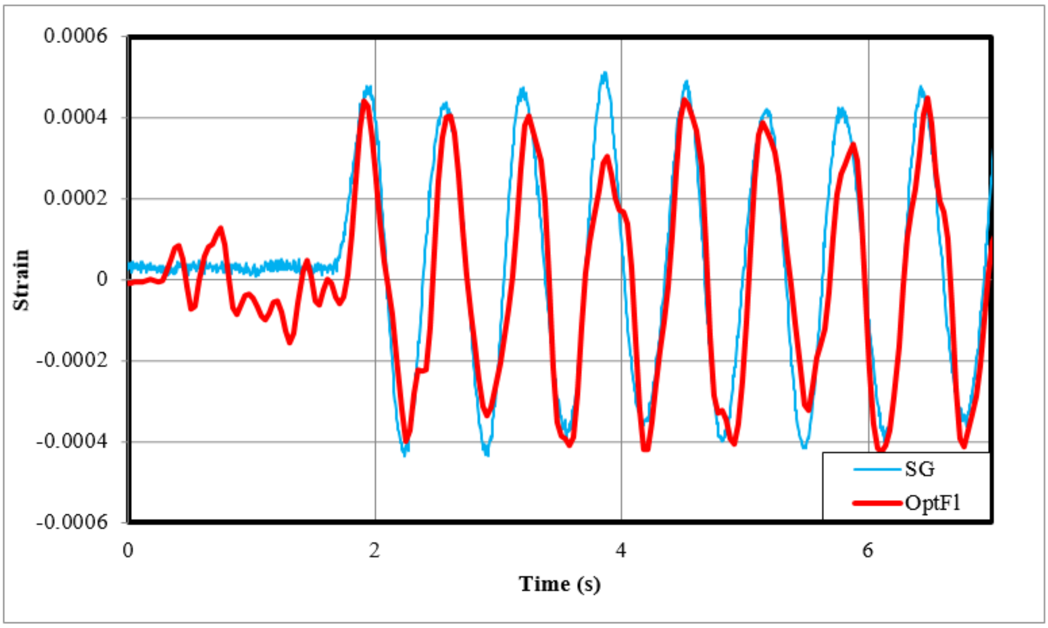

Figure 5.50. Comparison of Strain Gauge (SG) and Image-Based (OptFl) strain measurements.

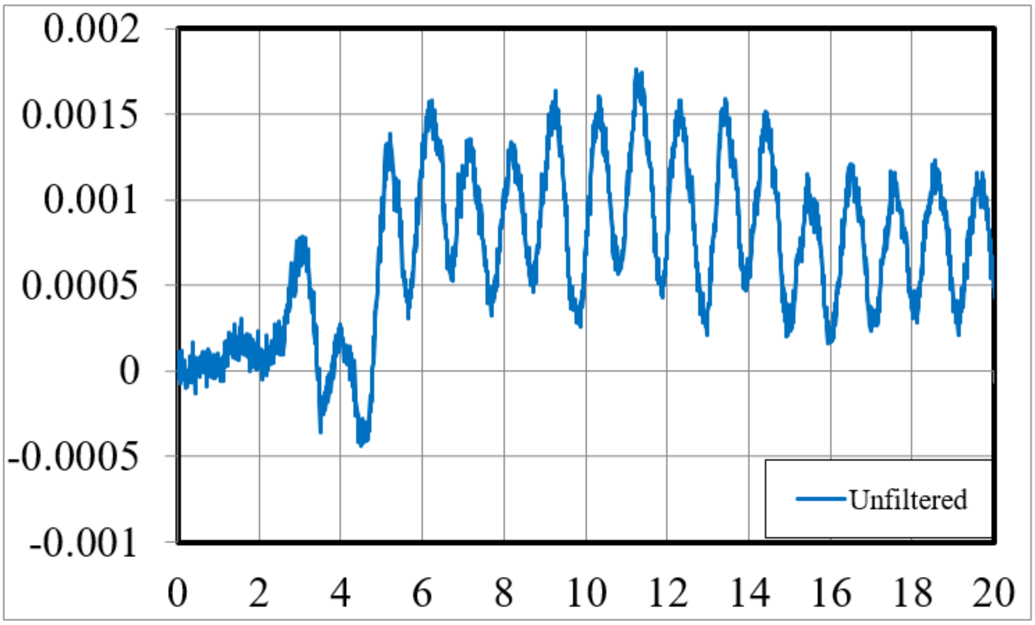

Figure 5.51. Unfiltered strain data extracted by image-based methods.

Results of these experiments showed that the recording system and algorithm needed to be developed further to extract strains under dynamic motion. The existing low frequency noise distorted the data. When this low frequency signals were filtered out, some data belonging to the actual displacement signals were also eliminated.

During these experiments, video cameras were placed quite close to the specimen and shaking the specimen manually distorted the camera's stationary position. Therefore, equipment that stabilizes the video camera must be properly installed during recording.

5.7. Results of MDOF Full Scale Experiments

This video record provided a useful information to extract displacements of the model in each story. The image record with Northridge Earthquake Ground Motion was analyzed and the results were compared with the accelerometers measured on each story. Results of these experiments are presented in figures from Figure 5.52 to Figure 5.59.

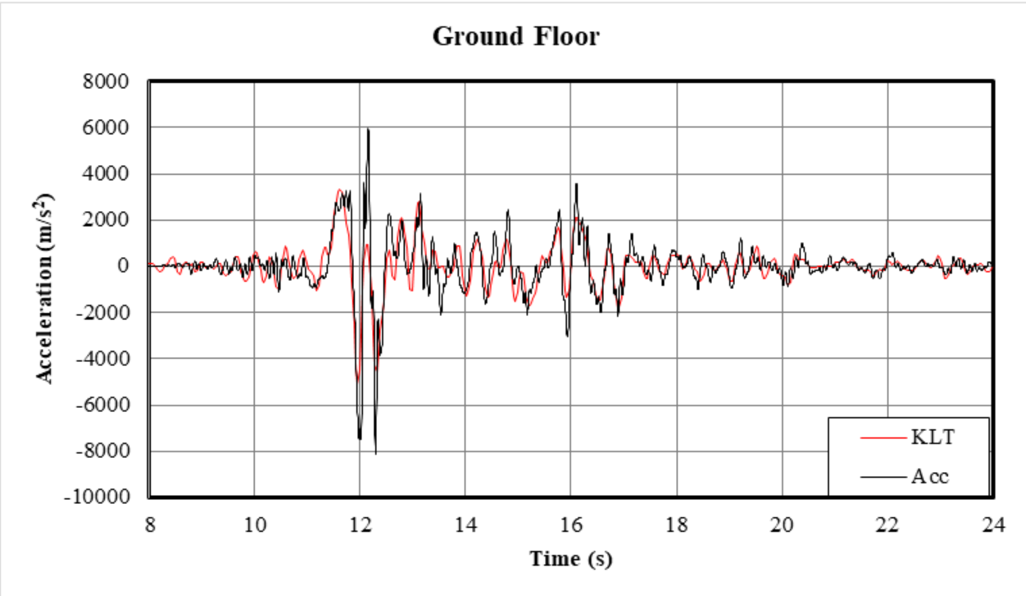

Figure 5.52. Ground Acceleration comparison graphic of accelerometer (Acc) and video record 640p, 30 fps EQ Record: Northridge.

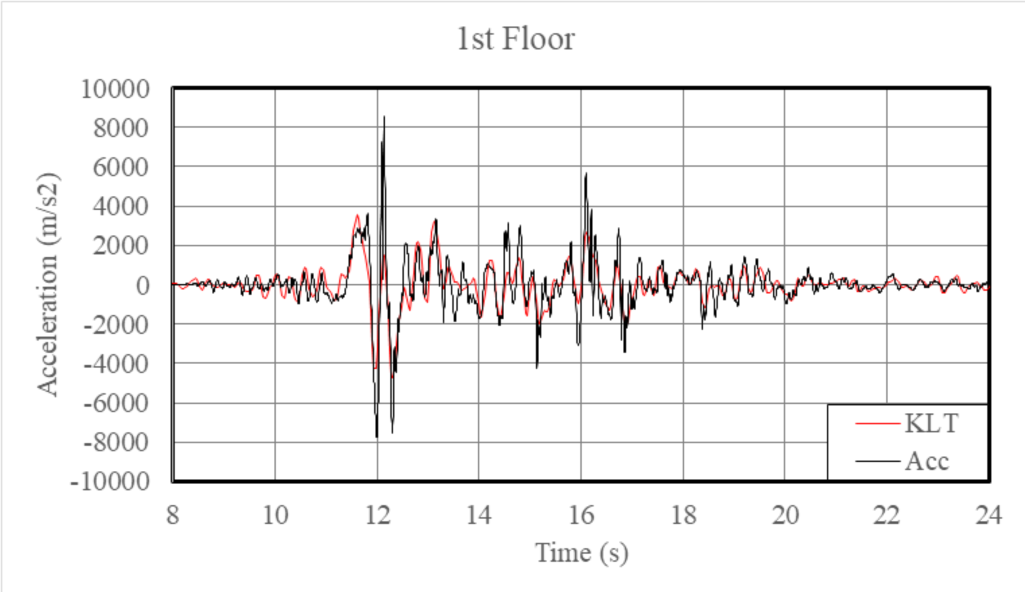

Figure 5.53. 1^{st} Floor Acceleration comparison graphic of accelerometer (Acc) and video record 640p, 30 fps EQ Record: Northridge.

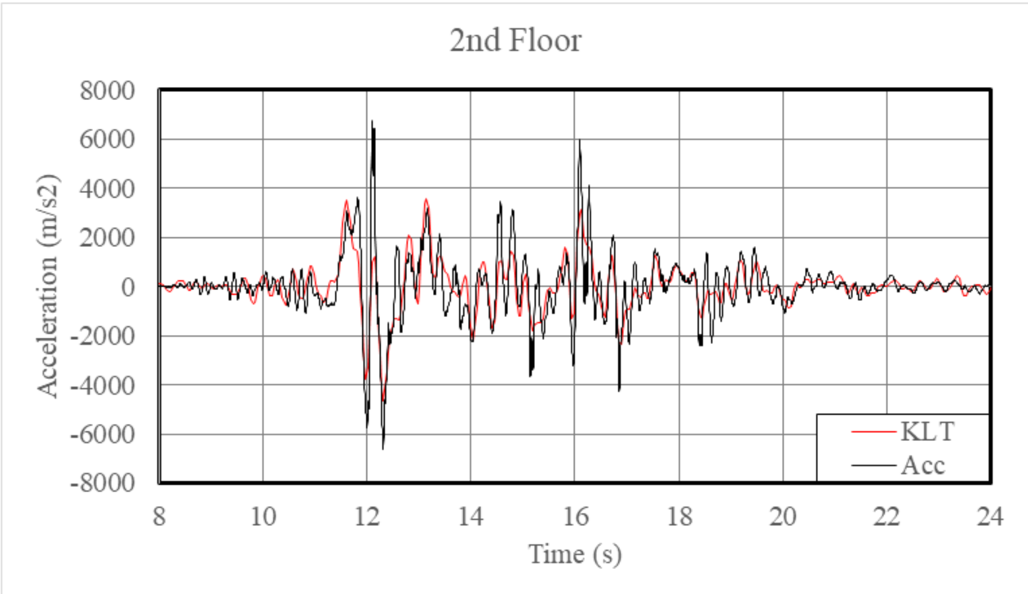

Figure 5.54. 2^{nd} Floor Acceleration comparison graphic of accelerometer (Acc) and video record 640p, 30 fps EQ Record: Northridge.

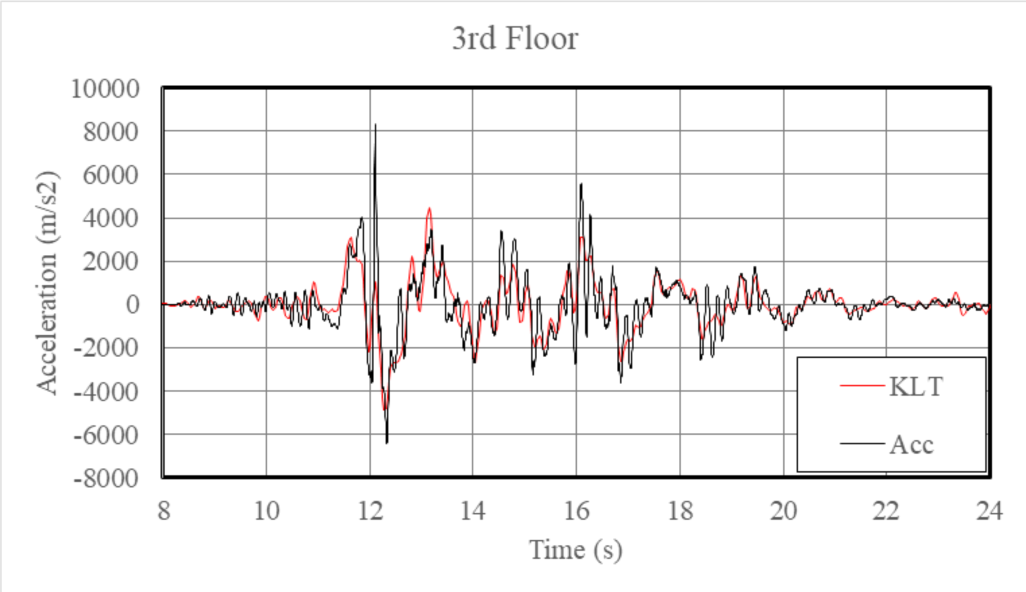

Figure 5.55. 3^{rd} Floor Acceleration comparison graphic of accelerometer (Acc) and video record 640p, 30 fps EQ Record: Northridge.

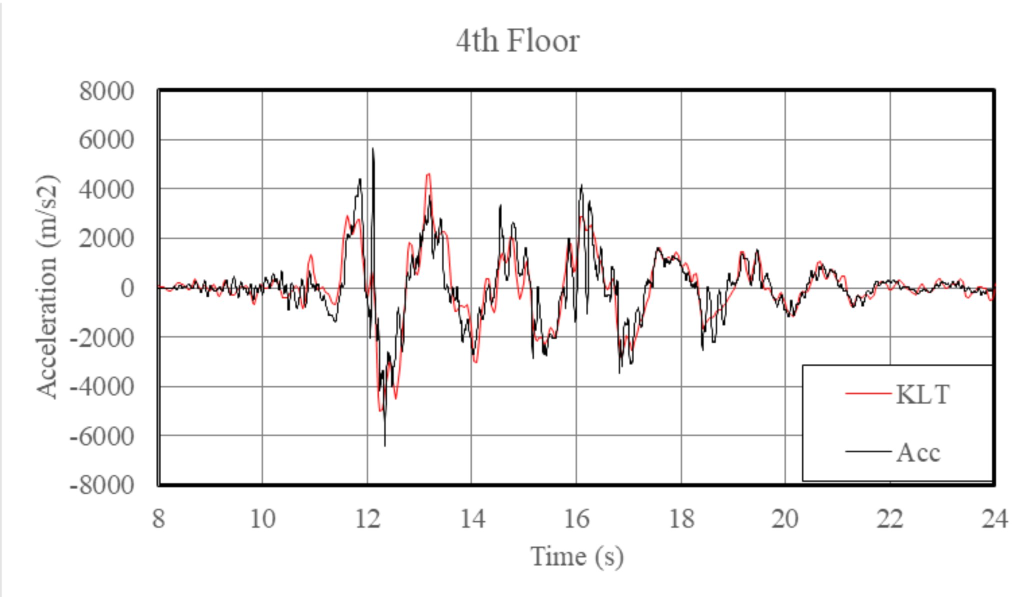

Figure 5.56. 4^{th} Floor Acceleration comparison graphic of accelerometer (Acc) and video record 640p, 30 fps EQ Record: Northridge.

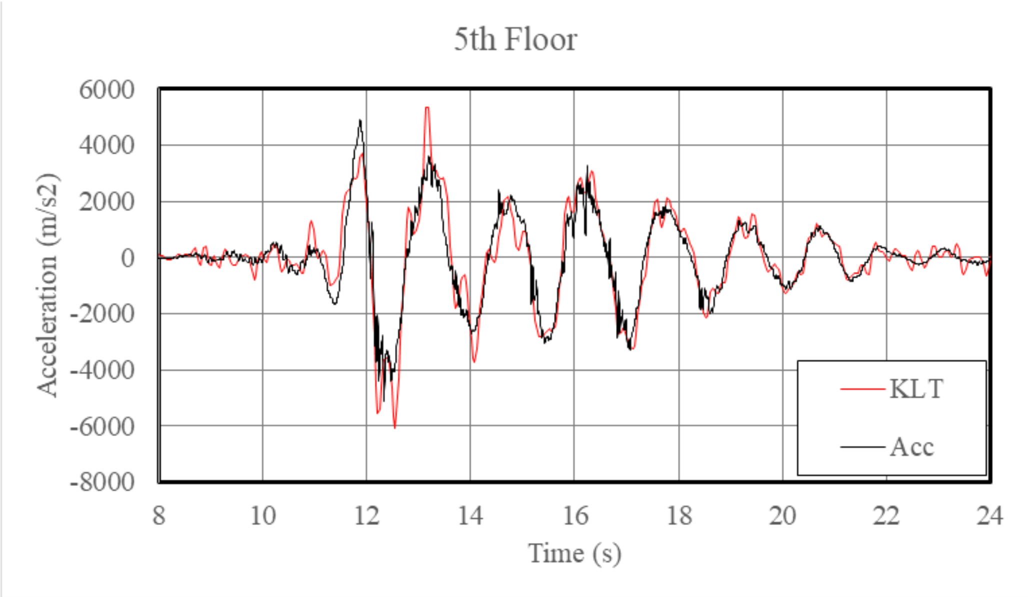

Figure 5.57. 5^{th} Floor Acceleration comparison graphic of accelerometer (Acc) and video record 640p, 30 fps EQ Record: Northridges.

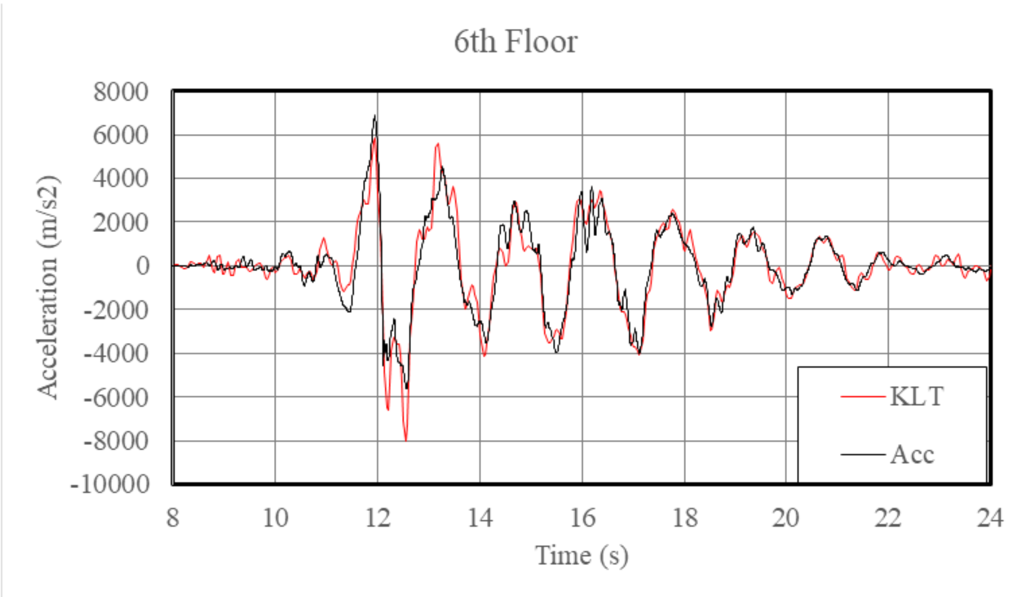

Figure 5.58. 6^{th} Floor Acceleration comparison graphic of accelerometer (Acc) and video record 640p, 30 fps EQ Record: Northridge.

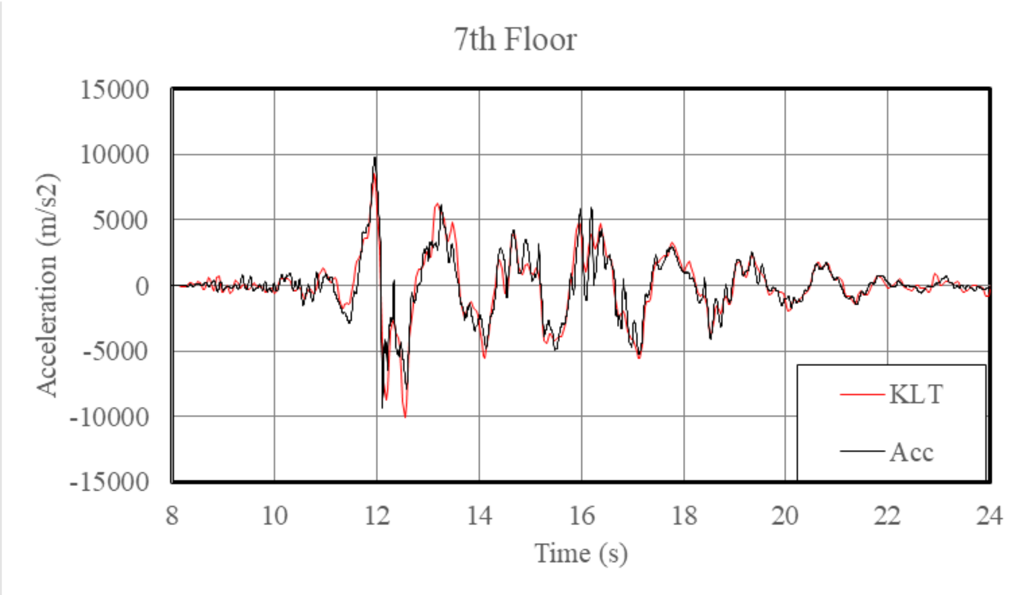

Figure 5.59. 7^{th} Floor Acceleration comparison graphic of accelerometer (Acc) and video record 640p, 30 fps EQ Record: Northridge.

Results of these measurements were considered quite promising in terms of the future studies of extracting the responses of real buildings during earthquakes. The video record was not intended to capture displacements or any other measurements. Its purpose was to record the testing event which took place. Using this video record, acceleration results extracted from this video were accurately matched with actual measured accelerometer data. Main problem observed was again mismatch in some peaks in the motion. These incidental peaks in motions are crucial to identify the structural behavior. Maximum acceleration and displacement experienced during the ground excitation are essential indicators of the structural condition after the earthquake. The absence of the matching the two sources of data considered to be the cause of the low sampling rate of the video camera.

The video records by stable video cameras provided promising results, but during an earthquake, motion of these cameras should also be considered. In order to determine earthquake responses, a method that reveals the motion of the camera should be developed. A single video recorder was able to capture the entire motion of the degrees of freedoms in this example. However, motions of a structure during an earthquake would be in three-dimensional space. In that more than one camera should record the motion of structure to cover all components of it.

Since the sampling rates of the compared data were different, coefficient of variation (COV) was not utilized in this study. However, another characteristic which is quite valuable for evaluating the effects of vibration was investigated. This characteristic is the range of the responses. Peak to peak values of compared data were found and the ratio between them were calculated. Table 5.1 presents the highest and lowest peak to peak ratios of different cases.

Table 5.1. Highest and Lowest Peak to Peak Ratios of Experimental Results.

	Highest Peak to peak ratio	Highest Peak to peak ratio case	Lowest Peak to peak ratio	Lowest Peak to peak ratio case
Elastic SDOF	0.9949	Erzincan T=0.667 Displacement	0.6324 (Due to noise)	Loma Prieta T=0.667 Acceleration
Plastic SDOF	0.9939	Acceleration m=94.4 kg	0.8585	Acceleration m=147 kg
Elastic MDOF	0.9677	HAD 165, Ground Displacement Scale Factor: 0.2	0.8587	San Salvador 3rd Floor Acceleration Scale Factor: 0.2
Plastic MDOF	0.9788	San Salvador Ground Displacement Scale Factor: 1.5	0.8887	San Salvador 3rd Floor Acceleration Scale Factor: 0.75
Full Scale MDOF	0.9704	7th Floor Acceleration	0.5944	Ground Acceleration
Strain	0.9241	Free Vibration	-	-

Table 5.1 shows the success of each case. However as indicated in the Table 5.1, the lowest value of the SDOF specimen stem from an unexpected distortion and its effects on the acceleration data. Except strain measurements, maximum ratios are above 96% success. On the other hand, minimum ratios were around 85% except acceleration of the SDOF case with unexpected noise and Ground motion of the full-scale model case. This ground motion contained sudden peaks which could not be detected by the video record with low sampling rate. These results indicated the

importance of the stable environmental conditions and high frequency sampling. The video of the full-scale model had 30 Hz sampling rate which was not sufficient in this case. A video record with 60 Hz sampling rate would have a great capability to capture these sudden motions.

6. CONCLUSIONS

Experiments conducted in this study included different structural cases, measurement tools and recording options. Consumer product video cameras were utilized in this study. The results showed that consumer product cameras and mobile phone video records could easily be used for extracting displacements of structures in shake table tests. In this study, Statistical Threshold method and a light source correction algorithm in LED tracking method were developed, and their performances were evaluated. Also KLT tracking algorithm was used to extract displacement in various experimental cases. Results obtained from image-based methods were similar to the conventional methods in general. When the certain conditions such as required sampling rate, distinctive shape or color characteristics on specimens as targets and stabilization of the recorder were met, these methods could be presented as powerful alternative measurement tools. Main conclusions that could be drawn in this study are as the followings:

- Conventional devices used in this study were strain gauges, LVDTs and accelerometers. If these devices were set up properly and did not have any functional problems, results obtained from these devices could be quite reliable. Their high sampling rate and accuracy provides advantages over image-based methods. However, experiencing such set up and functional problems are frequently observed in experiments. On the other hand, setting up the recorder that was used for image-based methods was quite easy and functional problems were never experienced during tests. When the frequency of the motion was within the range of the recorder, image-based methods were quite robust. However, motions with frequencies beyond this range could not be properly detected. Sampling rates of the recorders used in this study was 30 Hz and 60 Hz. However, conventional measurement devices had 200 Hz sampling rates. Proper comparison between these two methods should be conducted by devices with same sampling rates.
- When two motion tracking methods utilized in this study were compared, first conclusion could be drawn as the strength of KLT Tracking method in experi-

mental video records with lower resolution was apparent. As the resolution of the video record increased, results that were extracted with two different methods converged. However, KLT method was more vulnerable to changing background light conditions. Features detected by this method might disappear and results might not indicate the real dynamic responses. Existence of a light source on the specimen increased the robustness of image-based methods.

- As mentioned above, one crucial condition was that the true comparison of these two methods which took place was the existence of same sampling rate for both methods. However increased sampling rate meant lower resolution for a recorder. This low resolution reduced the accuracy of the image-based methods, especially LED-based statistical method. Hence, in order to use the LED-based statistical method in these comparisons, professional cameras with 200 Hz sampling rate and high resolution, at least 1080p, must be used. However, using such cameras would defeat the purpose of effectiveness in terms of the cost. On the other hand, KLT method did not possess such disadvantage under proper background light conditions.
- Effect of sampling rate and resolution were considered for both methods. While the effect of resolution was not highly crucial on the method based on KLT, high resolution significantly improved the performance of LED-based statistical method. Sampling rate played a crucial role in the determination of acceleration of the ground motion. Displacement of this ground motion could be extracted accurately, but when the acceleration data were derived, increment in the margins of errors was observed due smoothening effect of Savitzky-Golay derivatives.
- ? Main function of these recorders used in this study was to provide video record with best achievable resolution. However, in many cases, high frequency motions might occur, and larger sampling rates were required. The ground motion data of the Full-Scale building showed that 30 fps video record was sufficient. It is concluded that if a higher sampling rate, such as 60 fps, were used, results would be significantly improved.
- Video records of full-scale experiments provided promising results to extract the response of a real structure in an earthquake. However, a robust method that considering the motion of the video camera needed to be developed. In addition,

as one video camera could only record a single plane, more than one camera from different angles could be more beneficial in the determination of responses more reliable.

- In order to extract real strains on the specimens, low frequency noise should be eliminated. This elimination could be provided by experimental setup or a developed computer vision technique. Filtering the signal could lead to the elimination of the real data.

To expand the understanding in this research area, future works might consider performing a comparison of high-frequency professional recorders and commercial cameras. One other possible object of a future study might be conducting dynamic experiments and measurement of any displacement in three-dimensional space preferably with more than one recording source.

REFERENCES

Alemdar, Z.F., J.A. Browning and J. Olafsen, “Photogrammetric Measurements of RC Bridge Column Deformations”, *Engineering Structures*, Vol. 33, No. 8, pp. 2407-2415, 2011.

Baqersad, J., P. Poozesh, C. Niezrecki and P. Avitabile, “Photogrammetry and Optical Methods in Structural Dynamics - A review”, *Mechanical Systems and Signal Processing*, Vol. No. 86, pp. 17-34, 2017.

Birchfield, S., Derivation of kanade-lucas-tomasi tracking equation, Unpublished Notes, 1-2. http://vigir.missouri.edu/ gdesouza/ Research/ Tracking/ Derivation of Kanade - Lucas - Tomasi Tracking Equation Stan Birchfield.pdf, accessed at June 1997.

Cha, Y.J., J.G. Chen and O. Büyüköztürk, “Output-Only Computer Vision Based Damage Detection Using Phase-Based Optical Flow and Unscented Kalman Filters”, *Engineering Structures*, Vol. 132, pp. 300-313, 2017.

Chang, C.C. and Y.F. Ji, “Flexible Videogrammetric Technique for Three-Dimensional Structural Vibration Measurement”, *Journal of Engineering Mechanics*, Vol. 133, No. 6, pp. 656-664, 2007.

Chen, J.G., A. Davis, N. Wadhwa, F. Durand, W.T. Freeman and O. Büyüköztürk, “Video Camera - Based Vibration Measurement for Civil Infrastructure Applications”, *American Society of Civil Engineers*, Vol. 1, pp. 1-11, 2014.

Chen J.G., N. Wadhwa, Y.J. Cha, F. Durand, W.T. Freeman and O. Büyüköztürk, “Modal Identification of Simple Structures with High-Speed Video Using Motion Magnification”, *Journal of Sound and Vibration*, Vol. 345, pp. 58-71, 2015.

Choi, H.S., J.H. Cheung, S.H. Kim and J.H. Ahn, “Structural Dynamic Displacement

Vision System Using Digital Image Processing", *NDT and E International*, Vol. 44, No. 7, pp. 597-608, 2011.

Chu, T.C., W.F. Ranson and M.A. Sutton, "Experimental Mechanics", *Experimental Mechanics*, Vol. 25, pp. 232, 1985.

Güllü, A. *Seismic Analyses and Response Tuning of Structures Through Energy Equations*, M.S. Thesis, School of Civil Engineering, the University of Tehran, 2005.

Hoult, N.A., W. Andy Take, C. Lee and M. Dutton, "Experimental Accuracy of two Dimensional Strain Measurements Using Digital Image Correlation", *Engineering Structures*, Vol. 46, pp. 718-726, 2013.

Jurjo, D.L.B.R., C. Magluta, N. Roitman and P.B. Gonçalves, "Experimental Methodology for the Dynamic Analysis of Slender Structures Based on Digital Image Processing Techniques", *Mechanical Systems and Signal Processing*, Vol. 24, No. 5, pp. 1369-1382, 2010.

Kim, S.W. and N.S. Kim, "Multi-Point Displacement Response Measurement of Civil Infrastructures Using Digital Image Processing", *Procedia Engineering*, Vol. 14, pp. 195-203, 2011.

Lin, J.J., A.R. Liu, Q.C. Yu and J.D. Deng, "Deformation and Energy-Based Seismic Damage Evaluation of Steel Reinforced Concrete and Reinforced Concrete Piers", *Applied Mechanics and Materials*, Vol. 1, pp. 580-583, 2014.

Liu, X., X. Tong, X. Yin, X. Gu and Z. Ye, "Videogrammetric Technique For Three-Dimensional Structural Progressive Collapse Measurement", *Journal of the International Measurement Confederation*, Vol. 63, pp. 87-99, 2015.

Lu, L., H. Li, X. Liu and X. Lu, "Shaking Table Test on Seismic Performance of Controlled Rocking Reinforced Concrete Frame", *Jianzhu Jiegou Xuebao/Journal of Building Structures*, Vol. 37, No. 3, pp. 156-166, 2016.

Lucas, B.D. and K. Takeo, “An Iterative Image Registration Technique with an Application to Stereo Vision”, *Proceedings of the 7th International Joint Conference on Artificial Intelligence*, Vol. 1, pp. 674-679, 1981.

Mar, W., E. Sierra, J. Marrugo, C. Camacho, L.A. Romero and A.G. Marrugo, “A Vision-Based System for the Dynamic Measurement of In-Plane Displacements, 2014 3rd International Congress of Engineering Mechatronics and Automation”, *CIIMA 2014 - Conference Proceedings*, Vol. 1, pp. 3-6, 2014.

McAndrew, A., “An Introduction to Digital Image Processing with Matlab Notes for SCM2511”, *Image Processing 1.*, 2004.

McCarthy, D.M.J., J. H. Chandler and A. Palmeri, “Monitoring Dynamic Structural Tests Using Image Deblurring Techniques”, *10th International Conference on Damage Assessment of Structures*, pp. 569-570, 2013.

McCormick, N. and J. Lord, “Digital Image Correlation”, *Materials Today*, Vol. 13, No. 12, pp. 52-54, 2010.

Morlier, J., P. Salom and F. Bos, “New Image Processing Tools for Structural Dynamic Monitoring”, *Key Engineering Materials*, Vol. 347, pp. 239-244, 2007.

Nayyerloo, M., J.G. Chase, A. Millane, C. Muller, A. Malherbe, X.Q. Chen and G.A. MacRae, “Seismic structural displacement measurement using a line-scan camera: Camera-pattern calibration and experimental validation, *Journal of Civil Structural Health Monitoring*, Vol. 1, No. 3-4, pp. 113-124, 2011.

Newmark, N.M., “A Method of Computation for Structural Dynamics, *Journal of the Engineering Mechanics*, 1959.

Nogueira, F. M., F.S. Barbosa and L.P.S. Barra, “Evaluation Of Structural Natural Frequencies Using Image Processing, *Experimental Vibration Analysis For Civil Engineering Structures*, pp. 1-7, 2005.

Okuyan, S., *Scaling of Input Seismic Energy of SDOF Systems Through Experimental and Analytical Investigation*, M.S. Thesis, Bogiziçi University, 2017.

Park, J.W., J.J. Lee, H.J. Jung and H. Myung, Vision-Based Displacement Measurement Method For High-Rise Building Structures Using Partitioning Approach, *NDT and E International*, Vol. 43, No. 7, pp. 642-647, 2010.

Peters, W.H., W. F. Ranson, "Digital Imaging Techniques In Experimental Stress Analysis", *Optical Engineering*, Vol. 21, No. 3, pp. 213-427, 1982.

Ribeiro, D., R. Calçada, J. Ferreira and T. Martins, 2014, "Non-Contact Measurement of the Dynamic Displacement of Railway Bridges Using an Advanced Video-Based System", *Engineering Structures*, Vol. 75, pp. 164-180.

Savitzky, A. and M.J.E. Golay, "Smoothing and Differentiation of Data by Simplified Least-Squares Procedures", *Analytical Chemistry*, Vol. 36, pp. 1627-1639, 1964.

Shi, J. and C. Tomasi, "Good Features to Track", *IEEE Conference on Computer Vision and Pattern Recognition*, pp. 593-600, 1994.

Tomasi, C. and T. Kanade, "Detection and Tracking of Point Features", *Computer Science Department, Carnegie Mellon University*, 1991.

Tosun, U., R. Aghazadeh, C. Sert and M.B. Özer, 2017, Tracking Free Surface And Estimating Sloshing Force Using Image Processing", *Experimental Thermal and Fluid Science*, Vol. 88, pp. 423-433.

Uang, C.M. and V.B. Vitelmo, "Evaluation of Seismic Energy in Structures", *Earthquake Engineering and Structural Dynamics*, Vol. 19, No.1, pp. 77-90, 1990.

Wu, L.J., F. Casciati and S. Casciati, "Dynamic Testing of a Laboratory Model Via Vision-Based Sensing", *Engineering Structures*, Vol. 60, pp. 113-125, 2014.

Zdenek, K., M. Krystian and M. Jiri, "Forward-Backward Error: Automatic Detection of Tracking Failures", *Proceedings of the 20th International Conference on Pattern Recognition*, Vol. 1, pp. 2756-2759, 2010.